The Basil Cu-Co deposit, Huckitta project area, Harts Range, N.T., Australia: a possible metamorphosed volcanogenic massive sulphide deposit.

Thesis submitted in accordance with the requirements of the University of Adelaide for an Honours Degree in Geology

Kelly Ann Sharrad

November 2012

THE UNIVERSITY of ADELAIDE

THE BASIL CU-CO DEPOSIT, HUCKITTA PROJECT AREA, HARTS RANGE, N.T., AUSTRALIA: A POSSIBLE METAMORPHOSED VOLCANOGENIC MASSIVE SULPHIDE DEPOSIT.

BASIL CU-CO DEPOSIT: A POSSIBLE METAMORPHOSED VOLCANOGENIC MASSIVE SULPHIDE DEPOSIT.

ABSTRACT

Contemporary exploration models that link the common characteristics of a certain ore type depend upon an understanding of the mechanisms of ore formation and how these relate to the geological environment in which they occur. The Basil Cu-Co deposit located in the Harts Range, Central Australia. The deposit is hosted by a sequence that has been metamorphosed to amphibolite and granulite facies conditions twice (480-460 Ma and 450-300 Ma). As a result, many of the primary mineralisation textures and other characterising features have been destroyed, thus making it difficult to place the deposit within traditional genetic categories. Mineralogical, petrographic and geochemical studies of host rocks and sulphides in the zone of mineralisation, focussing on preserved textures and mineral relationships, allow some constraints to be placed on the genetic history of the deposit.

Results permit several genetic models to be ruled out. Firstly, whole rock geochemistry and garnet compositions suggest that the deposit is not a hydrothermal skarn system. Secondly, the lack of any significant Ni-signature, and presence of abundant zircons in amphibolite (indicating that not all host rocks are mafic in character), makes a magmatic-hosted Ni-Cu-(PGE) system unlikely. Tentatively, Basil is assigned to a volcanogenic massive sulphide (VMS)-style of mineralisation, formed on the seafloor, within basaltic, sedimentary and mixed tuffaceous host rocks typical of such deposit settings. The lack of a recognisable hydrothermal alteration zone is consistent either with destruction of the alteration zone during metamorphism or detachment of the ore from alteration either following formation, or during syn-metamorphic deformation.

The occurrence of sulphide inclusions within garnet and amphibole infers that the sulphides must be syn-metamorphic or earlier. Partitioning of trace elements between pyrite and co-existing pyrrhotite suggests (re)crystallisation occurred under equilibrium conditions. The composition of sphalerite coexisting with pyrite and pyrrhotite, points to crystallisation at pressures of 10 kbar.

CU-CO DEPOSIT, HARTS RANGE, REGIONAL METAMORPHOSED, SULPHIDE PETROGRAPHY, ORE GENESIS, LARAPINTA EVENT, VOLCANOGENIC MASSIVE SULPHIDE

TABLE OF CONTENTS

LIST OF FIGURES AND TABLES

INTRODUCTION

The Basil Cu-Co deposit, located in the Harts Range Group within the Irindina Province, in Central Australia, was discovered in 2009 (www.mithrilresources.com.au). The deposit is poorly understood in terms of its mineralogy and genesis, and in particular, the relationship and relative timing of ore formation, metamorphism and deformation.

A common problem in mineralized metamorphic terranes is that the timing of mineralisation relative to tectonic and metamorphic events is uncertain. Structural overprinting events can destroy the original geometry. Metamorphic and metasomatic overprinting and potential remobilisation of the ore and gangue minerals may obscure primary ore textures. The timing of mineralisation, especially if pre-metamorphic, may be difficult to ascertain. In the worst case, metamorphic overprinting may also make it very difficult or impossible to determine the original genetic type or the processes by which the mineralization formed.

The Basil deposit shows characteristics of some conventional deposit categories, such as sub-marine volcanic-associated hydrothermal deposits resulting in deposition of sulphide minerals on the ocean floor (e.g. Besshi-style mafic volcanogenic massive sulphide (VMS) deposit; (Mattinen & Bennett 1986); replacement and alteration of a chemically reactive host rock via the contact and transport of hydrothermal fluids through a limestone or calc-silicate rock (i.e. hydrothermal skarn; (Meinert 1992); and the formation of a deposit via the segregation and concentration of droplets of liquid sulphide from mafic and ultramafic magma from the silicate melt (e.g. Ni-Cu-(PGE) Deposit; (Naldrett 1999). The Basil deposit has key criteria missing which allow definitive classification into any one of these conventional categories.

The Basil deposit has most likely undergone deformation and metamorphic overprinting which would have resulted in destruction of the original geometry; this would make classification of the Basil deposit difficult and most certainly controversial.

This study applies mineralogical, petrological and geochemistry techniques to identify processes of ore formation and also sets out to address the impact which metamorphism and deformation have had on the ore system. In addition, the research seeks to understand the tectonic controls on the mineralisation. Establishing a genetic model for Basil will facilitate future mineral exploration in the region.

This project will develop an improved understanding of the Basil Cu-Co deposit and the processes involved in its formation and its relative age. An attempt will be made to eliminate specific genetic models for mineralisation by studying the geometry and whole rock geochemistry of alteration and comparing this with the surrounding mafic rocks. This approach focuses on major oxides and elements whose distribution may indicate alteration (via either enrichment or depletion).

BACKGROUND

The Harts Range is located in the Irindina Province in the south-eastern part of the Arunta Complex, central Australia (Buick et al., 2008) (Fig. 1). This area can be divided into the Harts Range Metamorphic Complex and the Entia Gneiss Complex/Bruna Gneiss (Hand *et al.* 1999a), which together constitute the Harts Range Metamorphic Complex (Hand *et al.* 1999a). The Entia Gneiss Complex and Bruna Gneiss forms a Palaeoproterozoic (~1800-1700 Ma; (Wade *et al.* 2008) basement to the Neoproterozoic-Cambrian Harts Range Group, which consists of metasediments and metabasites (Buick *et al.* 2005). The Harts Range Metamorphic Complex has undergone three major tectonomagmatic events: (1) 1780–1730 Ma arc-related magmatism (Wade *et al.* 2008), which affected the basement; (2) the 480–460

Ma Larapinta Event (Mawby *et al.* 1999, Buick *et al.* 2005) which metamorphosed and intensively deformed the Harts Range Group at amphibolite and granulite facies (Mawby *et al.* 1999, Buick *et al.* 2005, Maidment *et al.* 2012); and (3) the 450–300 Ma Alice Springs Orogeny, which resulted in amphibolite grade metamorphism (Mawby *et al.* 1999, Hand *et al.* 1999b, Buick *et al.* 2008).

The Basil Cu-Co deposit is hosted in the c. 520 Ma Riddock Amphibolite (Fig. 1). This is a metamorphosed extrusive sequence traceable for >120 km within the Harts Range Group (Maidment *et al.* 2012). One of the principal questions that require clarification is whether the Basil deposit has experienced the high-grade Ordovician Larapinta Event. If it has, it should be considered whether ore genesis is related to the magmatic processes associated with mafic volcanism during this event. Metamorphism and deformation events could be expected to have modified the primary geometry, remobilised the ore or gangue minerals and could have obliterated textures relating to the initial mineralisation event. Due to this amphibolite to granulite facies overprinting, trying to identify primary mineralisation styles is problematic. Conversely, if mineralisation has not been overprinted by the Larapinta Event, consideration is required as to whether the deposit formed post-Larapinta, or represents an ore that has been remobilised from an earlier location during that event. The difference between these scenarios has important implications for regional exploration models (i.e. stratigraphic verses structural).

GEOLOGICAL SETTING

The Harts Range can be divided into two major lithological associations; these include the Harts Range Metamorphic Complex (HRMC) and the structurally underlying Entia Gneiss Complex (EGC) (Miller *et al.* 1997, Buick *et al.* 2001; Fig. 1). Within that, the Harts Range

Metamorphic Complex can be further divided into two main packages; the Irindina Supracrustal Assemblage, which includes Fe- rich metapelite-mafic gneiss association,

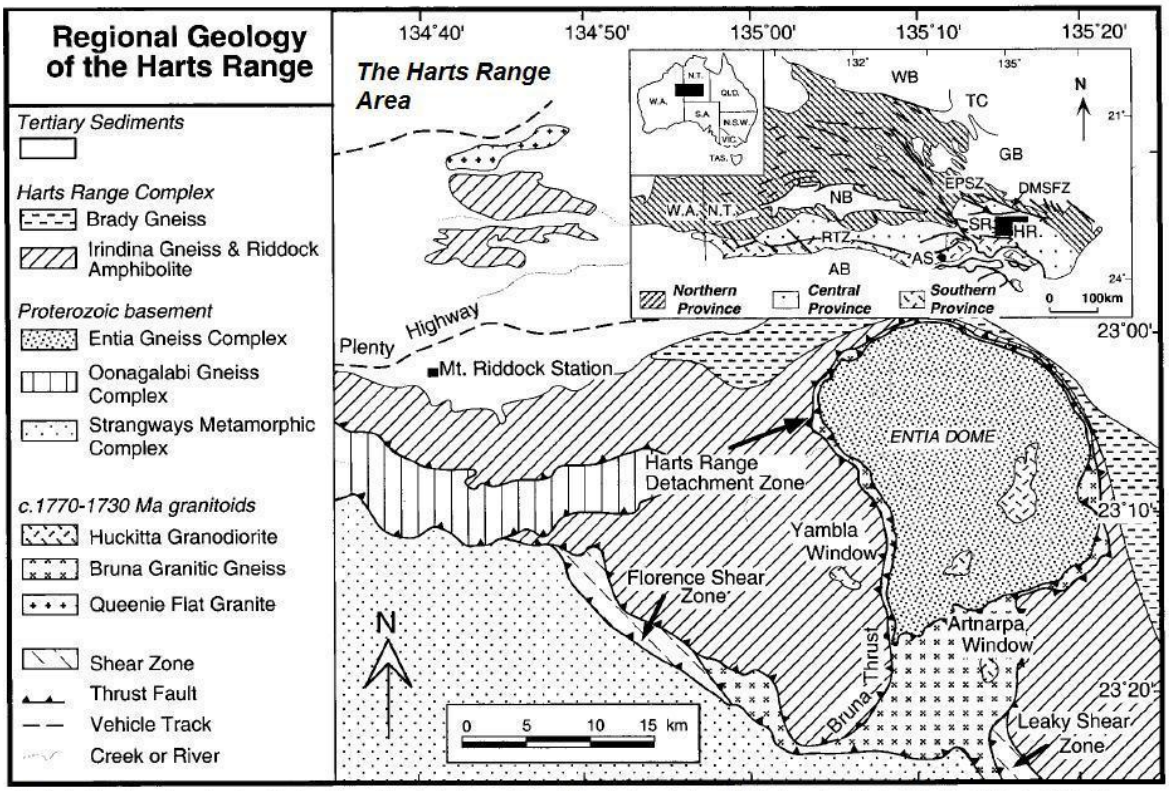

Figure 1: Location and regional geology of the Harts Range Area. Abbreviations in insert: AB – Armadeus Basin; NB – Ngalia Basin; WB – Wiso Basin; TC – Tennant Creek; GB – Georgina Basin; RTZ – Redbank Thrust Zone; EPSZ – Entire Point Shear Zone; DMFSZ – Delny-Mount Sandhill Shear Zone; HR – Harts Range; SR – Strangeways Range; AS – Alice Springs; The small black box inside the inset map shows the location of the main map within the Arunta Inlier. Modified after Miller et al. (1997) and Buick et al. (2001).

marble, calc-silicate and voluminous metabasic rocks (Riddock Amphibolite) (Buick *et al.* 2001), and the Harts Range Metaigneous Complex, which includes metabasic, meta-anorthositic and meta-ultrabasic rocks (Das *et al.* 2000). The EGC is dominated by mafic to felsic orthogneisses (Das *et al.* 2000). The HRMC and EGC are divided by a high-grade, low-angle shear zone (Harts Range Detachment Zone). The shear zone contains a sheet-like body of granitic gneiss called the Bruna Granitic Gneiss, which forms sheets of megacrystic metagranite that has been deformed heterogeneously to form augen gneiss (Das *et al.* 2000). The protoliths to the Harts Range Metamorphic Complex were deposited in an EW to SE-NW-trending rift (Buick *et al.* 2005). The rift, the Irindina sub-basin (Fig. 2), was located

between the present-day Amadeus and Georgina basins (Buick *et al.* 2005). From a recent study on detrital zircon from the Irindina Gneiss and inherited zircon from a c. 387 Ma granite with intrusive relationship into the HRMC, a range of ages from c. 1.3 Ga to c. 520 Ma (Buick *et al.* 2001, Buick *et al.* 2005) have been measured, which can give an inferred age of deposition of the sedimentary and igneous precursors at c. 520–500 Ma (Buick *et al.* 2005). The extensive mafic magmatism, which may have formed part of the continental-wide magmatic province at c. 520–500 Ma (Buick *et al.* 2005).

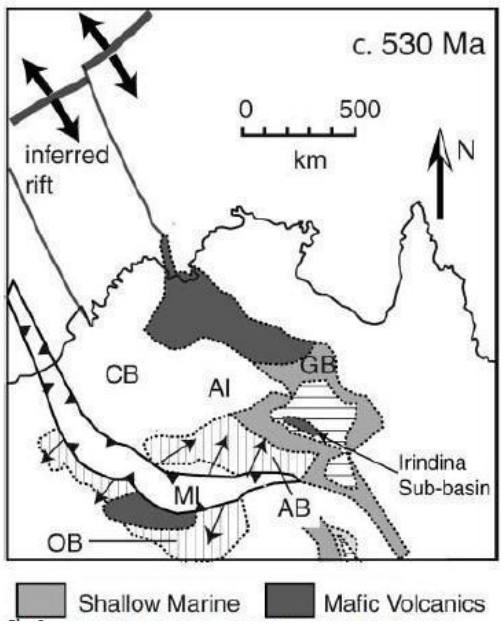

Figure 2: Location of the Irindina Sub-basin at the time of the deposition of sediments that are the protoliths to the Harts Range Metamorphic Complex. AB – Armadeus Basin; AI – Arunta Inlier; CB – Canning Basin; GB – Georgina Basin; MI – Musgrave Inlier; OB – Officer Basin. Adapted from Buick et al. (2005).

No more than 40 Ma after deposition of the Harts Range Metamorphic Complex, the Irindina sub-basin sediments and mafic volcanic rocks were metamorphosed to amphibolite and granulite grade during the 480–460 Ma Larapinta Event (Das *et al.* 2000, Buick *et al.* 2001, Buick *et al.* 2005). The structurally highest and lowest levels of the Harts Range Metamorphic Complex experienced peak metamorphic P-T conditions of 6–7 kbar and 650–700 °C and 8–10 kbar and 800–850 °C, respectively (Miller *et al.* 1997, Mawby *et al.* 1999, Hand *et al.* 1999b) . In the structurally deepest levels, decompressional cooling to 6 kbar and c. 700 °C (Miller *et al.* 1997, Mawby *et al.* 1999) was associated with the formation of recumbent, mylonitic shear fabrics that developed during NE–SW-directed tectonic movement during or after the Larapinta Event (Mawby *et al.* 1999, Hand *et al.* 1999b). The Larapinta Event was also accompanied by the intrusion of mafic to ultramafic dykes, plugs and sills, and the deposition of fine-grained sediments in an extensional setting (Mawby *et al.* 1999).

Between the Larapinta Event and the Alice Springs Orogeny, the setting may have been switched from regionally extensional to compressional, which resulted in the transport of high-grade rocks over lower-grade units along a sub-horizontal mid-crustal detachment (Mawby *et al.* 1999). This, sub-horizontal mid-crustal detachment (Harts Range Detachment Zone) contains the Bruna Granitic Gneiss. The age acquired from a three-point Sm-Nd isochron from a garnet-hornblende migmatite indicates that this movement occurred at 449 ± 10 Ma (Mawby *et al.* 1999).

The Harts Range Metamorphic Complex was then subject to the Alice Springs Orogeny (ASO) at 450–300 Ma (Hand *et al.* 1999a, Das *et al.* 2000, Buick *et al.* 2001). This resulted in metamorphism to amphibolite grade with peak P–T conditions reaching 6 kbar and 600 °C (Ballèvre *et al.* 2000). The ASO involved a long-lived, episodic intra-plate reworking. Amphibolite to granulite facies rocks of the Arunta region were exhumed and are preserved as a polyphase, predominantly south-vergent, thrust system (Buick *et al.* 2008).

The Alice Springs Orogeny marks the end of tectonic activity in the Arunta Inlier. The compressional nature of the intraplate orogeny is suggested to be the cause of exhumation of the Arunta Inlier from beneath the continuous Neoproterozoic to late Paleozoic intracratonic Centralian Superbasin (Shaw *et al.* 1991). The cooling history of the south-eastern Arunta Inlier from 400 to 300 Ma during the Alice Springs Orogeny suggests that exhumation of the Arunta Inlier probably occurred in a series of pulses, with relatively rapid exhumation first occurring at 400 Ma and again at approximately 350 and 310 Ma (Hand *et al.* 1999a).

Mithril Resources currently has 14 exploration tenements in the Harts Range. A wide variety of different mineralisation styles are represented within these tenements. These include; magmatic-hosted Ni-Cu sulphides, vein hosted gold deposits, Iron-Oxide-Copper-Gold (IOCG) deposits and Cu mineralisation of unknown genetic type (Fig. 3).

Basil, in the centre of the tenement area (Fig. 3), is one of the largest in the region. Assay results show values up to 6.3 % Cu (Fig. 3). A JORC-compliant inferred resource of 26.5 Mt

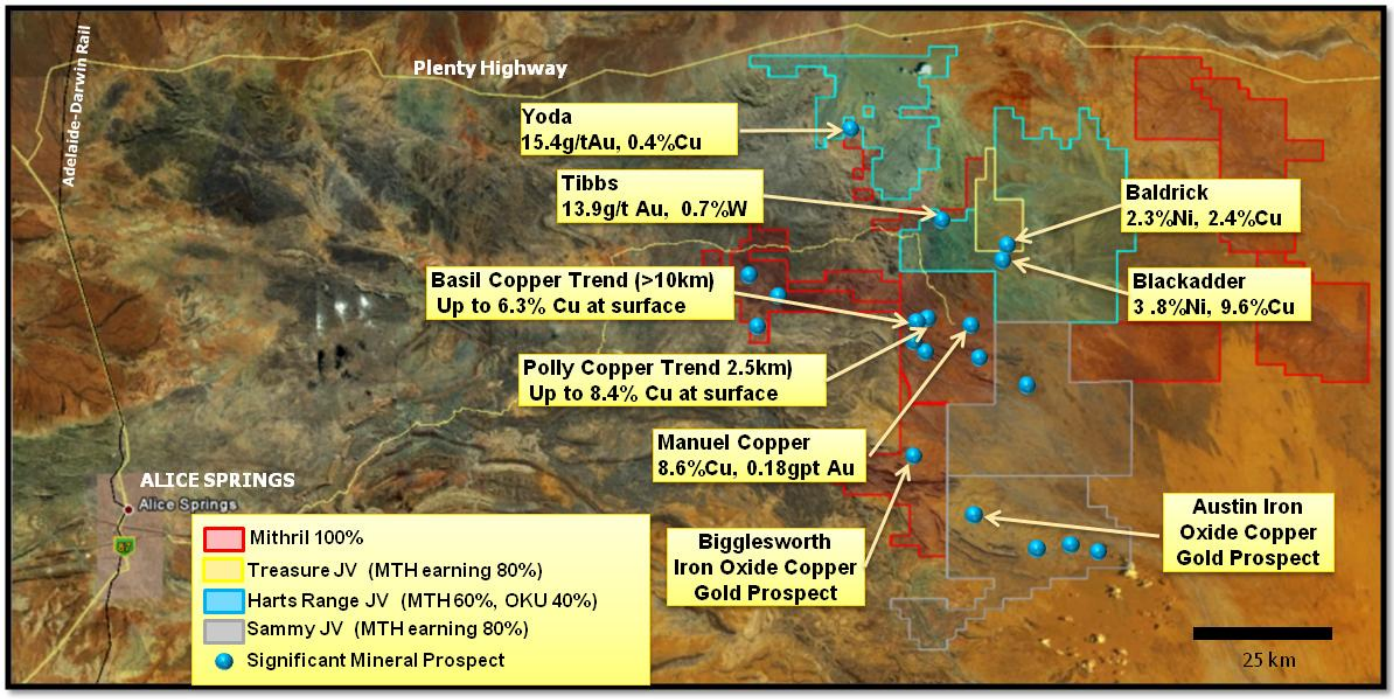

Figure 3: Location of Mithril's tenements within the Harts Range. Baldrick and Blackadder are magmatic-hosted Ni-Cu sulphide deposits. Yoda and Tibbs are vein hosted Gold deposits. Basil is the unknown Cu deposit. Adapted from Mithril Resources (2012).

@ 0.57% Cu, 0.05% Co was released in 2012 (Mithril Resources, 2012)

The Basil deposit lies within the Harts Range Metamorphic Complex; the host rock being the Riddock Amphibolite (Fig. 4). This is a Fe-rich metapelite-mafic gneiss association, with marble, calc-silicate and voluminous metabasic rocks. The Basil Copper Trend can be recorded for >10 km on the surface (Figs. 3 and 5). The 2011 drill programme of Mithril Resources was aimed at sampling 4.5 km of this strike length (Fig. 4). The Basil Fault (Fig. 6) is the only currently known structural control on the deposit. Mineralisation has been observed to be controlled by the Basil Fault. The morphology of the Basil deposit itself is certainly not uniform. An interpretation of the zones of mineralisation between drillholes LB027DD and LB035DD has been attempted based on assay results (Fig. 7). This shows one or two strongly mineralised zones, each 10-20 m in thickness, and one weaker mineralised zone dipping to the NW at ~45°.

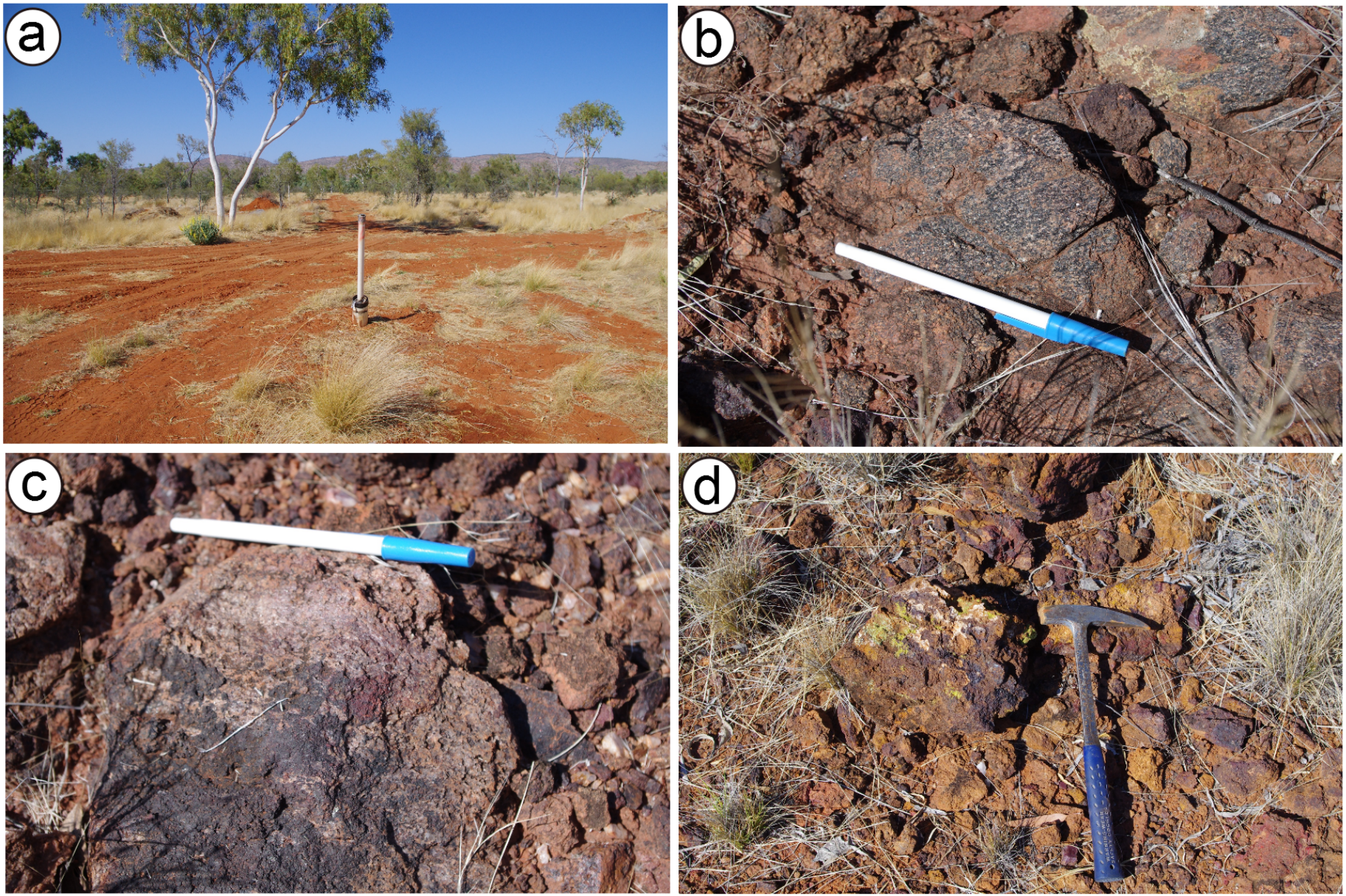

Figure 4: (a) Photograph showing LB035DD looking down strike of the drillhole. (b) Photograph showing the Riddock Amphibolite in outcrop at the relative location of drill holes LB027DD and LB035DD. (c) Photo of outcrop of Riddock Amphibolite with coarse-grained garnet. (d) Photograph showing the surface expression of the mineralisation zone as a Gossan. This photograph was taken at Rotten Hill, where the two drillholes of interest are both located.

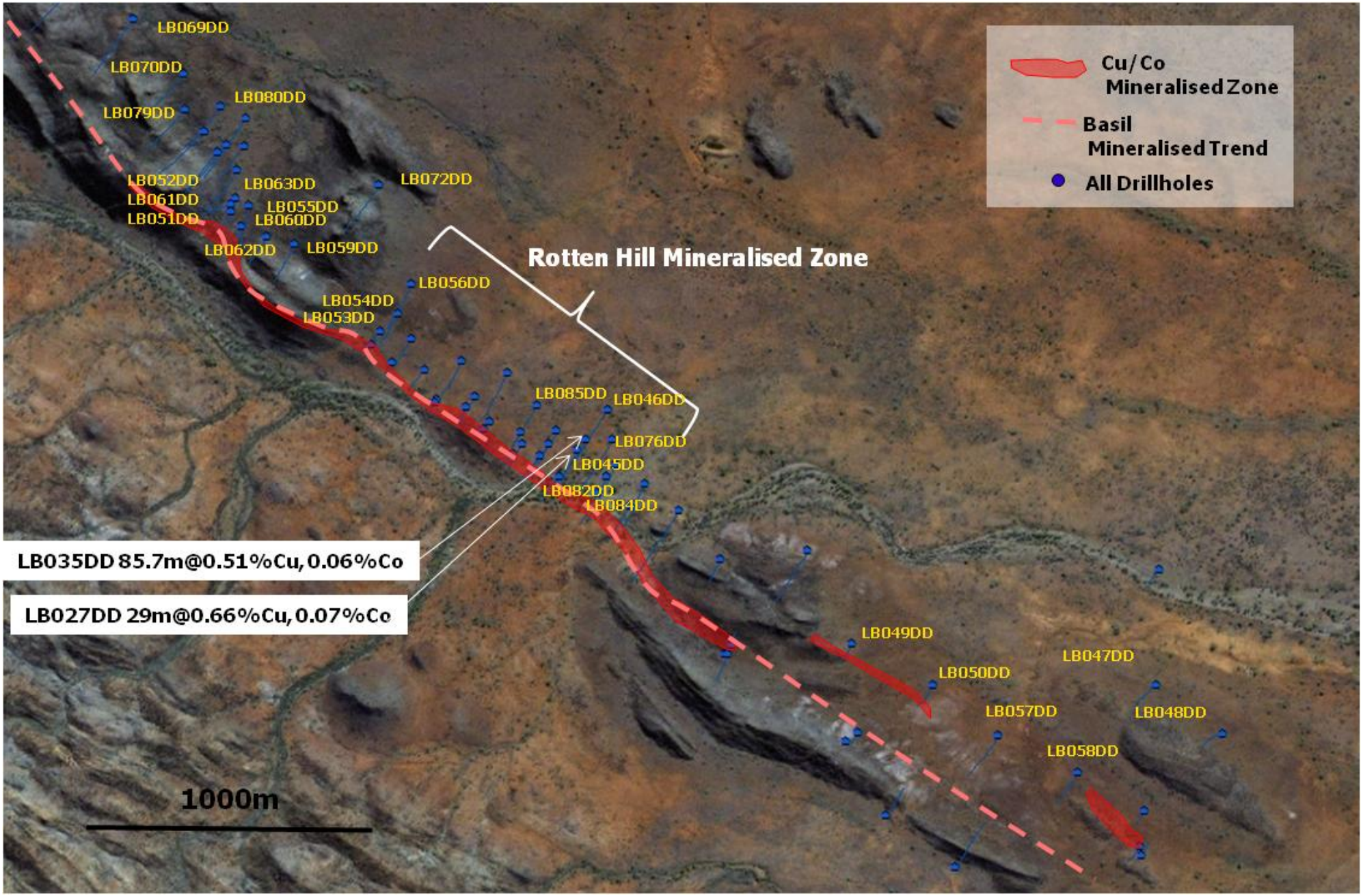

Figure 5: Location of the 4.5 km drilling program executed by Mithril Resources. LB027DD and LB035DD are the two drillholes that all samples were selected from. These drillholes are located in Rotten Hill, which was the first piece of evidence that there was mineralisation on this tenement. Adapted from Mithril Resources (2012).

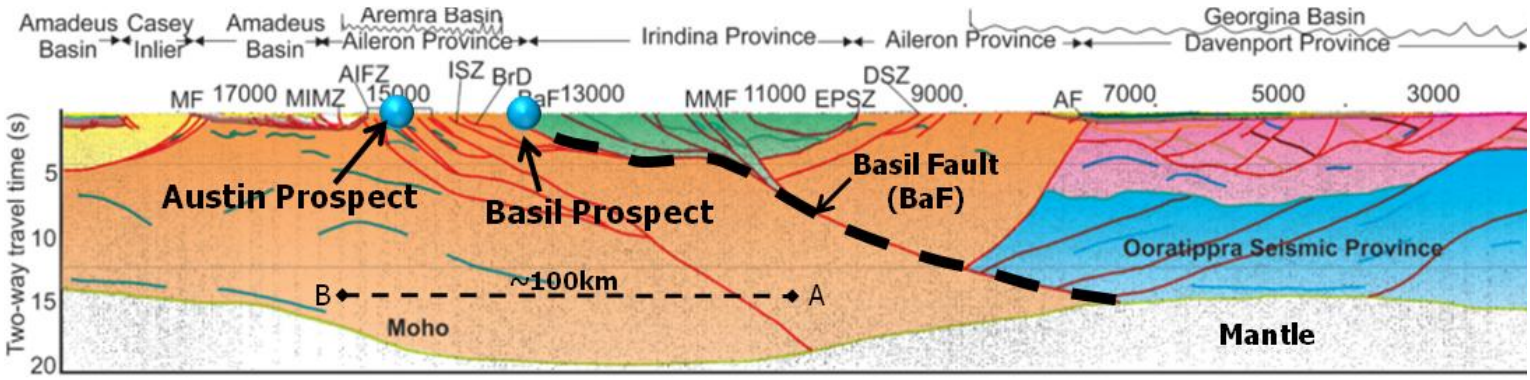

Figure 6: Regional migrated seismic section from Georgina-Arunta seismic line 09GA-GA1 showing interpretation and key provinces. The Basil Prospect is in direct contact with the Basil Fault. Adapted from (Korsch *et al.* 2011).

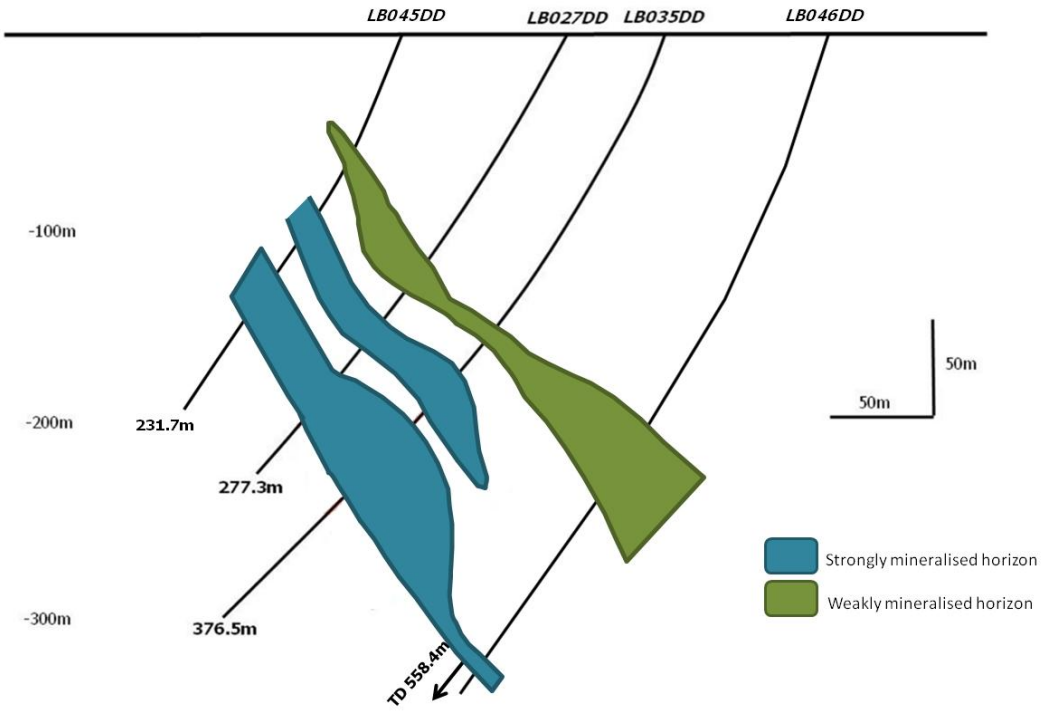

Figure 7: Diagrammatic interpretation of the zones of mineralisation that are present in drillholes LB027DD and LB035DD. The next set of drillholes on the outer edges of the zone of mineralisation do not pick up any mineralisation horizons. Cross-section adapted from Mithril Resources (2012).

Unpublished reports on the Basil deposit have made some suggestions regarding possible ore-forming process and genetic model. Pontifex and Associates, Adelaide-based petrography specialists, viewed various thin section samples, including the garnet-rich amphibolite described below. From these petrographic samples, the mineralisation in the Basil deposit was interpreted as a hydrothermal skarn. A second confidential report suggested the possibility that the mineralisation represented a Ni-Cu sulphide deposit originating via magmatic processes.

METHODS

To understand the mineralogy and ore-forming processes involved in the formation of the Basil Cu-Co deposit, 37 samples were collected from two diamond drill holes (LB027DD and LB035DD). Prior to sampling, both holes were extensively logged to define rock units and as a result, areas of interest. From these 37 samples, 15 were made into 1" polished blocks to study the ore mineralogy and the other 22 were made into 1" x 3" thin sections to study the host rock mineralogy. Appendices A and B are a detailed list of all samples selected, and an outline of sampling/analytical strategy, respectively.

All samples were studied under the Nikon Petrographic microscope at Adelaide Microscopy, to note the mineralogy, textures and any other features of interest.

Scanning Electron Microscopy (SEM) work was carried out using the Phillips XL30 instrument (Adelaide Microscopy) focusing on sulphides and any minerals that could not be identified optically. It was operated at 20eV accelerating voltage, a spot size of 4 and the samples were viewed under the back-scatter electron (BSE) detector.

Laser-Ablation Inductively Coupled Plasma Mass Spectroscopy (LA-ICP-MS) spot analysis of pyrite and pyrrhotite was undertaken using the Agilent HP-7500 Quadrupole ICPM instrument at Adelaide Microscopy. The instrument is equipped with a New Wave UP-213 Nd:YAG laser ablation system equipped with MeoLaser 213 software. Data reduction was performed using Glitter software (GEMOC 2005). Measurements were recorded for isotopes Ag, Au, Bi, Co, Cr, Cu, Hg, Mn, Mo, Ni, Pb, Sb, Se, Te, Tl, V and Zn. Electron Microprobe Analysis of pyrrhotite, sphalerite, and garnet was undertaken using a CAMECA SX-51 instrument with wavelength dispersive spectrometers (Adelaide Microscopy). Work focussed on determining the compositional variation in pyrrhotite and sphalerite. Garnet transects were undertaken to determine the presence or absence of metamorphic growth rims or other zonation patterns within single grains.

Whole rock geochemistry was performed by Genalysis' Adelaide Laboratory. Analysis was undertaken on each rock unit present, selecting one representative sample from each drill hole. Seventy-one elements were analysed for using various methods (Appendix B).

LA-ICP-MS element mapping was undertaken on representative garnet grains from the garnet-rich sample (sample KS-37). Mapping was conducted using a Resonetics M-50-LR 193-nm Excimer laser microprobe coupled to an Agilent 7700cx Quadrupole ICP-MS housed at Adelaide Microscopy. Images were performed by ablating sets of parallel line rasters in a grid across the sample. A beam size of 10 μm and a scan speed of 16 μm/s was chosen for the first garnet grain and a beam size of 14 μm and a scan speed of 20 μm/s was chosen for the second garnet grain. This resulted in the desired sensitivity of the elements of interest and adequate spatial resolution. Images were compiled and processed using the program Iolite developed by the Melbourne Isotope Group at Melbourne University (Woodhead *et al.* 2007). Iolite is an open source software package for processing ICP-MS data, and is an add-in for the data analysis program Igor developed by WaveMetrics.

RESULTS

Lithology

There are 4 main lithological units (Table 1): amphibolite (Fig. 8a-b); garnet-rich amphibolite (Fig. 8c-d); epidote-amphibole schist (Fig. 8e-f); and weakly-foliated amphibolite (Fig. 8g). Each of these units varies in terms of the abundance and diversity of minerals present (Fig. 9 and 10). Chlorite/carbonate alteration (Fig. 8h) is restricted to the amphibolite and weakly-foliated amphibolite lithologies.

In the zone of mineralisation (intersected in both LB027DD (Fig. 9) and LB035DD (Fig. 10) and Appendix C), the gangue mineral assemblage includes magnesiohornblende and andesine (confirmed by SEM-EDAX analysis), quartz, garnet, hematite, ilmenite, and magnetite.

Sulphides may comprise as much as 60% of the rock volume. Pyrite and pyrrhotite are approximately equal in abundance, both approaching 50% of the bulk rock but varying in their relative abundance from sample to sample. Some individual samples are notably pyrite- or pyrrhotite-rich. There are also very distinct barriers between pyrite- and pyrrhotite-rich zones (Fig. 11a). This was observed in a transition from a pyrite-rich to pyrrhotite-rich zone with the main mineralisation in drillhole LB035DD. Chalcopyrite comprises up to 3% of the total sulphides. The sulphides tend to be disseminated throughout the rock, locally giving it a semi-massive appearance (Fig. 11b). There are no obvious textures present in the zone of mineralisation. The late veining, which hosts sulphides and cross-cuts the dominant foliation defined by metamorphic minerals, suggests that mineralisation also occurred during the late stages of metamorphism (Fig. 11c).

Cross-cutting features throughout the sequence include quartz "sweats", which are described as thin (0.5-1 cm) veinlets of quartz that either runs parallel to the direction of foliation or cross-cut the foliation.

Whole rock geochemistry

Whole rock geochemical analysis (Appendix B) was performed on two samples of each rock unit in an attempt to define the presence or absence of hydrothermal alteration. Although complicated by the lack of unaltered rocks in the available sample suite, comparison of major oxides and trace elements in the different units, including fresh amphibolites most distant to mineralization, indicated no substantial differences among them, suggesting there is no obvious alteration halo present. Notably, there is no indication of any marked potassic, calcic or sodic alteration in the rocks enclosing the ores, which has been observed in the assay work done by Mithril. Potassic, sodic and calcic are the three most common types of hydrothermal alteration (Robb 2005).

Table 1: Lithological unit description of units present within drill holes LB027DD and LB035DD.

Lithological Unit	Minerals and Abundance	Grain Size	Comments
Amphibolite	**Primary assemblage** Magnesiohornblende (40%) Andesine (25%) Quartz (10%) **Accessory minerals** Titanite (10%) Ilmenite (10%) Zircon (3%) Apatite (2%) Rutile (1%)	 Coarse grained Medium grained Medium grained Fine grained Fine grained Very fine grained Very fine grained Very fine grained	(Fig. 8a-b) Magnesiohornblende can vary from brown to green in colour, suggesting varying Mg-enrichment. Titanite is pervasive, found as inclusions in all minerals. Minor sulphides are present, usually in the form of pyrite or pyrrhotite. Minor garnet has been found in some samples. Zircons are observed as inclusions in magnesiohornblende and titanite.
Garnet-rich Amphibolite	**Primary assemblage** Garnet (60%) Magnesiohornblende (20%) Quartz (7%) **Accessory minerals** Ilmenite (10%) Apatite (2%) Chlorite (1%)	 Very coarse grained Coarse grained Fine grained Medium grained Very fine grained Fine grained	(Fig, 8c-d) Magnesiohornblende is green. Quartz, magnesiohornblende and sulphides are present as inclusions in garnet. No evidence of optical zonation or orientation of grains. Sulphides often enclose garnets in a matrix.
Epidote Amphibole Schist	**Primary assemblage** Magnesiohornblende (25%) Epidote (25%) Andesine (15%) Orthopyroxene (15%) Quartz (10%) **Accessory minerals** Titanite (10%) Scapolite (2%) Dolomitic Carbonate (2%) Calcite (1%)	 Coarse grained Medium grained Medium grained Medium grained Fine grained Fine grained Fine grained Medium grained Medium grained	(Fig. 8e-f) Epidote and magnesiohornblende are in equal abundance. Magnesiohornblende is brown-green. Titanite is pervasive and present as inclusions in all minerals. Zircons are present in high abundance.
Weakly Foliated Amphibolite	**Primary assemblage** Magnesiohornblende (40%) Clinopyroxene (20%) Andesine (20%) Quartz (10%) **Accessory minerals** Titanite (10%)	 Coarse grained Medium grained Medium grained Fine grained Fine grained	(Fig. 8g)Very weak almost non-existent foliation. Magnesiohornblende is brown. Titanite is abundant and found as inclusions in all minerals.
Carbonate/Chlorite Alteration	**Primary assemblage** Chlorite (60%) Calcite (30%) Magnetite (10%)	Coarse grained Medium grained Fine grained	(Fig. 8h) These minerals are interchangeable throughout the two drillholes. Bother calcite and chlorite alteration can occur or just one type. Magnetite is fine grained and abundant.

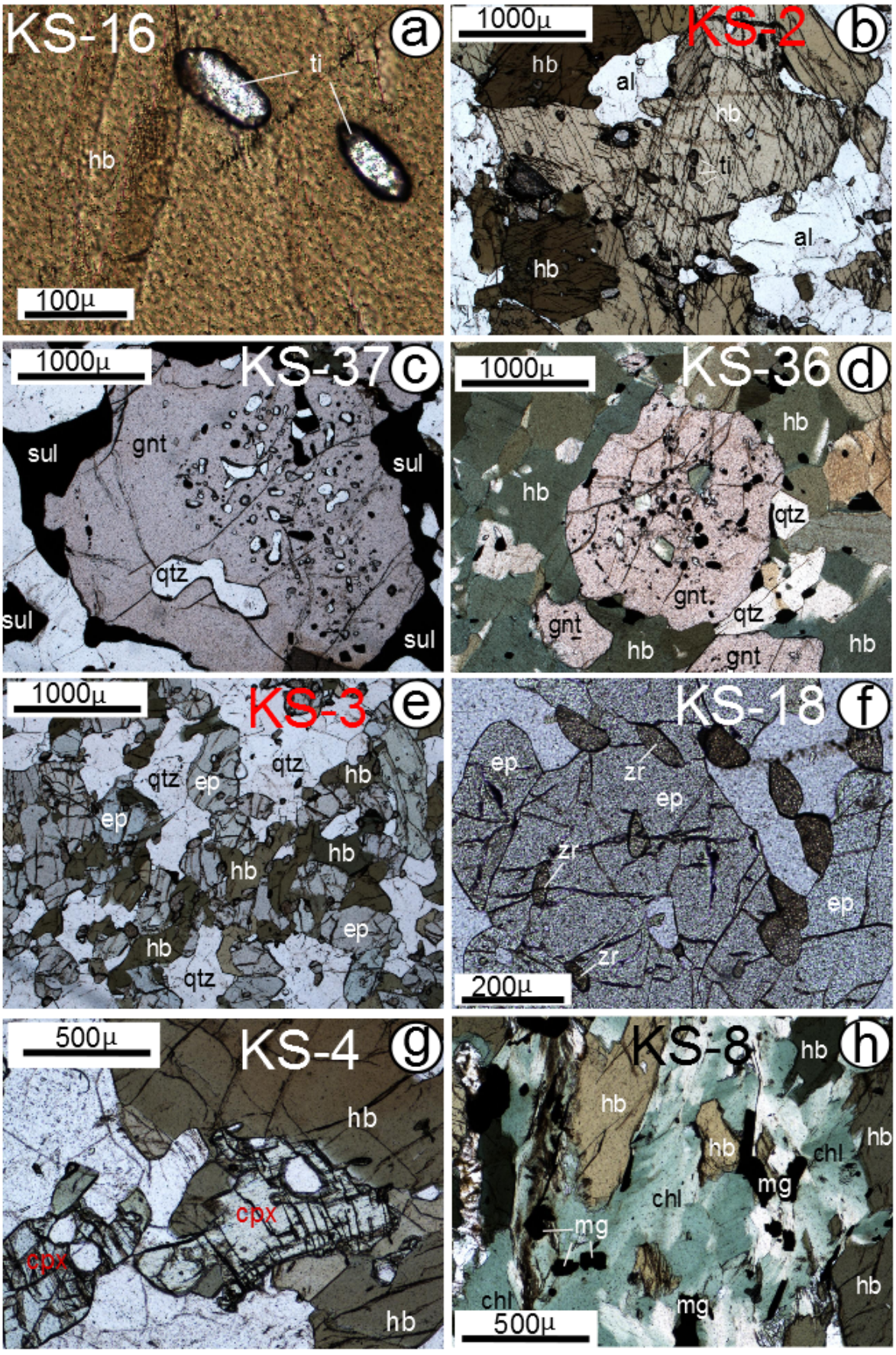

Figure 8: Transmitted light microphotographs illustrating important silicate mineral textures. (a) The occurrence of the mineral leucoxene. (b) Brown and green hornblende. (c) Sulphides forming a matrix around garnet grain. (d) Inclusions of sulphide, hornblende and quartz in garnet grain. (e) Coarse grained mineral assemblage of epidote, hornblende and quartz. (f) Occurrence of zircon. (g) Occurrence of kyanite. (h) Chlorite alteration accompanied with the presence of magnetite. Abbreviations: al=albite, chl=chlorite, cpx=clinopyroxene, ep=epidote, gnt=garnet, hb=hornblende, mg=magnetite, qtz=quartz, sul=sulphide, ti=titanate, zr=zircon.

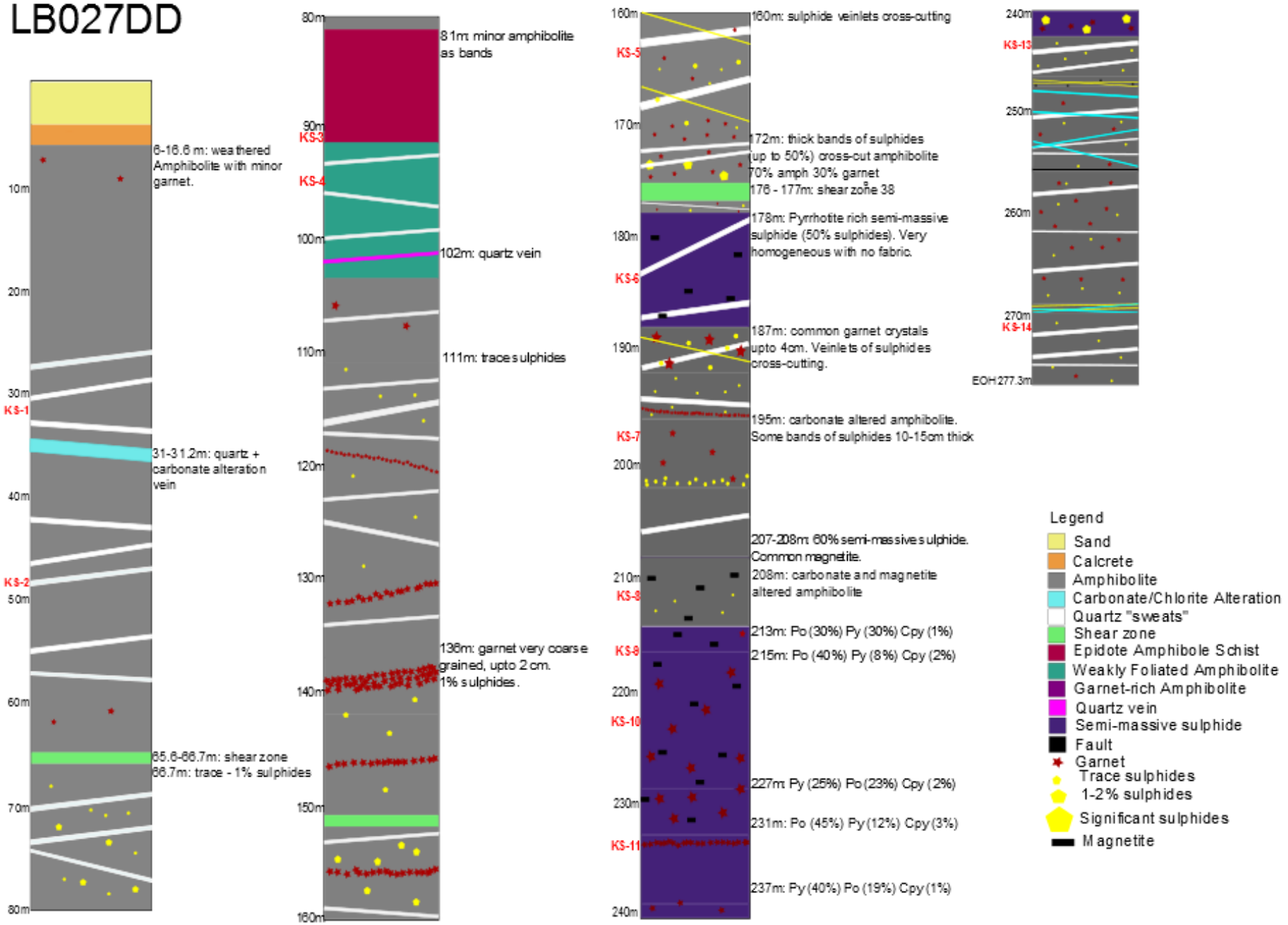

Figure 9: Descriptive log of drillhole LB027DD with information about the lithologies, the presence and abundance of sulphides (yellow pentagons), and structural features. Red labels on left hand side of stratigraphic column indicate where samples KS-1 to KS-14 was selected. Abbreviations: cpy – chalcopyrite; po – pyrrhotite; py – pyrite. The appearance of symbols for sulphides or minerals indicate their presence in the core.

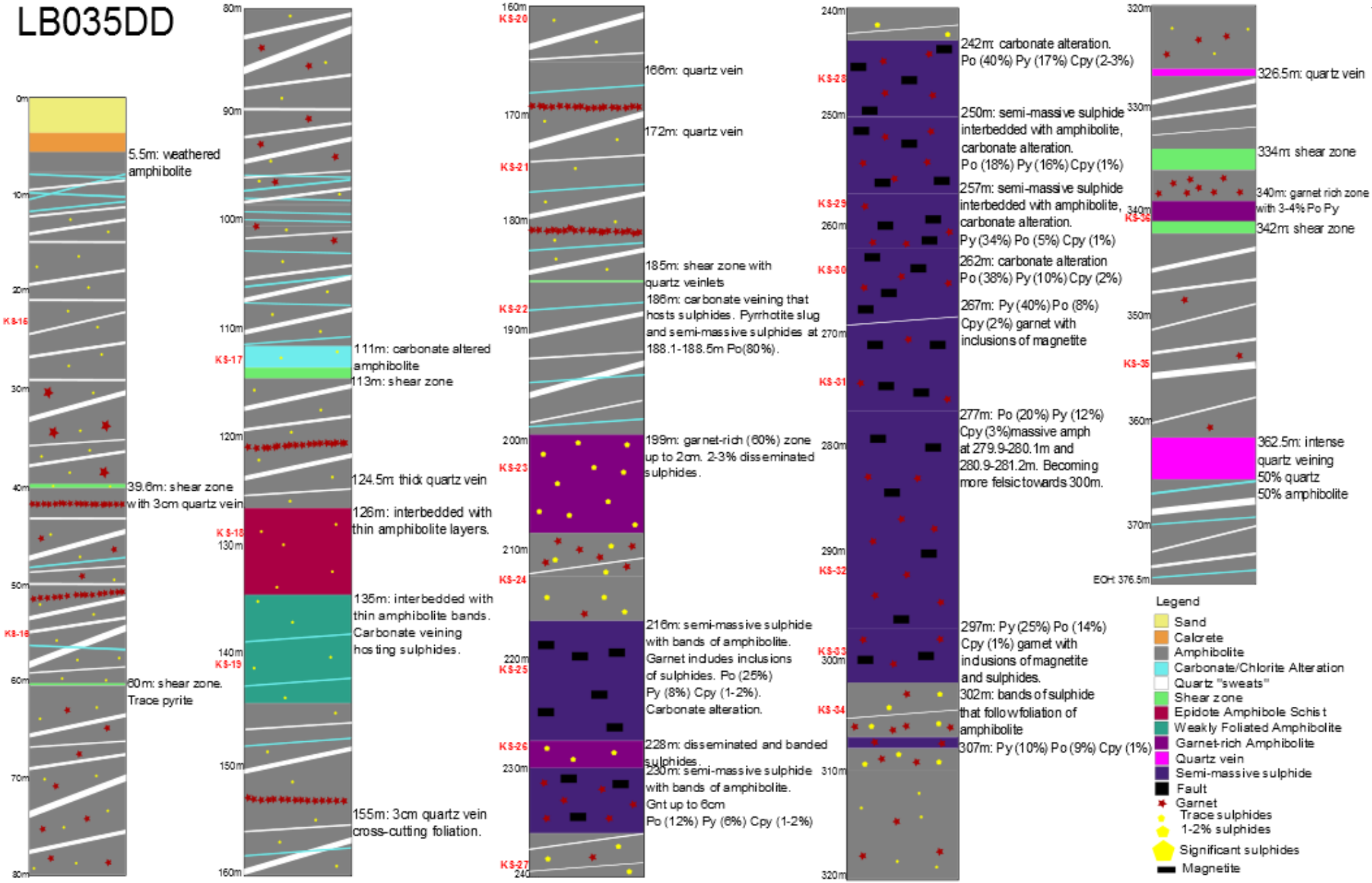

igure 10: Descriptive drillcore log of LB035DD with information about lithologies, the presence and abundance of sulphides (yellow pentagons), and structural features (i.e. veining and teration). Red labels on left hand side of stratigraphic column indicate where samples KS-14 to KS-36 was selected. Abbreviations: cpy – chalcopyrite; po – pyrrhotite; py – pyrite. The ppearance of symbols for sulphides or minerals indicate their presence in the core.

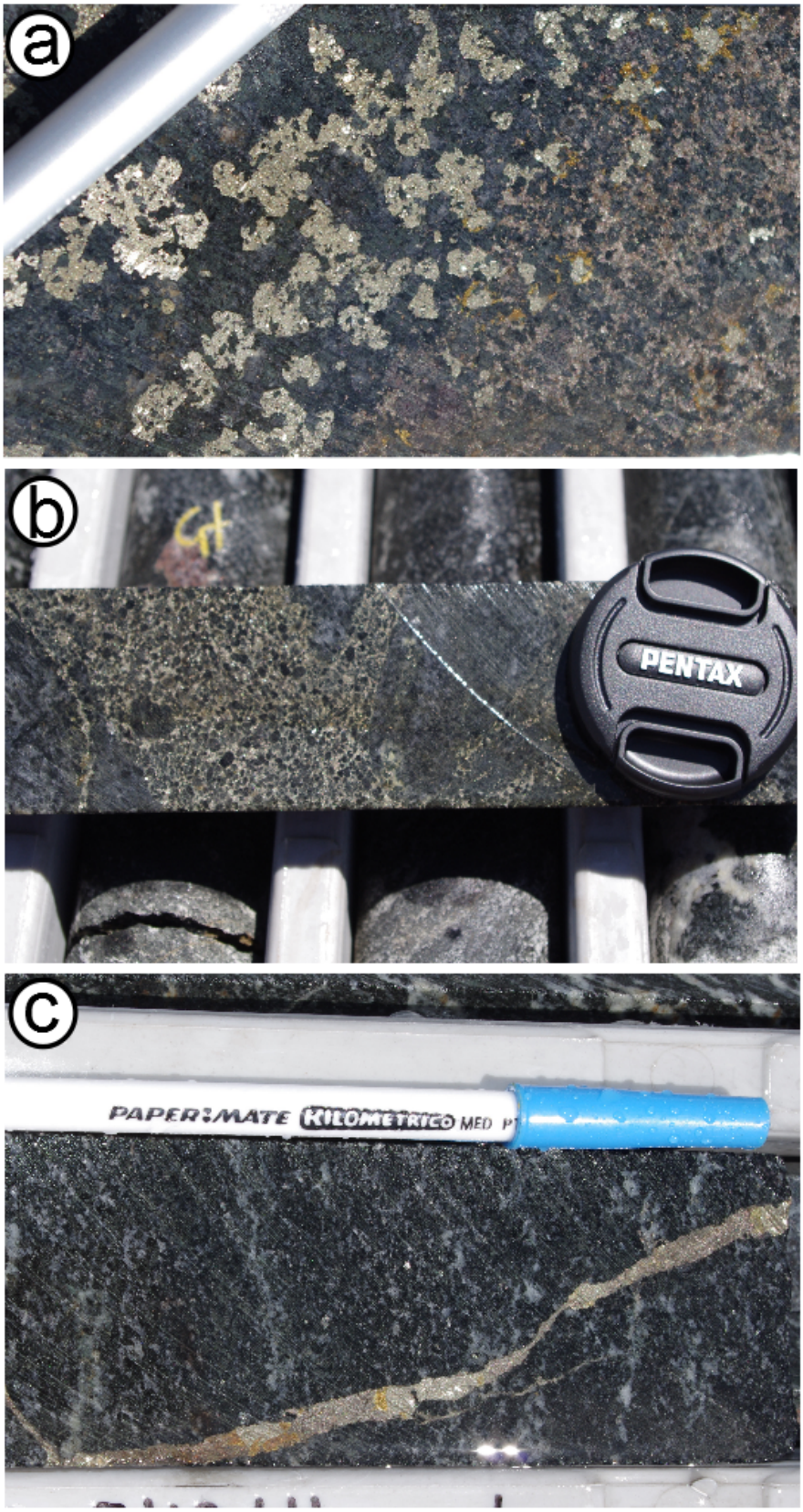

Figure 11: (a) Distinct boundary between coarse-grained pyrite (left) and fine-grained pyrrhotite (right). (b) Disseminated texture of sulphides. The amphibolite (dark grey) has had the sulphides invade any available space, "squeezing" into the host rock. (c) Late carbonate-sulphide vein cross-cutting the foliation of the amphibolite.

Table 2 summarises the geochemical differences between the host rock and the mineralization zone. Based on a calculation that corrects for the high volume of sulphide in the ore (Appendix B), the non-sulphide part of the mineralization zone would seem to be characterised by a marked decrease in mobile elements such as Na, K and Sr, but only negligible change in characteristically immobile elements such as Zr and Ti. Sample index and pictures of representative samples in Appendix B.

Table 2: Whole rock geochemistry of each rock unit recorded in the two sampled drillholes. Analysis included one representative sample for each rock unit and was selected from both drill holes. An average value was calculated for each rock unit from the two samples that were selected. Note that characteristically mobile elements such as Na, K and Sr are significantly lower in the zone of mineralisation whereas there is only negligible change in characteristically immobile elements such as Zr and Ti. Abbreviations: SMS=semi-massive suphide; av=average

ELEMENTS	Ag	Al_2O_3	As	Ba	Bi	CaO	Cd	Ce
UNITS	ppm	%	ppm	ppm	ppm	%	ppm	ppm
DETECTION	0.05	0.02	0.5	0.5	0.01	0.02	0.02	0.5
Amphibolite av.	0.06	14.51	11.48	41.33	0.03	10.62	0.08	18.88
Calc-silicate av.	0.00	13.93	10.15	100.50	0.00	14.98	0.01	14.35
Gneiss av.	0.00	15.91	11.00	42.50	0.05	11.45	0.10	12.80
Amphibolite + garnet av.	0.04	14.21	13.95	60.80	0.12	10.46	0.23	17.50
Garnet rich zone av.	0.08	14.49	7.85	13.95	0.07	3.91	0.62	4.75
Po-rich SMS av.	**1.99**	**12.15**	**11.80**	**33.06**	**1.44**	**7.76**	**3.18**	**14.11**
Equal Po-Py SMS av.	**1.23**	**8.28**	**16.71**	**286.80**	**2.36**	**5.64**	**2.60**	**8.53**
Py-rich SMS av.	**1.62**	**5.37**	**21.88**	**53.10**	**2.96**	**5.31**	**4.38**	**7.90**
ELEMENTS	Co	Cr	Cs	Cu	Dy	Er	Eu	Fe_2O_3
UNITS	ppm	ppm	ppm	ppm	ppm	ppm	ppm	%
DETECTION	0.1	20	0.05	1	0.05	0.05	0.05	0.02
Amphibolite av.	51.50	189.50	0.04	59.00	6.86	4.23	1.67	11.98
Calc-silicate av.	20.25	246.00	0.09	10.00	6.45	4.00	1.33	6.23
Gneiss av.	34.80	196.50	0.08	52.00	3.94	2.37	0.96	6.20
Amphibolite + garnet av.	49.45	194.50	0.08	146.50	6.73	4.02	1.64	12.86
Garnet rich zone av.	77.30	182.00	0.18	482.00	6.66	4.41	1.20	27.66
Po-rich SMS av.	**547.60**	**176.97**	**0.19**	**5642.50**	**5.82**	**3.79**	**1.18**	**42.73**
Equal Po-Py SMS av.	**929.50**	**97.16**	**0.58**	**4203.00**	**2.96**	**1.89**	**0.67**	**44.84**
Py-rich SMS av.	**1464.90**	**61.40**	**0.12**	**1656.50**	**2.54**	**1.59**	**0.63**	**45.12**
ELEMENTS	Ga	Gd	Ge	Hf	Ho	In	K_2O	La
UNITS	ppm	ppm	ppm	ppm	ppm	ppm	%	ppm
DETECTION	0.1	0.05	0.05	0.1	0.02	0.005	0.02	0.2
Amphibolite av.	20.33	6.16	0.68	3.55	1.38	0.10	0.22	7.30
Calc-silicate av.	17.55	5.57	0.96	2.95	1.31	0.06	0.17	5.30
Gneiss av.	16.20	3.44	0.88	2.05	0.80	0.04	0.19	4.65
Amphibolite + garnet av.	19.30	6.05	0.74	3.40	1.36	0.09	0.27	6.30
Garnet rich zone av.	14.45	5.16	0.23	3.00	1.41	0.12	0.05	1.65
Po-rich SMS av.	**19.61**	**4.82**	**0.88**	**3.19**	**1.23**	**0.33**	**0.11**	**6.78**
Equal Po-Py SMS av.	**17.44**	**2.55**	**0.71**	**1.91**	**0.60**	**0.43**	**0.10**	**4.09**
Py-rich SMS av.	**15.22**	**2.19**	**0.74**	**1.16**	**0.52**	**0.24**	**0.05**	**3.72**
ELEMENTS	Li	Lu	MgO	MnO	Mo	Na_2O	Nb	Nd
UNITS	ppm	ppm	%	%	ppm	%	ppm	ppm
DETECTION	0.1	0.02	0.02	0.02	0.1	0.02	0.05	0.1
Amphibolite av.	4.33	0.59	6.57	0.16	0.58	3.45	2.54	14.48
Calc-silicate av.	6.45	0.54	6.73	0.10	0.15	3.40	1.37	12.10
Gneiss av.	5.35	0.33	6.41	0.10	0.40	3.84	2.14	9.25
Amphibolite + garnet av.	4.25	0.56	6.41	0.24	0.60	3.10	2.71	13.95
Garnet rich zone av.	8.55	0.67	6.99	0.35	1.25	0.58	1.40	5.35
Po-rich SMS av.	**6.61**	**0.56**	**7.11**	**0.40**	**7.50**	**1.20**	**2.57**	**10.20**
Equal Po-Py SMS av.	**6.51**	**0.27**	**4.69**	**0.21**	**11.30**	**1.28**	**1.78**	**6.08**

Py-rich SMS av.	**5.72**	**0.19**	**2.86**	**0.25**	**21.90**	**0.60**	**0.93**	**5.50**
ELEMENTS	Ni	P_2O_5	Pb	Pr	Rb	Re	S	Sb
UNITS	ppm	%	ppm	ppm	ppm	ppm	ppm	ppm
DETECTION	1	0.03	5	0.05	0.1	0.002	50	0.05
Amphibolite av.	47.25	0.18	1.50	2.85	3.40	0.00	1943.50	0.08
Calc-silicate av.	49.50	0.15	2.50	2.29	1.65	0.00	112.50	0.08
Gneiss av.	32.00	0.08	3.00	1.93	1.75	0.00	1617.00	0.03
Amphibolite + garnet av.	52.00	0.20	9.00	2.69	3.05	0.00	3957.50	0.16
Garnet rich zone av.	41.00	0.07	5.50	0.84	1.60	0.00	13700.50	0.14
Po-rich SMS av.	**86.50**	**0.10**	**13.54**	**2.00**	**3.90**	**0.04**	**152500.00**	**0.15**
Equal Po-Py SMS av.	**86.50**	**X**	**14.67**	**1.21**	**4.72**	**0.05**	**197850.00**	**0.13**
Py-rich SMS av.	**8.00**	**0.08**	**17.85**	**1.12**	**0.86**	**0.07**	**251050.00**	**0.25**
ELEMENTS	Sc	Se	SiO_2	Sm	Sr	Tb	Te	Th
UNITS	ppm	ppm	%	ppm	ppm	ppm	ppm	ppm
DETECTION	10	0.5	0.03	0.05	0.2	0.02	0.05	0.05
Amphibolite av.	42.50	0.28	49.74	4.70	261.88	0.99	0.00	1.33
Calc-silicate av.	44.00	0.00	52.18	4.14	399.95	0.93	0.04	0.65
Gneiss av.	41.50	1.75	54.32	2.79	296.65	0.59	0.04	1.32
Amphibolite + garnet av.	43.50	0.25	49.86	4.54	204.50	0.97	0.00	0.99
Garnet rich zone av.	45.00	2.30	45.03	2.93	16.75	0.89	0.04	0.12
Po-rich SMS av.	**35.88**	**14.83**	**49.23**	**3.38**	**127.22**	**0.81**	**0.65**	**0.22**
Equal Po-Py SMS av.	**21.27**	**19.49**	**45.83**	**1.86**	**135.01**	**0.41**	**0.70**	**0.12**
Py-rich SMS av.	**15.00**	**16.08**	**46.12**	**1.68**	**124.04**	**0.35**	**0.23**	**0.10**
ELEMENTS	TiO_2	Tm	V	Y	Yb	Zn	Zr	
UNITS	%	ppm	ppm	ppm	ppm	ppm	ppm	
DETECTION	0.02	0.05	10	0.5	0.05	1	1	
Amphibolite av.	1.85	0.61	308.00	40.03	3.77	92.25	131.00	
Calc-silicate av.	1.62	0.58	295.00	38.15	3.61	22.00	108.00	
Gneiss av.	0.91	0.34	201.50	22.75	2.17	36.00	77.50	
Amphibolite + garnet av.	1.87	0.58	327.50	38.55	3.60	157.50	122.00	
Garnet rich zone av.	1.52	0.65	272.00	41.65	4.15	267.00	112.00	
Po-rich SMS av.	**1.69**	**0.56**	**272.66**	**35.41**	**3.50**	**587.00**	**122.76**	
Equal Po-Py SMS av.	**0.97**	**0.28**	**175.24**	**18.38**	**1.85**	**605.00**	**75.35**	
Py-rich SMS av.	**0.69**	**0.24**	**131.15**	**15.46**	**1.41**	**799.50**	**47.05**	

Mineralogy and Petrography

The amphibolite observed at Basil contains hornblende, andesine (An_{40-50}) and quartz as the dominant minerals. Hornblende is brown or green in colour, suggesting variation in Mg/(Mg+Fe) ratio; SEM-EDAX analysis showed compositions corresponding to magnesiohornblende is dominant (Mg/(Mg+Fe) = 0.6-0.8). Biotite has been observed in some samples but it is generally rare. Titanite is abundant, fine-grained, and occurs as inclusions in all minerals but is particularly concentrated within the magnesiohornblende (Fig. 12a, b). Fine-grained zircon is an abundant accessory (Fig. 12b, c).

The epidote-amphibole schist contains epidote, magnesiohornblende, quartz, andesine,

titanite, with minor scapolite, orthopyroxene, calcite and dolomitic carbonate. Scapolite is a very rare mineral in this unit and only one small grain, in one of the two samples of epidote-amphibole schist (KS-3), was observed. In hand sample, this unit displays a very distinct fabric or layering defined by epidote and magnesiohornblende, however viewed macroscopically, the fabric/layering is not discernible. In terms of mineral abundance, of the two samples that were selected, one (KS-3) is rich (25 vol.%) in epidote, and the other (KS-18) rich (15 vol.%) in orthopyroxene.

The weakly-foliated amphibolite is similar in appearance to the amphibolite, minus the strong foliation. Main minerals include magnesiohornblende, clinopyroxene, andesine, titanite and quartz. Clinopyroxene is observed in both samples selected. Titanite is observed as single fine grains and medium grained 'clumps' within the samples.

The garnet-rich amphibolite consists of up to 80% garnet, plus lesser magnesiohornblende, sulphides, quartz as inclusions in garnet and small (~1%) amounts of chlorite. The garnet grains are coarse-grained, ranging from 2-3 mm to 5 cm in size. They preserve inclusions of quartz, magnesiohornblende and sulphides. Apatite is a minor accessory phase (Fig. 12d). There is no evidence to suggest optical zonation or any reactions between the garnets and any other minerals.

Chlorite and carbonate alteration has been observed in the amphibolite and weakly-foliated amphibolite. Chlorite (Mg-rich clinochlore; EDAX analysis) has been observed to grow in radial patterns on magnesiohornblende (Fig. 8h).

Pyrite occurs mostly as euhedral grains, especially in the pyrrhotite-rich samples (Fig. 13 and Appendix D); these grains are rimmed by pyrrhotite and chalcopyrite. Chalcopyrite and pyrrhotite are often seen intergrown with one another (Fig. 13a). This may suggest equilibrium crystallisation from an initial *intermediate solid solution* phase in the system Cu-Fe-S (Cabri 1973).

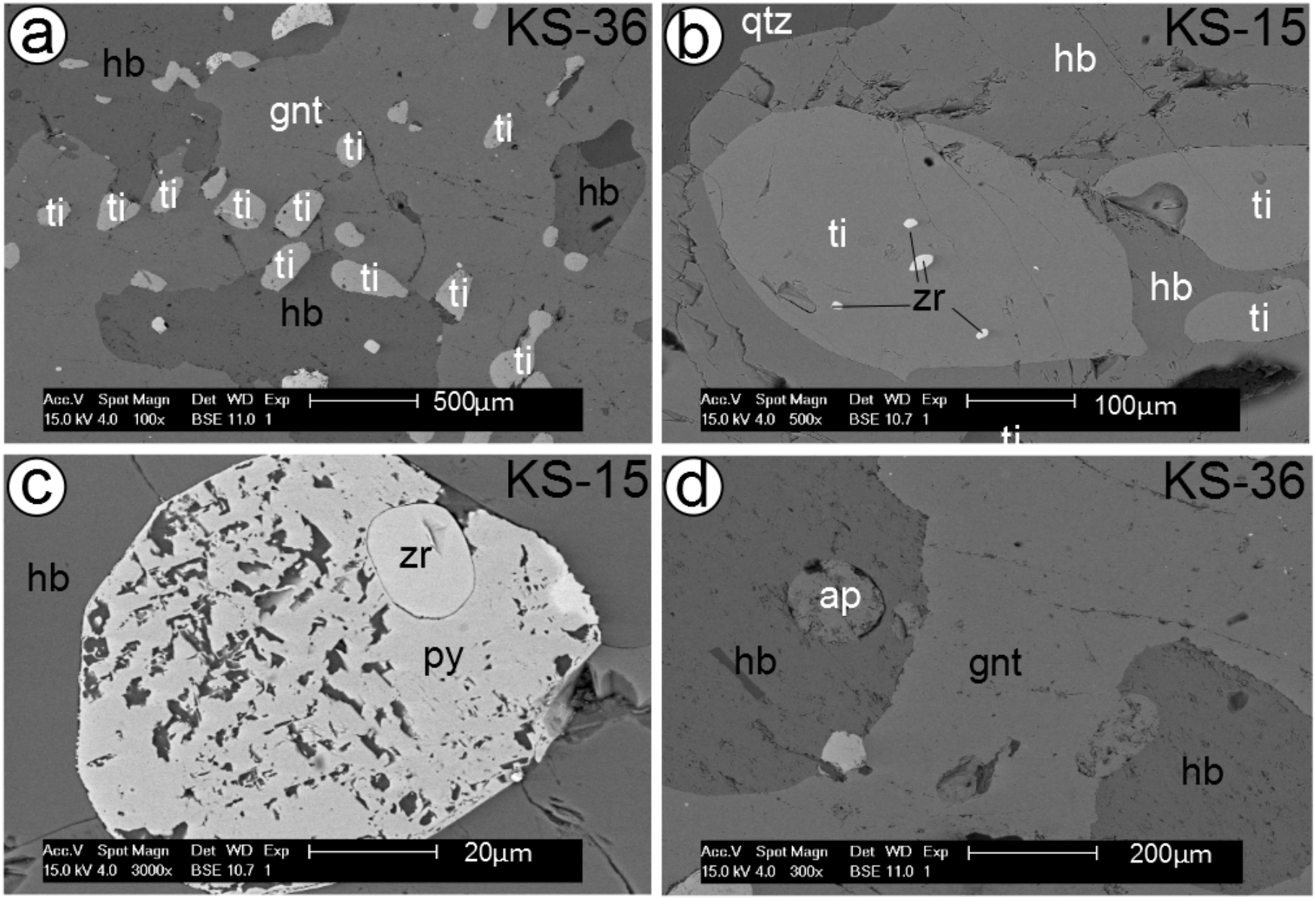

Figure 12: Back-scatter electron images illustrating relevant relationships between minerals. (a) Abundant inclusions of titanite within garnet and amphibole. (b) Inclusions of zircon within titanite. (c) Inclusion of zircon within pyrite. (d) occurrence of apatite grains as inclusions within hornblende, which is included within garnet. Abbreviations: ap=apatite, hb=hornblende, gnt=garnet, py=pyrite, qtz=quartz, ti=titanate, zr = zircon.

Chalcopyrite is usually only found in association with pyrite or as small "blobs" elsewhere in the zone of mineralisation. There also appears to be a second generation of pyrite (Fig. 13b) which is in very low abundance (<0.5 vol.%) throughout the samples. Secondary pyrite appears as a rim around other minerals, including magnetite, and is very fine-grained with respect to the minerals occurring around it. It is distinguishable from the earlier generation of pyrite due to: (i) its lack of euhedral morphology; (ii) it does not occur as "blobs" in pyrrhotite-rich samples; and (iii) it does not display a massive, matrix-supporting texture in pyrite-rich samples.

In more sulphide rich, semi-massive samples, the gangue minerals appear to be "suspended" in the sulphide matrix (Fig. 13c). Exsolution of ilmenite within hematite is also observed within the zone of mineralisation (Fig. 13d). Opaque inclusions in garnet were determined to be pyrrhotite, pyrite, hematite, ilmenite and quartz (Fig. 13e). This indicated that sulphides were present during garnet growth. Scanning electron microscopy of ore zone samples reveals the presence of minor amounts of baryte (Fig. 13f), molybdenite (Fig. 13g) and sphalerite (Fig. 13h).

Laser-Ablation Inductively-Coupled Plasma Mass Spectroscopy (LA-ICP-MS)

LA-ICP-MS trace element spot analysis of pyrite and pyrrhotite in four representative ore samples was undertaken to identify which trace elements were present in these minerals and, if so, could they provide additional petrogenetic information. Pyrite contains up to 7,300 ppm Co but most other trace elements were at or close to their minimum detection limits (Table 3). Variation in Co within and between samples can be attributed to a subtle compositional zoning. Flat time-resolved depth profiles for Co suggest the element is present in the crystal lattice, consistent with solid solution in the system FeS_2-CoS_2-NiS_2 (Hawley & Nichol 1961). Pyrite contains low but detectable concentrations of Mn, Ni and Se. These are all

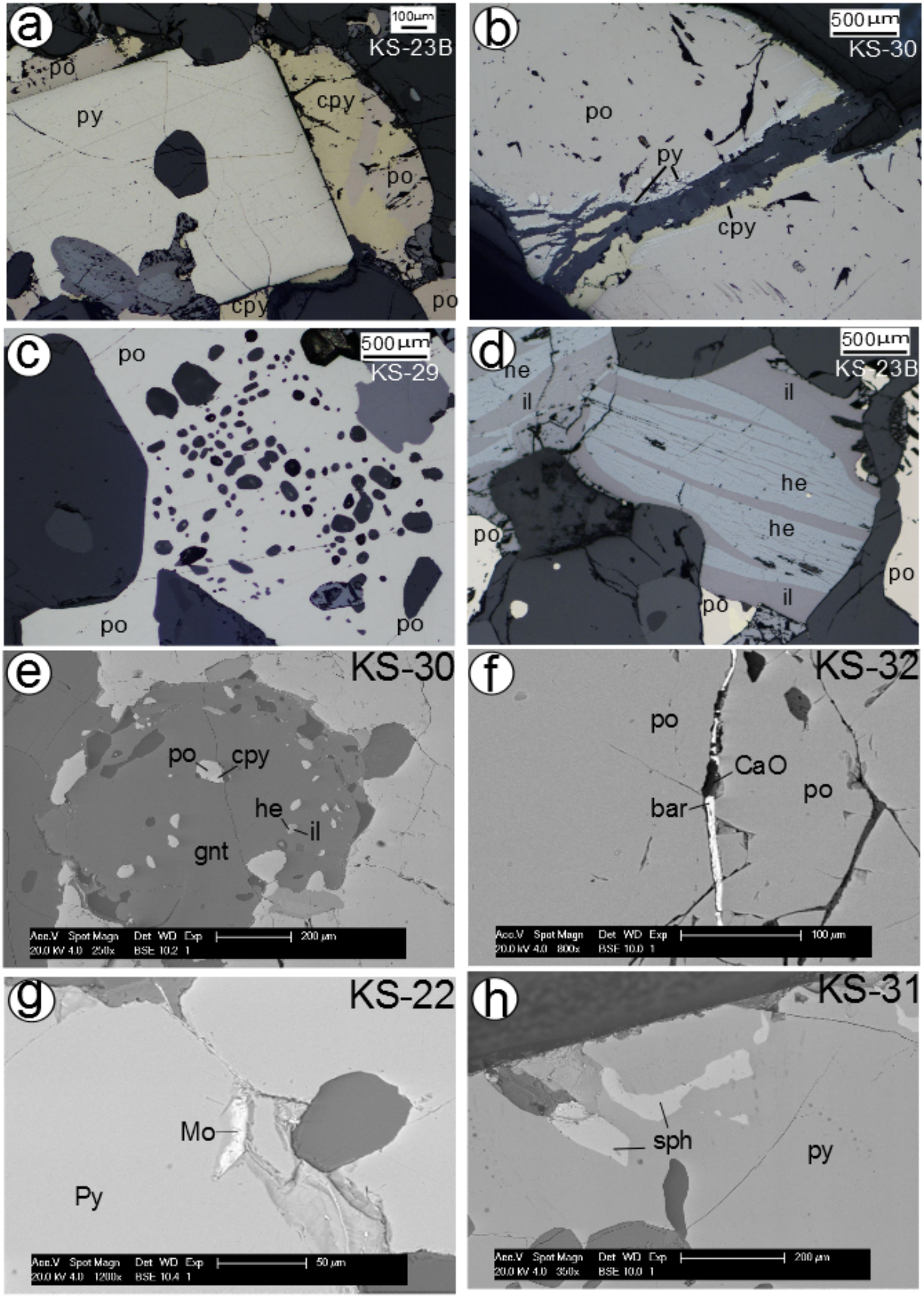

Figure 13: Reflected light photomicrographs illustrating relevant ore textures. (a) Typical euhedral pyrite and characteristic intergrowths of chalcopyrite and pyrrhotite in the matrix enclosing the pyrite. (b) Fine-grained secondary pyrite at the margins of coarse deformed pyrrhotite. (c) Gangue inclusions suspended in a matrix of pyrrhotite. (d) Exsolution of two Fe-(Ti)-oxides (hematite and ilmenite). Back-scatter electron images illustrating relevant mineral interactions. (e) Inclusions of sulphide in garnet. (f) Occurrence of baryte. (g) Occurrence of molybdenite. (h) Occurrence of sphalerite. Abbreviations: bar=baryte, CaO=calcite, cpy=chalcopyrite, gnt=garnet, he=hematite, il=ilmenite, mo=molybdenite, po=pyrrhotite, py=pyrite, sph=sphalerite

elements commonly found substituting for Fe in pyrite, or for S in the case of Se (Winderbaum *et al.* 2012). Upon metamorphic recrystallisation, incorporated trace and minor elements are often released (Cook *et al.* 2013). The complete dataset is given in Appendix E. Comparative analysis of pyrrhotite in six samples shows a similar range of trace elements in the sulphide lattice. The main exception is Ni, which occurs at concentrations up to 645 ppm (Table 4). There is some limited variation within and between samples, but in general, the Ni concentration is fairly homogeneous. Pyrrhotite also contains lesser amounts of Co, compared to pyrite, and minor Mn and Se. As for pyrite, the flat time-resolved depth profiles for Co and the other elements suggest that all these elements are present in the sulphide lattice. The complete dataset is given in Appendix F.

Figure 14 depicts the contents of Ni and Co in pyrite and pyrrhotite. The two Fe-sulphides define two very distinct groups: pyrite is enriched in Co (up to 7000 ppm) with low Ni content (<100 ppm); and pyrrhotite is enriched in Ni (up to 700 ppm) and only moderately enriched in Co (up to 1000 ppm).

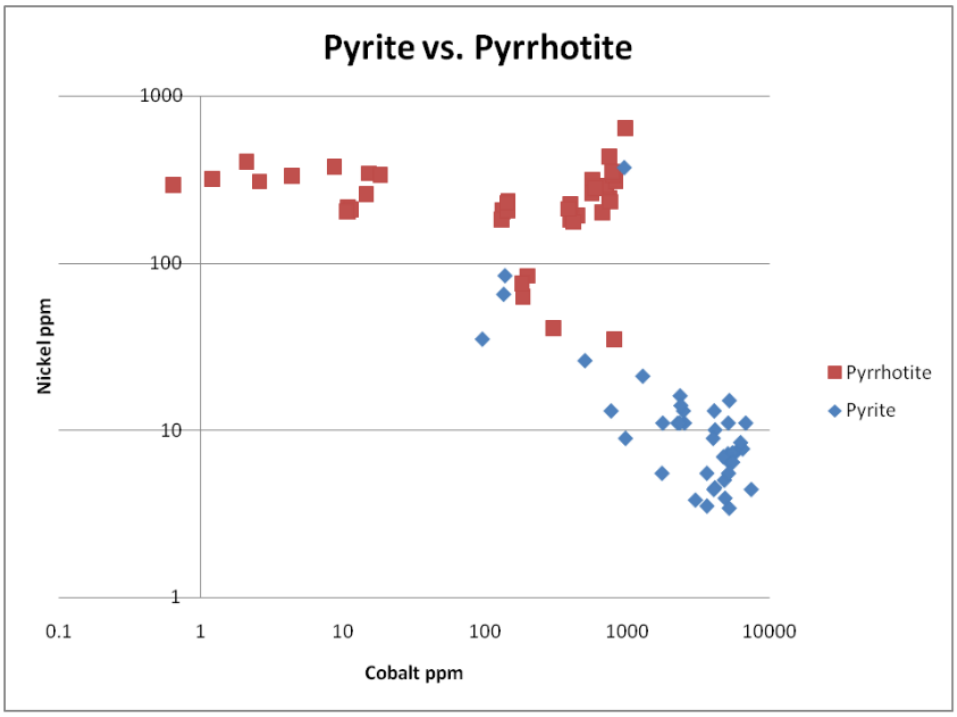

Figure 14: Diagram depicting LA-ICP-MS spot analytical data for Ni and Co in pyrite and pyrrhotite (logarithmic scales). Pyrrhotite is anomalous in Ni relative to pyrite, with lower concentrations of Co, whereas pyrite is enriched in Co with generally low concentrations of Ni.

Table 3: Summary of LA-ICP-MS spot trace element analytical data for pyrite grains from 4 representative samples. Euhedral pyrite grains were targeted. For each sample, a mean concentration value, standard deviation, maximum and minimum is given. Cobalt is the only element displaying strong enrichment.

	V	Cr	Mn	Co	Ni	Cu	Zn	Se	Mo	Ag	Sb	Te	Au	Hg	Tl	Pb	Bi
KS-25b																	
mean n=8	0.13	1.10	8.40	4845.00	54.00	0.74	0.73	13.00	0.08	0.67	0.03	-	-	0.14	-	0.05	0.05
std	0.09	0.72	18.45	1850.75	129.05	0.46	0.56	11.11	0.08	0.12	0.03	-	-	0.09	-	0.03	0.11
max	0.32	2.00	54.00	6754.00	373.00	1.70	1.70	39.00	0.25	0.37	0.09	<0.94	<0.09	0.29	<0.03	0.13	0.31
min	0.05	0.32	0.35	945.00	5.50	0.25	0.30	3.70	0.02	0.20	0.01	<0.01	0.00	0.06	0.00	0.20	0.00
KS-11																	
mean n=12	0.89	-	2.60	2420.00	12.00	1.17	0.73	5.80	0.64	0.04	0.04	0.30	0.03	0.13	0.01	0.20	0.47
std	2.59	-	2.03	1158.21	5.09	0.79	0.35	1.64	0.04	0.03	0.04	0.20	0.03	0.05	0.01	0.27	1.13
max	9.10	<2.6	5.80	4112.00	26.00	2.90	1.60	9.90	0.12	0.14	0.15	0.62	0.07	0.20	0.02	0.85	3.60
min	0.04	<0.38	0.27	500.00	5.50	0.37	0.46	3.50	0.00	0.02	0.01	0.06	0.00	0.04	0.00	0.02	0.00
KS-09																	
mean n=12	0.21	-	3.10	4889.00	5.30	1.50	0.87	11.00	0.06	0.13	0.06	0.29	0.01	0.17	0.01	0.69	0.78
std	0.20	-	2.72	1182.61	1.57	0.89	0.42	3.19	0.03	0.34	0.08	0.29	0.02	0.04	0.02	1.59	2.64
max	0.63	<3.1	6.60	7384.00	8.40	3.50	1.50	17.00	0.11	1.20	0.29	1.10	0.06	0.24	0.06	5.70	9.20
min	0.04	<0.48	0.32	2990.00	3.50	0.57	0.28	7.40	0.03	0.02	0.01	0.07	0.00	0.10	0.00	0.05	0.00
KS-30																	
mean n=9	0.17	-	3.30	1708.00	32.00	1.70	1.06	18.00	0.06	0.03	0.02	0.15	-	0.12	0.01	0.13	0.03
std	0.22	-	4.75	4183.42	54.37	2.19	2.35	26.78	0.12	0.02	0.03	0.26	-	0.09	0.01	0.22	0.13
max	0.31	<7.3	6.50	5181.00	84.00	4.30	4.10	42.00	0.19	0.04	0.05	0.37	<0.06	0.17	0.02	0.38	0.20
min	0.03	<0.5	0.38	95.00	3.40	0.45	0.28	3.90	0.01	0.02	0.01	0.02	0.00	0.05	0.00	0.02	0.00

Table 4: Summary of LA-ICP-Ms spot trace element analytical data for pyrrhotite grains from 6 representative samples. For each sample, a mean concentration, standard deviation, maximum and minimum is given. Nickel and cobalt are the only elements displaying strong enrichment.

Element	V	Cr	Mn	Co	Ni	Cu	Zn	Se	Mo	Ag	Sb	Te	Au	Hg	Tl	Pb	Bi
KS-6																	
mean=7	0.87	-	4.60	484.00	179.00	3.40	1.70	17.00	0.13	0.27	0.02	0.19	0.01	0.11	0.00	2.10	0.37
std	1.06	-	4.60	278.20	102.03	3.24	1.86	11.20	0.12	0.26	0.01	0.09	0.01	0.04	0.00	3.61	0.64
max	3.10	9.80	13.00	746.00	292.00	9.40	5.70	33.00	0.37	0.74	0.04	0.29	0.02	0.16	0.01	10.00	1.80
min	0.02	0.35	0.18	181.00	63.00	0.08	0.12	4.50	0.04	0.03	0.00	0.08	0.00	0.05	0.00	0.02	0.01
KS-11																	
mean=7	0.30	-	37.00	13.00	254.00	3.60	-	18.00	0.41	1.60	0.02	-	0.01	1.40	0.00	1.70	1.60
std	0.29	-	56.08	2.97	63.10	1.45	-	7.37	0.88	3.66	0.01	-	0.01	0.07	0.00	2.00	3.28
max	0.90	<28	127.00	18.30	346.00	5.60	<5.4	28.00	2.40	9.90	0.04	<0.46	0.02	0.30	0.01	5.90	9.00
min	0.10	<1.1	1.30	10.60	203.00	1.40	<0.58	9.70	0.05	0.09	0.00	<0.07	0.00	0.09	0.00	0.20	0.04
KS-28																	
mean=10	0.27	4.57	32.00	493.00	226.00	2.00	1.40	13.00	0.11	0.40	0.02	0.29	0.01	0.20	0.00	0.29	0.24
std	0.16	3.82	89.84	122.19	47.83	1.53	0.92	7.36	0.07	0.53	0.01	0.12	0.02	0.17	0.00	0.38	0.42
max	0.49	12.00	288.00	757.00	315.00	5.10	3.90	30.00	0.24	1.80	0.04	0.42	0.06	0.62	0.00	1.20	1.40
min	0.09	1.00	1.20	385.00	176.00	0.68	0.80	7.10	0.01	0.01	0.00	0.02	0.00	0.02	0.00	0.00	0.00
KS-30																	
mean=7	0.13	-	11.00	118.00	297.00	1.90	1.30	11.00	0.08	0.09	0.04	-	-	0.40	0.00	0.17	0.03
std	0.06	-	24.83	304.55	121.89	0.63	0.41	5.81	0.05	0.05	0.02	-	-	0.23	0.00	0.18	0.03
max	0.25	<1.6	67.00	809.00	407.00	2.50	1.90	19.00	0.19	0.20	0.09	<0.73	<0.02	1.40	0.00	0.56	0.07
min	0.07	<0.73	1.10	0.64	35.00	0.68	0.84	4.50	0.04	0.04	0.02	<0.18	<0	0.12	0.00	0.04	0.01
KS-32																	
mean=7	-	1.40	2.60	137.00	211.00	1.80	1.30	13.00	0.20	0.41	0.03	0.43	0.01	0.20	0.00	0.44	0.08
std	0.02	0.34	1.65	6.16	18.02	0.81	0.29	3.54	0.07	0.48	0.02	0.16	0.00	0.05	0.00	0.49	0.15
max	0.14	2.10	6.00	145.00	237.00	3.00	1.80	16.00	0.29	1.30	0.05	0.62	0.01	0.26	0.01	1.40	0.42
min	0.10	1.10	1.10	130.00	182.00	0.79	1.00	5.70	0.11	0.04	0.01	0.22	0.01	0.13	0.00	0.05	0.01
KS-25A																	
mean=5	0.21	4.00	2.80	823.00	416.00	4.80	2.40	17.00	0.25	0.82	0.03	0.61	0.01	0.23	0.00	0.41	0.11
std	0.15	3.59	1.95	86.81	135.76	5.27	2.30	4.64	0.08	1.44	0.01	0.62	0.00	0.18	0.00	0.42	0.13
max	0.46	9.80	5.60	968.00	645.00	14.00	6.50	22.00	0.35	3.40	0.04	1.70	0.01	0.53	0.00	1.10	0.32
min	0.10	1.10	0.90	742.00	311.00	1.00	1.10	11.00	0.15	0.11	0.01	0.19	0.00	0.08	0.00	0.08	0.01

Electron Probe Microanalysis (EPMA)

EPMA was used to analyse pyrrhotite to determine the mineral stoichiometry in terms of the Fe:S ratio. In some cases, the Fe:S ratio can be used to infer temperatures of crystallisation (e.g.(Becker *et al.* 2010). The dataset (Table 5) shows the composition is approximately $Fe_{0.9}S$ (i.e. Fe_8S_9), with remarkably little variation within and between sample populations. Significantly, the compositions of pyrrhotite occurring as inclusions within garnet and within the matrix of the ore zone were remarkably similar to one another (Table 5).

Table 5: Mean EPMA data for pyrrhotite grains in 6 representative samples. Spot analysis of pyrrhotite was undertaken to determine the ratio of Fe:S throughout the zone of mineralisation and as inclusions in garnet. Green-shaded columns indicate pyrrhotite that has formed throughout the mineralised system and the blue –shaded column indicates pyrrhotite grains occurring as inclusions within garnets. There is no significant difference in the element wt. % values or Fe:S ratio of the two populations.

Element (wt.%)	KS-11 mean (n=14)	KS-25a mean (n=15)	KS-30 mean (n=13)	KS-32 mean (n=15)	KS-23b mean (n=13)	KS-23b mean (n=11)
S	38.28	38.70	38.97	38.49	39.12	39.24
Fe	60.83	60.24	60.55	60.67	58.65	58.49
Co	0.00	0.11	0.00	0.00	0.11	0.10
Ni	0.03	0.06	0.03	0.04	0.22	0.22
Cu	0.02	0.01	0.01	0.02	0.02	0.05
Zn	0.01	0.01	0.01	0.02	0.03	0.02
As	0.07	0.04	0.05	0.06	0.06	0.05
Ag	0.02	0.02	0.02	0.02	0.02	0.03
Sb	0.01	0.01	0.01	0.01	0.03	0.01
Pb	0.13	0.13	0.15	0.13	0.17	0.15
Bi	0.10	0.09	0.09	0.10	0.12	0.09
Total	**99.50**	**99.43**	**99.91**	**99.59**	**98.55**	**98.45**
Formulae (calculated to S=1)						
Fe	0.953	0.939	0.941	0.949	0.861	0.856
Co	0.000	0.002	0.000	0.000	0.001	0.001
Ni	0.001	0.001	0.001	0.001	0.003	0.003
Cu	0.000	0.000	0.000	0.000	0.000	0.001
Zn	0.000	0.000	0.000	0.000	0.000	0.000
Ag	0.001	0.001	0.001	0.001	0.000	0.000
Pb	0.000	0.000	0.000	0.000	0.001	0.001
Total M	**0.913**	**0.891**	**0.892**	**0.906**	**0.866**	**0.862**
As	0.001	0.001	0.001	0.001	0.000	0.001
Sb	0.000	0.000	0.000	0.000	0.000	0.000
Bi	0.001	0.001	0.001	0.001	0.000	0.000
S	1.044	1.056	1.056	1.048	1.000	1.000

EPMA was conducted on sphalerite to determine the Fe content. When buffered by both pyrite and pyrrhotite, which is the case for the Basil deposit, the mol.% FeS content of sphalerite can be an efficient geobarometer, and can provide an estimate of the pressure conditions at which the sphalerite (and implicitly the other sulphides) formed (Scott 1973, 1976). The mol.% FeS content of sphalerite ranges from ~10 mol.% up to more than 25% (Table 6). The sphalerite geobarometer is temperature-independent up to ca. 600 °C, so assuming an arbitrary peak metamorphic temperature of 580 °C (realistic in terms of the minerals present), the lower mol.% FeS values (9-13 mol.% FeS) are consistent with formation at pressures exceeding 10 kBar. The sphalerite with higher

Table 6: Mean EPMA data for sphalerite in 4 representative samples. Spot analysis of sphalerite was undertaken for the application of mol.% FeS as a geobarometer.

Wt.%	KS-33 mean (n=3)	KS-29 mean (n=7)	KS-31 mean (n=6)	KS-23b mean (n=1)
S	32.10	32.58	31.33	31.87
Fe	6.43	11.23	10.48	6.97
Co	0.01	0.01	0.05	0.02
Cu	0.28	0.12	0.19	0.21
Zn	57.40	54.84	56.60	57.58
As	0.04	0.02	0.04	0.01
Ag	0.02	0.02	0.01	0.01
Cd	0.17	0.08	0.05	0
Pb	0.08	0.06	0.10	0.02
Bi	0.13	0.09	0.07	0.15
Total	**96.64**	**99.09**	**98.92**	**96.87**
Formulae (calculated to 2 a.p.f.u)				
Fe	0.12	0.20	0.19	0.13
Co	0.00	0.00	0.00	0.00
Cu	0.00	0.00	0.00	0.00
Zn	0.88	0.81	0.85	0.88
Ag	0.00	0.00	0.00	0.00
Cd	0.00	0.00	0.00	0.00
Pb	0.00	0.00	0.00	0.00
Bi	0.00	0.00	0.00	0.00
Total	**1.00**	**1.01**	**1.04**	**1.01**
As	0.00	0.00	0.00	0.00
S	1.00	0.99	0.96	0.99
Total	**1.00**	**0.99**	**0.96**	**0.99**
mol.% FeS	11.50	19.19	17.67	12.40
mol.% ZnS	87.75	80.47	81.78	87.20
mol.% CdS	0.00	0.00	0.02	0.00

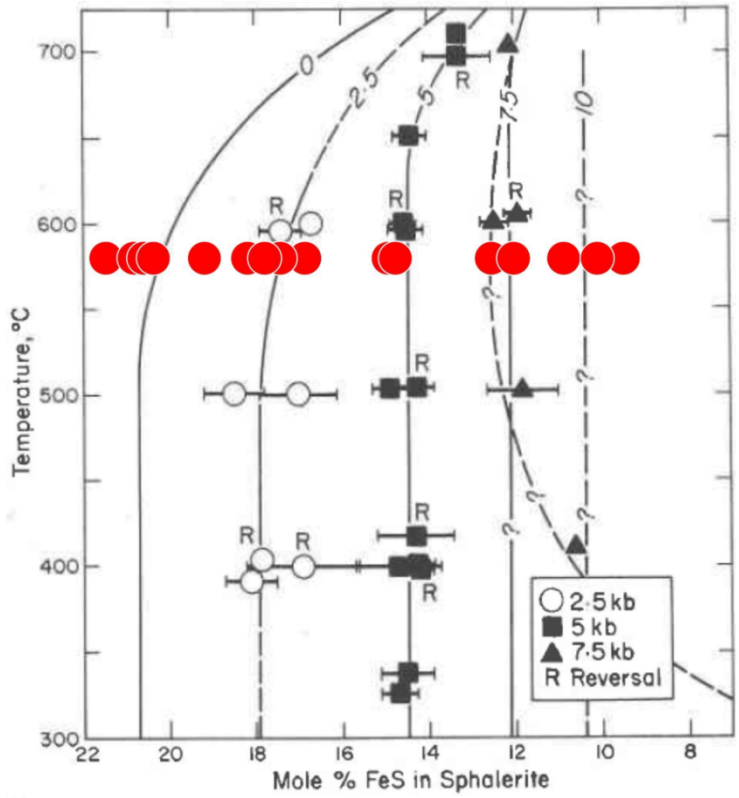

Figure 15: mol.% FeS vs. temperature diagram modified after Scott (1976) showing electron probe microanalysis of data for sphalerite (from Table 3) as red circles. A peak metamorphic temperature of 580 °C has been assumed. Assuming equilibrium crystallisation with pyrite and pyrrhotite, the lower values of mol.% FeS indicate mineralisation pressures of >10 kbar. Sphalerite with higher mol.% FeS are suggested to represent re-equilibration during the retrograde metamorphic path.

mol.% FeS (>15 mol.% FeS) most likely represents equilibration upon retrograde cooling or lack of equilibrium between sphalerite, pyrite and pyrrhotite (Cook *et al.* 1994). Individual mol.% FeS values are superimposed on the FeS vs. temperature diagram of Scott (1976) in Figure 15.

The sphalerite contains few other substituted elements. Cadmium, a common minor constituent of sphalerite was typically only 0-0.24 wt.% (Table 6).

Electron Probe Microanalysis (EPMA) data for garnet in sample KS-23b (Table 7) indicates that the compositions, with significant almandine and pyrope components (Mezger *et al.* 1992), are consistent with their appearance and paragenesis, indicating

they are metamorphic garnets. Skarn garnets are, in contrast, typically calcic with high grossular (Ca-Al) and andradite (Ca-Fe) components (Meinert 1992). There is negligible variation in major components across the four large garnet grains are essentially identical and there is no core-to-rim compositional variation. All show ~60 mol.% almandine content, ~30% pyrope, ~10% grossular and very minor spessartine.

Table 7: Electron probe microanalysis of 4 representative garnet grains in sample KS-23b. Each mean value given represents a 30-point transect across each garnet grain.

(Wt.%)	71733a_02 mean=30	71733a_06 mean=30	71733b_02 mean=30	71733b_03 mean=30
Ca	3.20	3.33	3.13	3.20
Na	0.01	0.05	0.02	0.01
K	0.01	0.01	0.00	0.01
Fe	27.09	28.51	28.75	28.89
Ti	0.02	0.02	0.02	0.04
Mg	8.24	8.32	8.00	8.07
Si	40.01	38.44	38.57	38.77
Mn	0.51	0.50	0.66	0.67
Cr	0.01	0.01	0.01	0.02
Al	21.05	21.44	21.68	21.68
Total	**100.16**	**100.63**	**100.85**	**101.35**
Mg	1.91	1.92	1.84	1.85
Fe	3.51	3.70	3.71	3.71
Mn	0.07	0.06	0.09	0.09
Ca	0.53	0.55	0.52	0.53
Total	**6.02**	**6.24**	**6.16**	**6.18**
Al (total)	3.85	3.91	3.95	3.93
Si	6.10	5.94	5.96	5.96
Al	0.10	0.06	0.06	0.04
Total	**6.14**	**5.99**	**5.98**	**5.98**
Al	3.81	3.86	3.93	3.91
Ti	0.00	0.00	0.00	0.00
Cr	0.00	0.00	0.00	0.00
Total	**3.81**	**3.86**	**3.93**	**3.91**
Na	0.00	0.02	0.01	0.00
K	0.00	0.00	0.00	0.00
TOTAL	**15.97**	**16.09**	**16.06**	**16.07**
Mol.% end-members				
Almandine	59.22	59.23	60.29	60.13
Pyrope	30.84	30.83	29.88	29.93
Spessartine	1.41	1.05	1.41	1.40
Grossular	8.54	8.90	8.42	8.54

LA-ICP-MS element mapping

LA-ICP-MS mapping of two selected garnet grains in sample KS-37 was undertaken to determine if there was any subtle compositional zoning that was not recognised in the EPMA study. Specifically, the mapping targeted elements concentrated in the garnet rim relative to the core which might reflect fluid evolution. The maps (Fig. 16, Appendix G) showed that the Heavy Rare Earth Elements (HREE; Dy, Er, Lu, Y and Yb), as well as Cr and V, are notably enriched in the rims relative to the core. Interestingly, the major elements which often define compositional zoning in garnet, such as Al, Ca and Fe (Argles *et al.* 1999) displayed no apparent zoning within the garnet (Fig. 16). Other elements mapped, including various Light Rare Earth Elements (LREE; Ce, Nb, Nd, Eu), and Sn, Ti and Zr, were either not present or were present at only negligible concentration (and thus are not shown in Fig. 16).

DISCUSSION

Relationships between sulphides and metamorphism

Petrographic examination of the ores and their host rocks shows that sulphides and rock-forming silicates are included within one another. In particular, the occurrence of sulphide inclusions within garnet and amphibole are suggestive of the entire package having undergone regional metamorphism at amphibolite to granulite facies. This infers that the sulphides must be pre- or syn-metamorphic in origin even if they recrystallised under metamorphism. This may have occurred during the ca. 480-460 Ma Larapinta Event (Mawby *et al.* 1999, Buick *et al.* 2005), or the 450-300 Ma Alice Springs Orogeny (Mawby *et al.* 1999, Hand *et al.* 1999b, Buick *et al.* 2008).

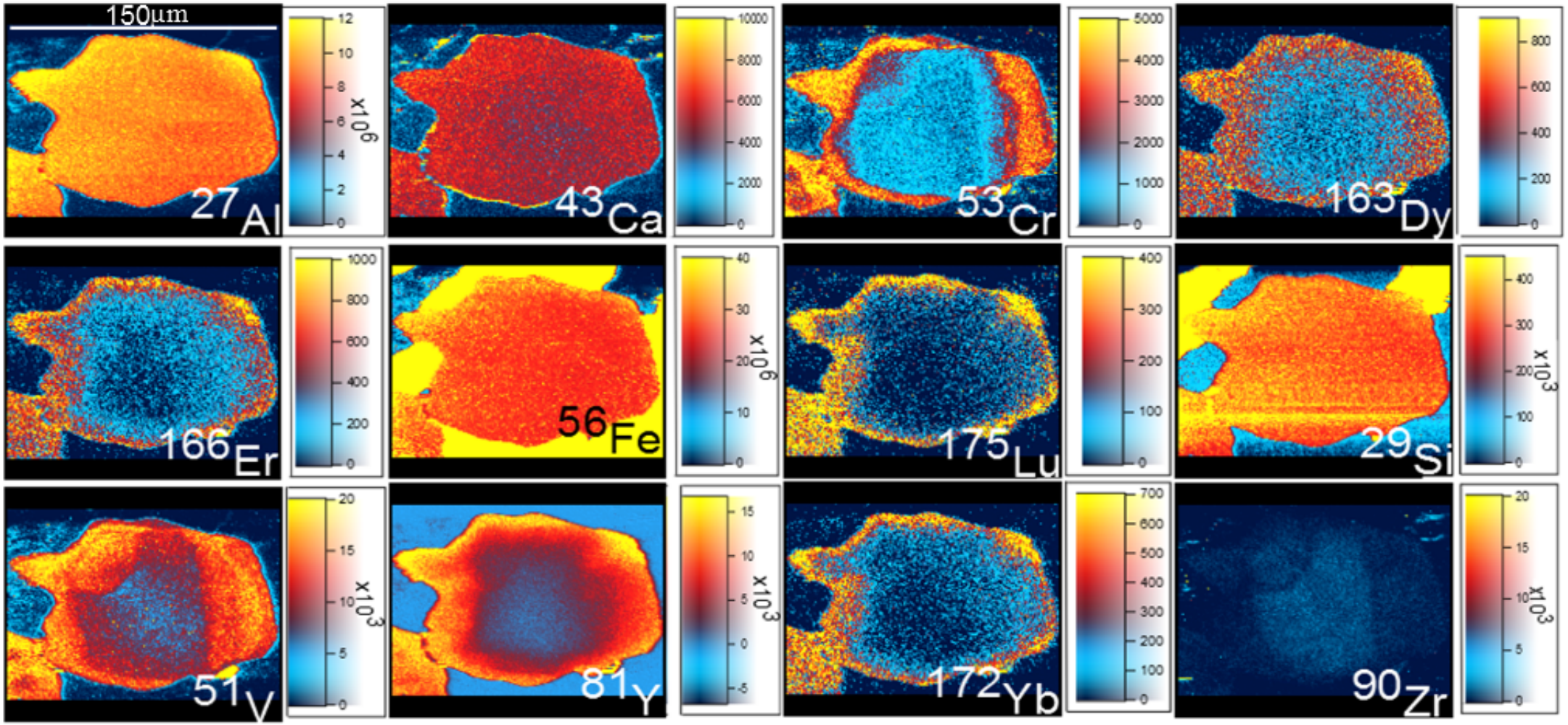

Figure 16: LA-ICP-MS element maps of a metamorphic garnet grain. Note that Y, HREE (Dy, Er, Yb and Lu), Cr and V all show compositional zoning, with a marked enrichment around the rim of the grain. In contrast, elements which usually define compositional zoning in metamorphic garnet, such as Al, Ca, Fe and Si, are uniformly distributed.

LA-ICP-MS spot analysis has confirmed that Co is contained within pyrite (Table 3) and Ni is incorporated within pyrrhotite (Table 4). No independent Co- or Ni-bearing minerals were observed. Cobalt (as Co^{2+}) and Ni (as Ni^{2+}) are isomorphously substituted in the respective sulphide lattices, where they replace Fe^{2+} (Hawley & Nichol 1961). Under equilibrium conditions, cobalt preferentially crystallises into pyrite and nickel will preferentially crystallise into pyrrhotite (Hawley & Nichol 1961). This relationship suggests equilibrium partitioning of the two elements between the two Fe-sulphides, presumably at the time of metamorphic recrystallisation. The coexistence of the two Fe-sulphides at the time of trace element partitioning further suggests that the system was close to the pyrite-pyrrhotite buffer in fS_2-fO_2 space at that time (Hall 1986). Sulphide recrystallisation during peak metamorphism is also supported by the composition of at least some of the sphalerite in the ore. Application of the sphalerite geobarometer (Scott 1973, 1976) is possible because of the pyrite-pyrrhotite equilibrium demonstrated by the Co/Ni partitioning above. EPMA data showing a sub-population of sphalerite with 10–12 mol.% FeS (Table 6) indicates metamorphic pressures in excess of 10 kBar, consistent with burial at up to 30 km. At conditions of 600 °C and >10 kbar, sulphide recrystallisation can be expected (McClay & Ellis 1983).

LA-ICP-MS spot analysis of pyrite (Table 3) has shown that, apart from Co, other trace elements common in pyrite are either absent or are present in only negligible concentrations. This observation is also consistent with complete recrystallisation of the sulphide assemblage during metamorphism (McClay & Ellis 1983). Any trace elements that had originally been incorporated in pyrite would be released to form discrete minerals, as for example shown for Au (Larocque *et al.* 1995); others such as Ni are partitioned into coexisting pyrrhotite.

It is proposed that the Basil Cu-Co deposit is either a metamorphosed (i.e., it formed pre-metamorphism) or a metamorphogenic deposit (syn-metamorphic). Three key mineral textures observed: the lack of plastically-deformed (euhedral) pyrite; pyrite overgrowing garnet and; the presence of relict pyrite in massive pyrrhotite-dominant ore; Fig. 13), are consistent with the metamorphic recrystallisation of pyrite (Craig & Vaughan 1994) in which the sulphide anneal during metamorphic cooling, forming 'new' euhedral grains. The textures shown in Figure 13, showing massive pyrite and pyrrhotite without any clear orientation (e.g. parallel to foliation) indicates that recrystallisation must have continued during the waning stages of the metamorphic cycle. Pyrite deforms either by plastic or brittle deformation and cannot grow statically under strain (Barrie *et al.* 2010).

Further evidence for a pre- or syn-metamorphic origin of sulphides comes from sulphide-silicate relationships. Pyrrhotite is observed as inclusions within metamorphic garnet (Fig. 13) suggesting that the sulphides must have been present at the time of garnet growth. This finding is endorsed by the EPMA compositional data that show that sulphides included within garnet are compositionally identical to those elsewhere in the ore system (Table 5), even if there is a possibility that these sulphides re-equilibrated during retrograde conditions.

Garnet compositions

LA-ICP-MS mapping of garnet (Fig. 16) has shown that the garnet rims are enriched in HREE (Dy, Er, Lu, Y and Yb), as well as Cr and V. Garnet can be an efficient concentrator of HREE relative to LREE and may show grain-scale compositional zoning with respect to HREE (e.g. cores that are strongly enriched in HREE relative to

the rims (Otamendi *et al.* 2002). For zoning of the type observed in the Basil deposit to occur, a HREE-rich fluid must have been available in the system during the final stage of garnet grown (presumably syn- or post-peak). A possible source of HREE would be the metamorphic breakdown of amphibolites facies minerals such as hornblende or biotite (Bingen *et al.* 1996) or most likely titanate, an excellent REE-host (Bingen *et al.* 1996, Hughes *et al.* 1997) as the system approaches granulite facies. Alternatively, HREE and Cr may have migrated to the rims via a process of solid-state diffusion, as has been demonstrated by (Carlson 2012), albeit at somewhat higher temperatures. The enrichment in Cr and V may have been derived from breakdown of magnetite or ilmenite, which both may carry significant Cr or V(Toft *et al.* 1993)

Hydrothermal alteration

In comparison with the rocks hosting the mineralization, the whole rock geochemistry of the mineralisation zone indicates a loss of more mobile elements (Ca, K, Na, and Sr) whereas the more immobile elements (Zr and Ti) are unchanged, even when adjusted for the large volumes of sulphide in the ore. This is concordant with a hypothesis involving flow of hydrothermal fluid, interaction with pre-existing minerals, and breakdown of alkali-bearing minerals. Importantly, this suggests that there could potentially be alteration markers that could be used in exploration for mineralization similar to the Basil deposit. Determination of the extent of this alteration, both laterally and vertically, would however require analysis of a greater number of samples including those from well outside the orebody (lacking in the present study). Reconstruction of pre-alteration, pre-mineralisation protolith lithology is however complicated by the wide variation in lithologies.

Origin of the host rock

The mineralogy of the amphibolite contains magnesiohornblende with lesser andesine and quartz. The amphibolite has also been observed to contain abundant, very fine-grained zircons. In terms of a protolith, the amphibolite that hosts the Basil Deposit has a chemistry consistent with formation in an intracontinental rift environment (Sivell & Foden 1985), possibly as a sequence of submarine basaltic flows (Lawrence *et al.* 1987). Given that there is generally only small or sporadic amounts of zircon as a primary magmatic mineral in mafic and ultramafic rocks (Heaman *et al.* 1990), and this amphibolite has abundant zircons, it is our interpretation that these zircons cannot igneous in origin and are more likely to be detrital zircons. It is suggested therefore that the protolith must contain a significant sedimentary component and is most likely a tuffitic rock containing both sedimentary and volcaniclastic material.

The presence of scapolite suggests the fluids that were present within the system were derived from evaporitic sediments (Ramsay & Davidson 1970), and the occurrence of orthopyroxene either suggests a mafic component or metamorphic growth in a pelitic sedimentary rock. The mineralogy of the weakly-foliated amphibolite suggests a tuff as the protolith to this unit.

The mineralogy of the garnet-rich amphibolite presents a number of potential alternative protoliths. Metamorphic garnets grow in certain conditions such as; Al- and Ti-rich chemistry. This garnet-rich amphibolite could have originally been abundant in aluminous minerals or rich in Ti-bearing minerals such as rutile or ilmenite.

It may however have been an extrusive, or mixed extrusive-sedimentary event. Identifying the primary lithology of the rocks hosting mineralization is difficult given the amphibolite- to granulite facies overprint. Nevertheless, a scenario can be put

forward in which initial pillow basalt formation in the Irindina sub-basin was accompanied by deposition of detrital tuffaceous material and sedimentary material, as discussed above. In terms of where the deposit is located with respect to the stratigraphy of the sub-basin, the Basil deposit is not located at the stratigraphically lower sections of the basin but further up in the sequence, in between successive units of pillow basalts and detrital material. This suggests that the host rock is not entirely mafic but rather volcaniclastic in origin with intercalated sediments.

Genetic Ore Types

From the evidence reported here, it is possible to dismiss some of the genetic ore types that were suggested above. A hydrothermal skarn style of deposit was suggested due to the presence of a garnet-rich (60-80%) lithology, which is a common characteristic of skarn deposits (Meinert 1992). However, the compositions of these garnets indicate a metamorphic and not a skarn origin. Moreover, there are few other indicators of a skarn setting such as carbonate or calc-silicate precursors, or the presence of diopside-hedenbergite, wollastonite or actinolite. The only clinopyroxene seen (Fig. 8g) does not co-exist with garnet. These lines of evidence lead to the conclusion that the Basil deposit is not of a skarn origin.

A second alternative presented in a confidential report was that the Basil deposit represents a magmatic sulphide Ni-Cu-(PGE) deposit formed in an intrusive setting. The lack of significant Ni (<100 ppm in all samples, no pendlandite or other Ni-minerals observed) and PGEs in the zone of mineralisation and presence of lithologies that cannot have been mafic intrusive protoliths is enough to suggest that this deposit type model can be dismissed.

If skarn and magmatic styles of mineralisation are ruled out by the available evidence, one is left with the final suggestion: that Basil formed via seafloor exhalative processes and is thus a possible VMS-type deposit. The evidence presented above support such a hypothesis. The geological setting in which the HRMC was formed is concordant with such an interpretation. Deposition of pillow basalts and clastic material took place in a sub-basin with the metals leached from the dominantly mafic underlying sequence, lending the mineralisation a Cu-dominant character.

The only difficulty with this hypothesis is the lack of any significant hydrothermal alteration halo enclosing the deposit. Zoned alteration halos are characteristic of many VMS deposits(Franklin *et al.* 2008). Despite this, the lack of a recognisable hydrothermal alteration zone is consistent either with destruction of the alteration zone during metamorphism or detachment of the ore from alteration either following formation (e.g. accumulation in a brine pool distal to the vent not as a proximal sulphide mound), or during syn-metamorphic deformation (e.g. shearing focussed along the mineralised zone; Cook et al. 1990).

CONCLUSIONS

The Basil deposit is metamorphosed, i.e., it is likely formed at least during the Alice Springs Orogeny, if not the earlier Larapinta Event. Syn-metamorphic sulphide recrystallisation occurred with equilibrium partitioning of trace elements between pyrite and co-existing pyrrhotite. The composition of the sphalerite buffered by the pyrite and the pyrrhotite points to crystallisation at pressures of 10 kBar.

Mineralogical, petrographic and geochemical evidence allow various suggested genetic

ore types to be disproved. Garnet compositions are typical of metamorphic origin and not the product of a hydrothermal skarn system. The lack of significant Ni in the mineralisation and presence of abundant detrital zircons in the amphibolite make a magmatic-hosted Ni-Cu-(PGE) deposit scenario unlikely. This leaves the possibility that the Basil deposit was originally formed as a volcanogenic massive sulphide by volcanogenic-exhalative processes at or near the seafloor. Whole rock geochemistry showed no significant evidence for a marked halo of hydrothermal alteration associated with the ore.

Doubtless, much will be written about the Basil deposit and its host rocks in the future as more data emerge that can further constrain what it is, and what it isn't. Above all, there is a clear need for reliable geochronological data for the mineralization and the host rocks, as well as a better-defined sequence of deformation events.

ACKNOWLEDGMENTS

Many thanks to all the employees at Mithril Rosources Limited. Whether the help was financially or knowledge based, this project would not have succeeded without your help. Thanks to Nigel Cook for his enthusiasm and willingness to take on this project, without him I wouldn't have produced a thesis. Much appreciation to Angus Netting and Benjamin Wade of Adelaide microscopy, without their help of collecting data, I would have had nothing to discuss. Mention and thanks to Pontifex and Assoc. for their preparation of all my samples and finally to Genalysis for their help.

REFERENCES

ARGLES T., PRINCE C., FOSTER G. & VANCE D. 1999. New garnets for old? Cautionary tales from young mountain belts. *Earth and Planetary Science Letters* **172**, 301-309.

BALLÈVRE M., MÖLLER A. & HENSEN B. J. 2000. Exhumation of the lower crust during crustal shortening: an Alice Springs (380 Ma) age for a prograde amphibolite facies shear zone in the Strangways Metamorphic Complex (central Australia). *Journal of Metamorphic Geology* **18**, 737-747.

BARRIE C. D., COOK N. J. & BOYLE A. P. 2010. Textural variation in the pyrite-rich ore deposits of the Røros district, Trondheim Region, Norway: implications for pyrite deformation mechanisms. *Mineralium Deposita* **45**, 51-68.

BECKER M., DE VILLIERS J. & BRADSHAW D. 2010. The Mineralogy and Crystallography of Pyrrhotite from Selected Nickel and PGE Ore Deposits. *Economic Geology* **105**, 1025-1037.

BINGEN B., DEMAIFFE D. & HERTOGEN J. 1996. Redistribution of rare earth elements, thorium, and uranium over accessory minerals in the course of amphibolite to granulite facies metamorphism: The role of apatite and monazite in orthogneisses from southwestern Norway. *Geochimica et Cosmochimica Acta* **60**, 1341-1354.

BUICK I. S., HAND M., WILLIAMS I. S., MAWBY J., MILLER J. A. & NICOLL R. S. 2005. Detrital zircon provenance constraints on the evolution of the Harts Range Metamorphic Complex (central Australia): links to the Centralian Superbasin. *Journal of the Geological Society* **162**, 777-787.

BUICK I. S., MILLER J. A., WILLIAMS I. S. & CARTWRIGHT I. 2001. Ordovician high-grade metamorphism of a newly recognised late Neoproterozoic terrane in the northern Harts Range,central Australia. *Journal of Metamorphic Geology* **19**, 373-394.

BUICK I. S., STORKEY A. & WILLIAMS I. S. 2008. Timing relationships between pegmatite emplacement, metamorphism and deformation during the intra-plate Alice Springs Orogeny, central Australia. *Journal of Metamorphic Geology* **26**, 915-936.

CABRI L. J. 1973. New data on Phase Relations in the Cu-Fe-S System. *Economic Geology* **68**, 443-454.

CARLSON 2012. Rates and Mechanisms of Y, REE. *American Mineralogists*, 522-533.

COOK N., KLEMD R. & OKRUSCH M. 1994. Sulphide mineralogy, metamorphism and deformation in the Matchless massive sulphide deposit, Namibia. *Mineralium Deposita* **29**, 1-15.

COOK N. J., CIOBANU C. L., MERIA D., SILCOCK D. & WADE B. P. 2013. Arsenopyrote-pyrite association in an orogenic gold ore: tracing mineralization history from textures and trace elements. *Economic Geology*.

CRAIG J. R. & VAUGHAN D. J. 1994. *Ore Microscopy and Ore Petrography*. **Second Edition:** 120-163. John Wiley & Sons, Inc., Canada.

DAS K., BUICK I. S., MILLER J. A., HAND M., MAWBY J., HENSEN B. & YOSHIDA M. 2000. Geology and Tectonic Evolution of Strangeways and Harts Range Region of Eastern Arunta Inlier, Central Australia - a Post-conference Geotraverse of

"Orogenesis in the Outback" (Alice Springs, July 1999). *Journal of Geosciences* **43**, 249-260.

FRANKLIN J. M., GIBSON H. L., JONASSON I. R. & GALLEY A. G. 2008. Volcanogenic massive sulphide deposits. *Economic Geology* **100**, 523-560.

HALL A. J. 1986. Pyrite-pyrrhotine redox reactions in nature. *Mineralogical Magazine* **50**, 223-229.

HAND M., MAWBY J. O., KINNY P. & FODEN J. 1999a. U–Pb ages from the Harts Range, central Australia: evidence for early Ordovician extension and constraints on Carboniferous metamorphism. *Journal of the Geological Society* **156**, 715-730.

HAND M., MAWBY M., MILLER J. A., BALLEVRE M., HENSEN B., MOLLER A. & BUICK I. S. 1999b. The Tectonothermal Evolution of the Harts Range and Strangeways Range Region. *Geological Society of Australia, Specialist Group in Geochemistry, Mineralogy and Petrology Field Guide* **4**.

HAWLEY J. E. & NICHOL I. 1961. Trace elements in pyrite, pyrrhotite and chalcopyrite of different ores. *Economic Geology* **56**, 467-487.

HEAMAN L. M., BOWINS R. & CROCKET J. 1990. The chemical composition of igneous zircon suites: implications for geochemical tracer studies. *Geochimica et Cosmochimica Acta* **54**, 1597-1607.

HUGHES J. M., BLOODAXE E. S., HANCHAR J. M. & FOORD E. E. 1997. Incorporation of rare earth elements in titanite: Stabilization of the *A2/a* dimorph by creation of antiphase boundaries. *American Mineralogists* **82**, 512-516.

KORSCH R. J., GOLEBY B. R., LEVEN J. H. & DRUMMOND B. J. 2011. Crustal architecture of central Australia based on deep seismic reflection profiling. *AGES*.

LAROCQUE A. C. L., HODGSON C. J., CABRI L. J. & JACKMAN J. A. 1995. Ion microprobe analysis of pyrite, chalcopyrite and pyrrhotite from the Mobrun VMS deposit in Northwestern Quebec: Evidence for metamorphic remobilisation of gold. *Canadian Mineralogist* **33**, 373-388.

LAWRENCE R., JAMES P. & OLIVER R. 1987. Relative timing of folding and metamorphism in the ruby mine area of the Harts Range, central Australia. *Australian Journal of Earth Sciences* **34**, 293-309.

MAIDMENT D. W., HAND M. & WILLIAMS I. S. 2012. Detrital zircon constraints on the deep intracratonic burial and regional high-grade metamorphism during basin formation. *Gondwana Research*.

MATTINEN P. R. & BENNETT G. H. 1986. The green mountain massive sulphide deposit. Besshi-style mineralization within the california foothills copper-zinc belt. *Journal of Geochemical Exploration* **25**, 185-200.

MAWBY J. O., HAND M. & FODEN J. 1999. Sm–Nd evidence for high-grade Ordovician metamorphism in the Arunta Block, central Australia. *Journal of Metamorphic Geology* **17**, 653-668.

MCCLAY K. & ELLIS P. 1983. Deformation and recrystallization of pyrite. *Mineralogical Magazine* **47**, 527-538.

MEINERT L. D. 1992. Skarn and Skarn Deposits. *Geoscience Canada* **19**, 145-162.

MEZGER K., ESSENE E. J. & HALLIDAY A. 1992. Closure temperatures of the Sm—Nd system in metamorphic garnets. *Earth and Planetary Science Letters* **113**, 397-409.

MILLER J. A., CARTWRIGHT I. & BUICK I. S. 1997. Granulite facies metamorphism in the Mallee Bore area, northern Harts Range: implications for the thermal evolution of the eastern Arunta Inlier, central Australia. *Journal of Metamorphic Geology* **15**, 613-629.

NALDRETT A. J. 1999. World-class Ni-Cu-PGE deposits: key factors in their genesis. *Mineralium Deposita* **34**, 227-240.

OTAMENDI J. E., DE LA ROSA J. D., DOUCE A. E. P. & CASTRO A. 2002. Rayleigh fractionation of heavy rare earths and yttrium during metamorphic garnet growth. *Geology* **30**, 159-162.

RAMSAY C. & DAVIDSON L. 1970. The origin of scapolite in the regionally metamorphosed rocks of Mary Kathleen, Queensland, Australia. *Contributions to Mineralogy and Petrology* **25**, 41-51.

ROBB L. J. 2005. Introduction to ore-forming processes. 129-215.

SCOTT S. D. 1973. Experimental Calibration of the Sphalerite Geobarometer. *Economic Geology* **68**, 466-474.

SCOTT S. D. 1976. Application of the sphalerite geobarometer to regionally metamorphosed terrains. *American Mineralogists* **61**, 661-670.

SHAW R. D., ETHERIDGE M. A. & LAMBECK K. 1991. Development of the late Proterozoic to mid-Paleozoic intracratonic Amadeus Basin in central Australia: a key to understanding tectonic forces in plate interiors. *Tectonics* **10**, 688-721.

SIVELL W. & FODEN J. 1985. Banded amphibolites of the Harts Range meta-igneous complex, central Australia: an early Proterozoic basalt-tonalite suite. *Precambrian Research* **28**, 223-252.

TOFT P., SCOWEN P., ARKANI-HAMED J. & FRANCIS D. 1993. Demagnetization by hydration in deep-crustal rocks in the Grenville province of Quebec, Canada: Implications for magnetic anomalies of continental collision zones. *Geology* **21**, 999-1002.

WADE B. P., HAND M., MAIDMENT D. W., CLOSE D. F. & SCRIMGEOUR I. R. 2008. Origin of metasedimentary and igneous rocks from the Entia Dome, eastern Arunta region, central Australia: a U - Pb LA-ICPMS, SHRIMP and Sm - Nd isotope study. *Australian Journal of Earth Sciences* **55**, 703-719.

WILSON S. A., RIDLEY W. I. & KOENIG A. E. 2002. Development of sulfide calibration standards for the laser ablation inductively-coupled plasma mass spectrometry technique. *Journal of Analytical Atomic Spectrometry* **17**, 406-409.

WINDERBAUM L., CIOBANU C. L., COOK N. J., PAUL M., METCALFE A. & GILBERT S. 2012. Multivariate Analysis of LA-ICP-MS Trace Element Dataset for Pyrite. *Mathematical Geosciences* **44**, 823-842.

WOODHEAD J. D., HELLSTROM J., HERGT J. M., GREIG A. & MAAS R. 2007. Isotopic and elemental imaging of geological materials by laser ablation inductively coupled plasma-mass spectrometry. *Geostandards and Geoanalytical Research* **31**, 331-343.

APPENDIX A: DESCRIPTIVE LIST OF ALL SAMPLES COLLECTED

Sample Number	Description	Interval of Sample (m)	Original Sample Number
KS-1	Garden variety Amphibolite	31.45-31.6	71711
KS-2	Low Cu amphibolite	49.1-49.25	71712
KS-3	Epidote Amphibole schist	90.1-90.2	71713
KS-4	Weakly foliated amphibolite	96.07-96.12	71714
KS-5	Amphibolite containing minor garnet	163.25-163.4	71715
KS-6	Semi-massive sulphide Po (50%) Py (8%) Cpy (1%)	184.45-184.48	71716
KS-7	Carbonate altered amphibolite	196.9-197	71717
KS-8	Carbonate-chlorite-magnetite Amphibolite	211-211.15	71718
KS-9	Semi-massive sulphide Po (30%) Py (30%) Cpy (1%)	215-214.17	71719
KS-10	"Clast" amphibole-magnetite in semi-massive sulphide	222-222.13	71720
KS-11	Semi-massive sulphide Po (45%) Py (12%) Cpy (3%)	234.7-234.85	71721
KS-12	Semi-massive sulphide Py (40%) Po (19%) Cpy (1%)	231.19-241.35	71722
KS-13	Amphibolite (base sulphides in alteration)	243.95-244.1	71723
KS-14	Garden variety Amphibolite	271.15-271.3	71724
KS-15	Low Cu Amphibolite	23.3-23.5	71725
KS-16	Average Cu Amphibolite	55.1-55.3	71726
KS-17	Amphibolite/Carbonate alteration zone contact	112.2-112.5	71727
KS-18	Epidote Amphibole schist	129.6-129.77	71728
KS-19	Weakly foliated amphibolite	141.4-141.55	71729
KS-20	Low Cu Amphibolite	161.7-161.85	71730
KS-21	Amphibolite containing minor garnet	175.17-175.25	71731
KS-22	Amphibolite containing sulphides	187.05-187.2	71732
KS-23A	Garnet-rich amphibolite (60% garnet)	203.8-204	71733
KS-23B	Garnet-rich amphibolite (60% garnet)	203.8-204	71733
KS-24	Mela Amphibolite	213.5-213.67	71734
KS-25A	Semi-massive sulphide Garnet and Mela Amphibolite clasts containing sulphides	220.95-221.15	71735

KS-25B	Semi-massive sulphide Garnet and Mela Amphibolite clasts containing sulphides	220.95-221.15	71735
KS-26	amphibolite-garnet-quartz rich 1% sulphides	228.85-229	71736
KS-27	Amphibolite	239.95-240.05	71737
KS-28	Semi-massive sulphides Po (40%) Py (17%) Cpy (2-3%)	246.1-246.27	71738
KS-29	Semi-massive sulphides Py (34%) Po (5%) Cpy (1%)	258.1 - 258.2	71739
KS-30	Semi-massive sulphides Po (38%) Po (10%) Cpy (2%)	264.45-264.7	71740
KS-31	Semi-massive sulphides Py (40%) Po (8%) Cpy (2%)	274.15-274.32	71741
KS-32	Semi-massive sulphides Po (20%) Py (12%) Cpy (3%)	291.15-291.35	71742
KS-33	Semi-massive sulphides Py (25%) Po (14%) Cpy (1%)	299.9-300.05	71743
KS-34	Amphibolite	303.55-303.75	71744
KS-35	Amphibolite	354.95-355.05	71745
KS-36	Garnet-rich amphibolite	340.4-340.5	71746

APPENDIX B: SAMPLING AND ANALYTICAL METHODOLOGY

Sample selection

To properly study and fully understand the Basil Cu-Co deposit, representative samples needed to be collected from diamond drill core. This sample suite formed the basis of the petrographic observations, SEM, LA-ICP-MS and EPMA analysis and whole rock geochemical work undertaken in this study to expand knowledge on Basil. Two drill holes were selected (LB027DD and LB035DD). Both are NQ-diameter (47.6 mm) diamond drill holes that intersect the area of mineralisation. Extensive logging was then undertaken, which included descriptions of rock types, rock-forming minerals, sulphides and any other comments that could not be documented elsewhere on the log sheet. Whist logging the drill holes, anything of visual interest was photographed and commented on in a separate note book, in case needed for reference later.

When the drill log was completed, 36 samples of interest were selected for polished blocks (15 samples) or thin sections (21 samples). At least one sample of every rock type was selected for a thin section, making sure to select an area on the drill core that was representative of the entire rock type and selecting the same units from both drill cores for later comparison. In most cases, multiple samples of every rock type were selected for thin sections and polished blocks. Samples from the zones of mineralisation were prepared as polished blocks, in this case, each type of mineralisation was selected (i.e. pyrrhotite-rich, pyrite-rich and even percentage zones), again ensuring that each sample was representative of its description and rock type.

To preserve the core for future reference, only half core was taken and samples were no sample exceeded 20 cm in length. The core was then photographed on both sides with a scale, both wet and dry, and, and the core was also photographed with reference to where the thin sections and polished blocks were from. The core samples were then sent to Pontifex & Associates to be prepared as 1” x 3” thin sections and 1” circular polished blocks.

Optical microscopy

All polished blocks were examined under reflected light using a Nikon Petrographic microscope, which has a magnification of up to 50x, located at Adelaide Microscopy. Emphasis was on photodocumentation, mineral identification and noting the texture of the sulphides in respect to the gangue minerals and any crystal morphologies expressed by the sulphides. By viewing these optically first, a better understanding of these samples can be gained, facilitating location of areas of interest on other instrumentation later.

All thin sections were examined under polarised and cross-polarised light, noting mineralogy, textures. Photomicrographs were taken to document aspects of interest.

XL30 (Scanning Electron Microscope)

SEM work was carried out using a Phillips XL30 SEM instrument at Adelaide Microscopy, equipped with an energy-dispersive X-ray spectrometer (EDAX) and back-scatter electron (BSE) detector. The SEM was operated at 20eV accelerating voltage, spot size 4 and beam size 4 μm. BSE imaging allowed for the observation of sulphides and other minerals on the micro-scale. The emphasis here was to focus on the pyrite and whether there was any evidence of compositional zonation, which would indicate more than one generation of pyrite. When looking through each sample, photographic images were taken of textures among the sulphides, the pyrite crystals and of any minerals that had not been identified during optical microscopy. To help with identification of minerals, spots were placed on minerals and semi-quantitative EDAX data were obtained. Photos that included EDAX spots

were saved in a PowerPoint presentation for future reference, with a "x" marking the location of the analytical spot.

Laser-Ablation Inductively-coupled Plasma Mass Spectrometry (LA-ICP-MS)

LA-ICP-MS spot analysis of pyrite and pyrrhotite was made using the Agilent HP-7500 Quadrupole ICPMS instrument at Adelaide Microscopy. The instrument is equipped with a New Wave UP-213 Nd:YAG laser ablation system equipped with MeoLaser 213 software. Data reduction was performed using Glitter software (GEMOC 2005).

Samples with suitable grains of pyrite and pyrrhotite were ablated, the pyrite was targeted to find out what trace elements were present and the pyrrhotite was targeted to find out what trace elements were present. Analyses were made with spot size diameter of 40 μm. The laser system was operated at pulse rates of 5 Hz and 75% power level; laser energy was typically 6-9 J/cm-2, giving an ablation rate of approx. 1.5μm/sec. The following isotopes were monitored ^{29}Si, ^{33}S, ^{34}S, ^{43}Ca, ^{51}V, ^{52}Cr, ^{55}Mn, ^{57}Fe, ^{59}Co, ^{60}Ni, ^{56}Cu, ^{66}Zn, ^{69}Ga, ^{75}Ag, ^{82}Se, ^{95}Mo, ^{107}Ag, ^{111}Cd, ^{115}In, ^{118}Sn, ^{121}Sb, ^{125}Te, ^{137}Ba, ^{184}W, ^{193}Ir, ^{197}Au, ^{202}Hg, ^{205}Tl, ^{208}Pb, ^{209}Bi. The analysis time for each sample was 90 seconds (20 second measurement of background with the laser off, 10 seconds with the laser on and the shutter closed and a 60 second analysis with the laser on).

Calibration was performed using the MASS-1 trace element sulphide standard (Wilson *et al.* 2002). The raw analytical data for each spot analysis is plotted as a line graph and the integration times for background and sample signal selected. The smooth button was also used, helping to select a more representative signal. Standards were run after each separate sample of unknowns and were converted to concentration values using known values of Fe in both pyrite and pyrrhotite.

LA-ICP-MS element mapping

LA-ICP-MS mapping was conducted using a Resonetics M-50-LR 193-nm Excimer laser microprobe coupled to an Agilent 7700cx Quadrupole ICP-MS housed at Adelaide Microscopy, University of Adelaide. The M-50 utilises a two-volume ablation cell designed by Laurin Technic Pty. Ablation was performed in an atmosphere of UHP He (0.71/min), and upon exiting the cell the aerosol sell is mixed with Ar (0.93 l/min) immediately after the ablation cell, after which the mix is passed through a pulse-homogenising device or "squid" prior to direction instruction into the torch. The ICPMS was optimised daily to maximise sensitivity on isotopes of the mass range of interest, while keeping production of molecular oxide species (i.e., ^{232}Th^{16}O/^{232}Th) and doubly-charged ion species (i.e., ^{140}Ce^{2+}/^{140}Ce+) as low as possible, and usually <0.2%.

Images were performed by ablating sets of parallel line rasters in a grid across the sample. A beam size of 10 μm and a scan speed of 16 μm/s was chosen for the first garnet grain and a beam size of 14 μm and a scan speed of 20 μm/s was chosen for the second garnet grain, which resulted in the desired sensitivity of the elements of interest, and adequate spatial resolution for the study. The spacing between the lines was 10 μm for the first garnet grain and 14 μm for the second garnet grain, to match the size of the laser beam used. The effect of redeposition during mapped was minimised by pre-ablating each line prior to its main data collection run. A laser repetition of 10 Hz was selected at a constant energy output of 100 mJ, resulting in an energy density of ~6 J/cm2 at the target. A set of 28 isotopes were analysed with dwell times for all masses set to 0.003 s, resulting in a total swipe time of ~0.08 s. A 30 second background acquisition was acquired at the start of every raster, and to allow for cell wash-out, gas stabilisation, and computer processing, a delay of 15 s was used after each line. Identical rasters were done on the standard glass NIST-610 at the start and end of a mapping run.

Images were compiled and processed using the program Iolite developed by the Melbourne Isotope Group at Melbourne University (Woodhead *et al.* 2007). Iolite is an open-source software package for processing ICP-MS data, and is an add-in for the data analysis program Igor developed by WaveMetrics. A typical mapping run was analysed over 9-12h session, in which significant instrument drift could occur. To correct for this, standards were analysed immediate before and after the run to assess drift and if present, was corrected for by applying a linear fit between the two sets of standards. Following this, for each raster and every element, the average background was subtracted from its corresponding raster, and the rasters were compiled into a 2-D image displaying combined background/drift corrected intensity for each element.

Electron Microprobe Analysis (EPMA)

Quantitative compositional data for sulphides (pyrrhotite, sphalerite and pyrite) and garnet in samples from both drill holes using a CAMECA SX-51 instrument with wavelength-dispersive spectrometers at Adelaide Microscopy. The instrument was operated at an accelerating voltage of 20 kV and a beam current of 20 nA. The following elements were analysed using the following X-ray lines and standards.

Whole rock geochemistry

Samples were selected from both drill holes that were representative of all the different rock units logged in LB027DD and LB035DD. Each sample was approximately a quarter of the drill core selected, to give the best sample representation. Analysis was undertaken at the Genalysis laboratory (Adelaide). Several different analytical methodologies were followed to obtain optimal results. These were:

(1) Ag, As, Bi, Cd, Co, Cs, Ge, In, Li, Mo, Nb, Re, Sb, Se, Te and Tl were analysed using the method 4A/MS (Multi-acid digest including HF, HNO_3, $HClO_4$ and HCl in Teflon tubes and analysed by Inductively-Coupled Plasma Mass Spectrometry).

(2) Al, Ca, Cr, Fe, K, Mg, Mn, Na, P, Sc, Si, Ti and V were analysed using the method FB6/OE (Lithium metaborate/tetraborate fusion and analysed by Inductively Coupled Plasma Optical (Atomic) Emission Spectrometry). The corresponding oxides (Al_2O_3, CaO, Fe_2O_3, K_2O, MgO, MnO, Na_2O, P_2O_5, SiO_2 and TiO_2) were subsequently calculated.

(3) Ba, Be, Ce, Dy, Er, Eu, Ga, Gd, Hf, Ho, La, Lu, Nd, Pr, Rb, Sm, Sn, Sr, Ta, Tb, Th, Tm, U, W, Y, Yb and Zr were analysed using the method FB6/MS (Lithium metaborate/tetraborate fusion and analysed by Inductively-Coupled Plasma Mass Spectrometry).

(4) Cu, Ni, Pb, S and Zn were analysed using the method 4A/OE (Multi-acid digest including HF, HNO_3, $HClO_4$ and HCl in Teflon tubes and analysed by Inductively-Coupled Plasma Optical (Atomic) Emission Spectrometry).

A calculation was applied to the raw whole rock geochemical data to correct for the amount of sulphide present in the zone of mineralisation that effectively dilutes elements not present in the sulphides. The modal percentage of sulphide was recorded during initial logging of the two holes. All elemental assay values were then multiplied by this percentage within the zone of mineralisation. This brings the silicates up to 100% concentration and the values are no long diluted by the sulphides present.

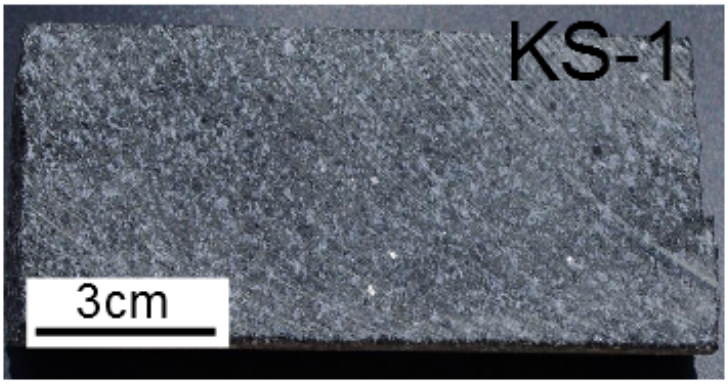
KS-1
3cm

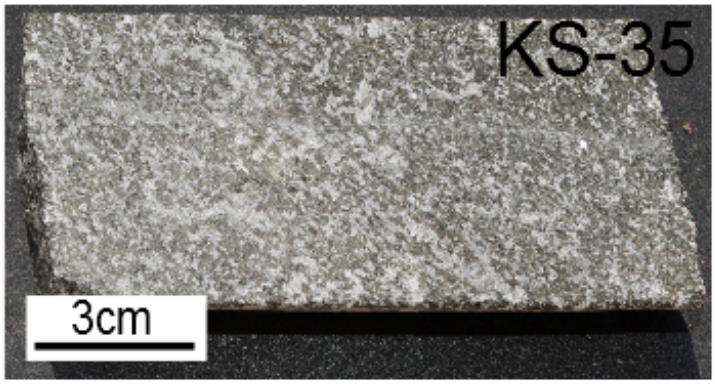
KS-35
3cm

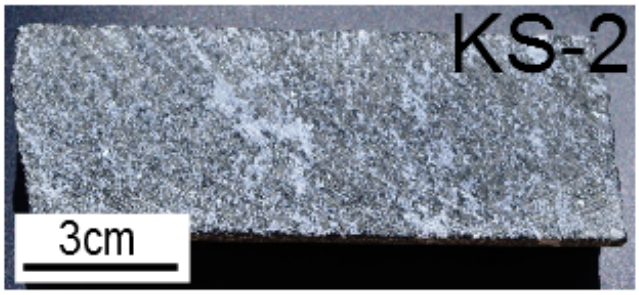
KS-2
3cm


KS-15
3cm

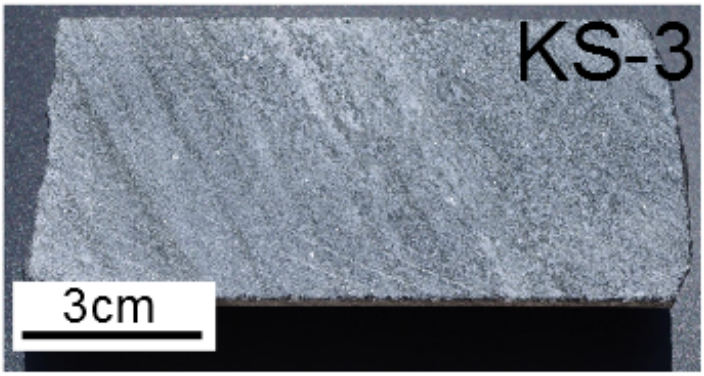
KS-3
3cm

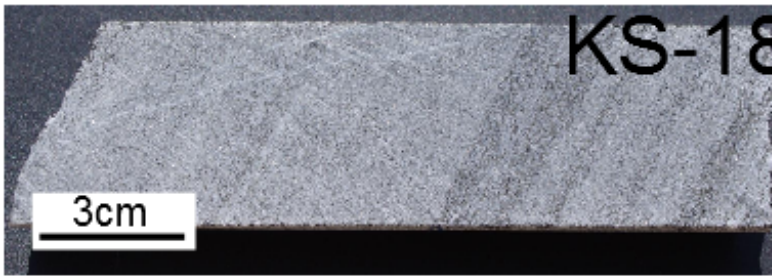
KS-18
3cm

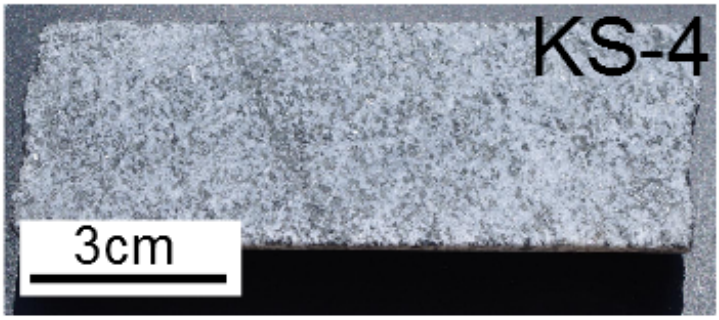
KS-4
3cm

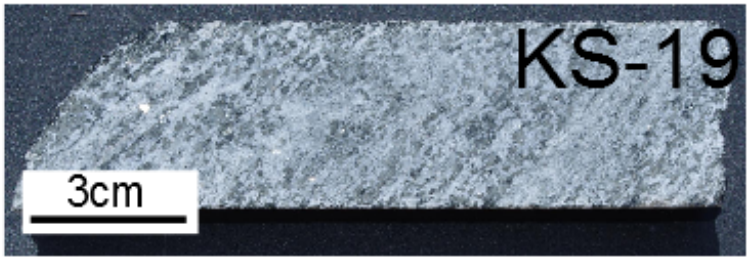
KS-19
3cm

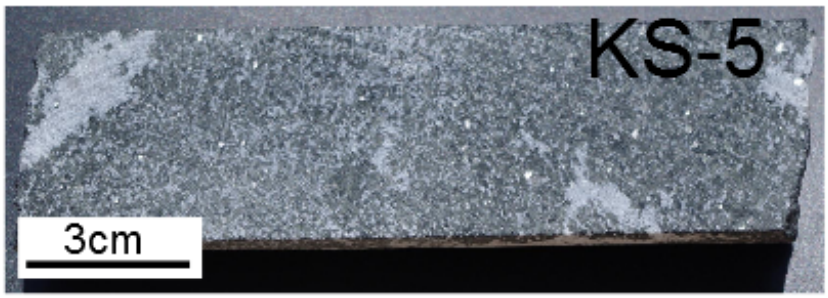
KS-5
3cm

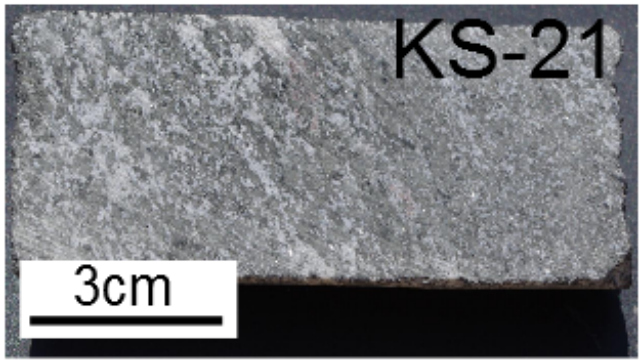
KS-21
3cm

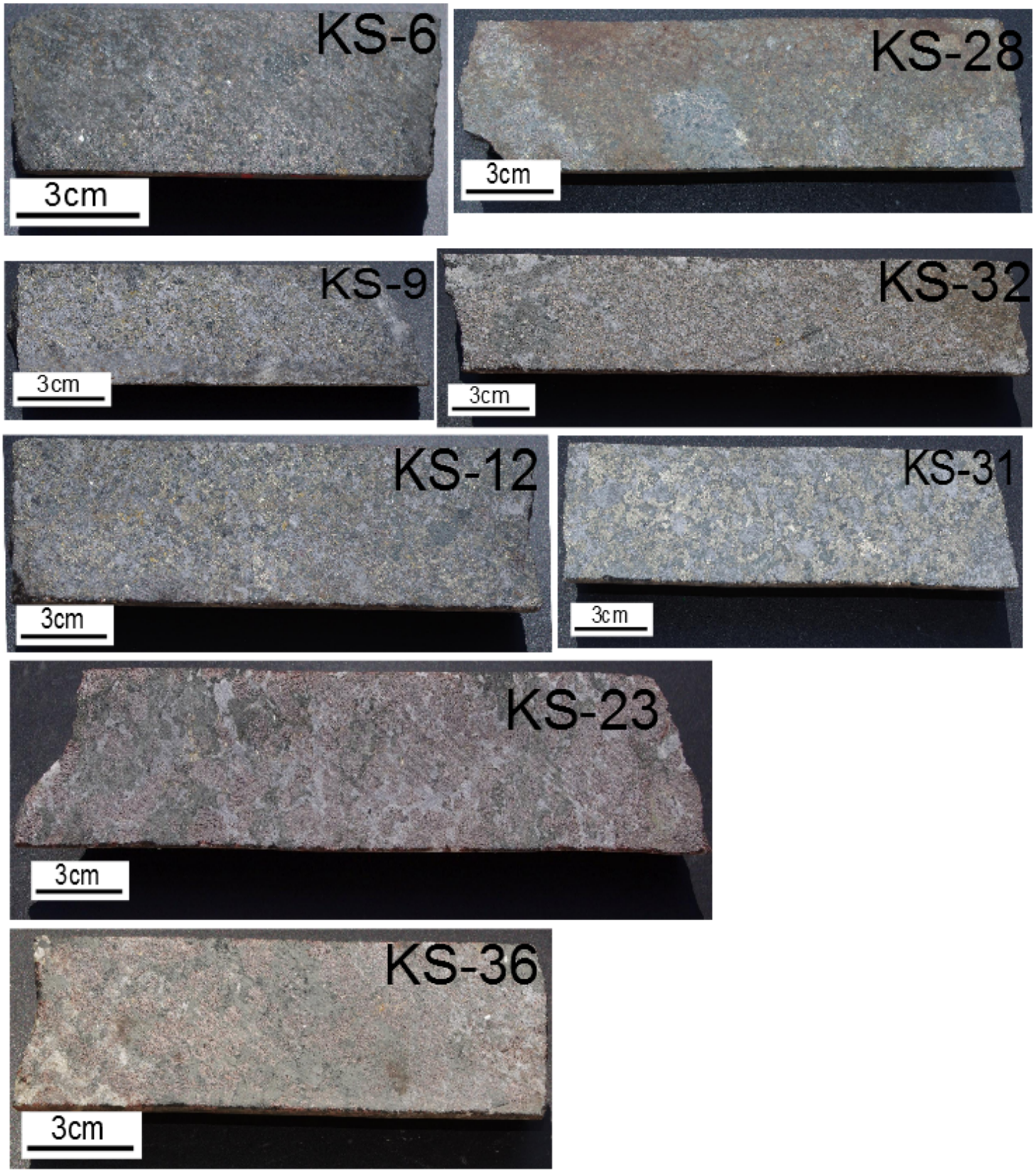

Photographs of the samples that were selected from each drillhole and used as the representative samples for the whole rock geochemistry analysis.

Rock unit	Sample number
Garden Variety Amphibolite	KS-1 and KS-35
Low Cu Amphibolite	KS-2 and KS-15
Epidote Amphibole Schist	KS-3 and KS-18
Weakly Foliated Amphibolite	KS-4 and KS-19
Amphibolite with minor Garnet	KS-5 and KS-21
Pyrrhotite-rich semi-massive sulphide	KS-6 and KS-28
Pyrrhotite-pyrite semi-massive sulphide	KS-9 and KS-32
Pyrite-rich semi-massive sulphide	KS-12 and KS-31
Garnet-rich Amphibolite	KS-23 and KS-36

Table displaying the various units that were analysed and where each representative sample was selected from.

APPENDIX C: PHOTOGRAPHS OF CORE FROM BASIL

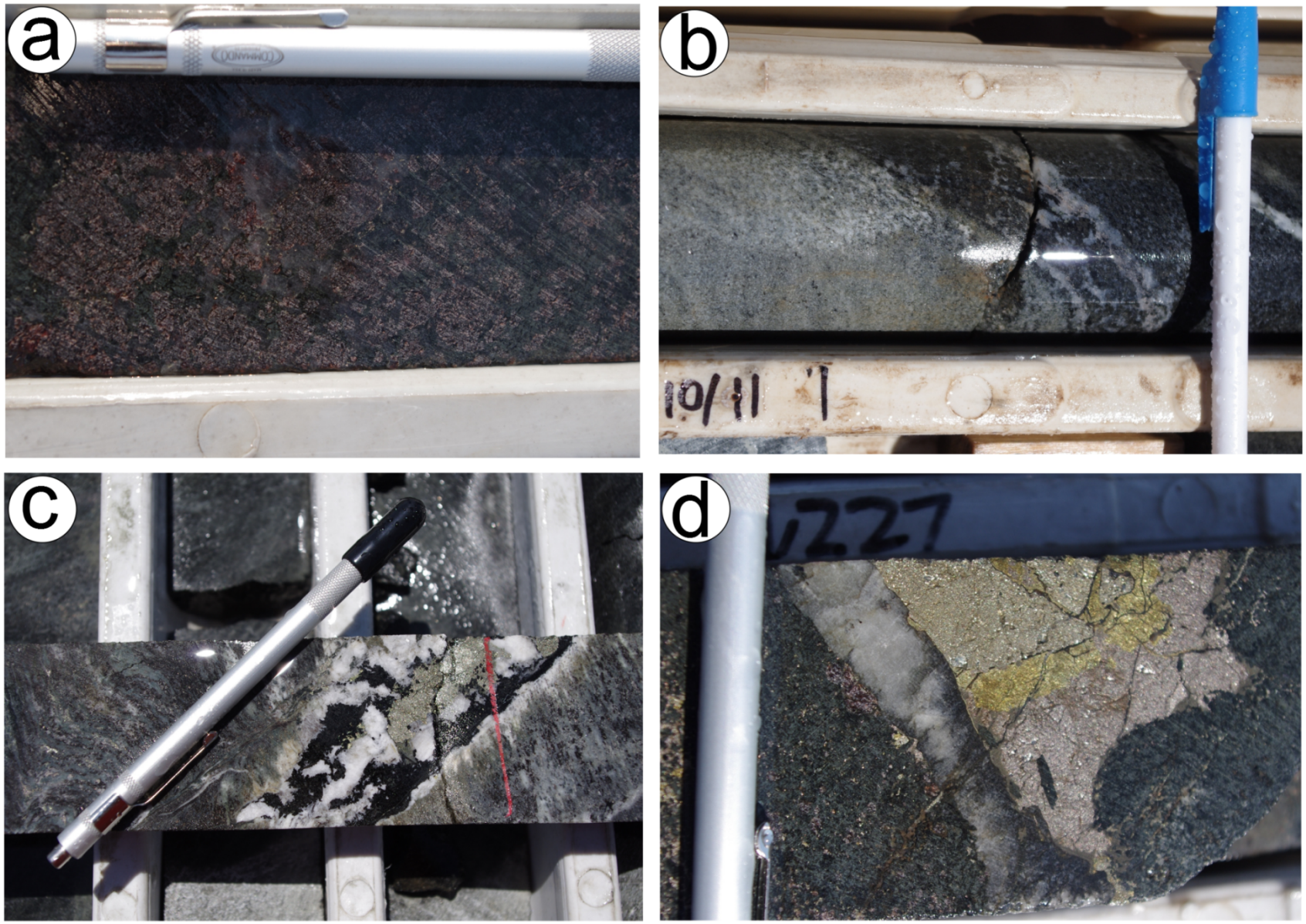

(a) Displays the garnet-rich zone found in both drill holes. (b) Displays the boundary between the epidote hornblende schist (left) and the amphibolite (right). (c) Displays a quartz vein that hosts magnetite (black) and sulphide (metallic), chlorite alteration (green) can be observed on both sides. (d) Displays the different colours of the three sulphide minerals that occur at Basil. Gold (chalcopyrite), silver-gold (pyrite) and pink-bronze (pyrrhotite).

APPENDIX D: REFLECTED LIGHT PHOTOMICROGRAPHS AND BACK SCATTER ELECTRON IMAGES

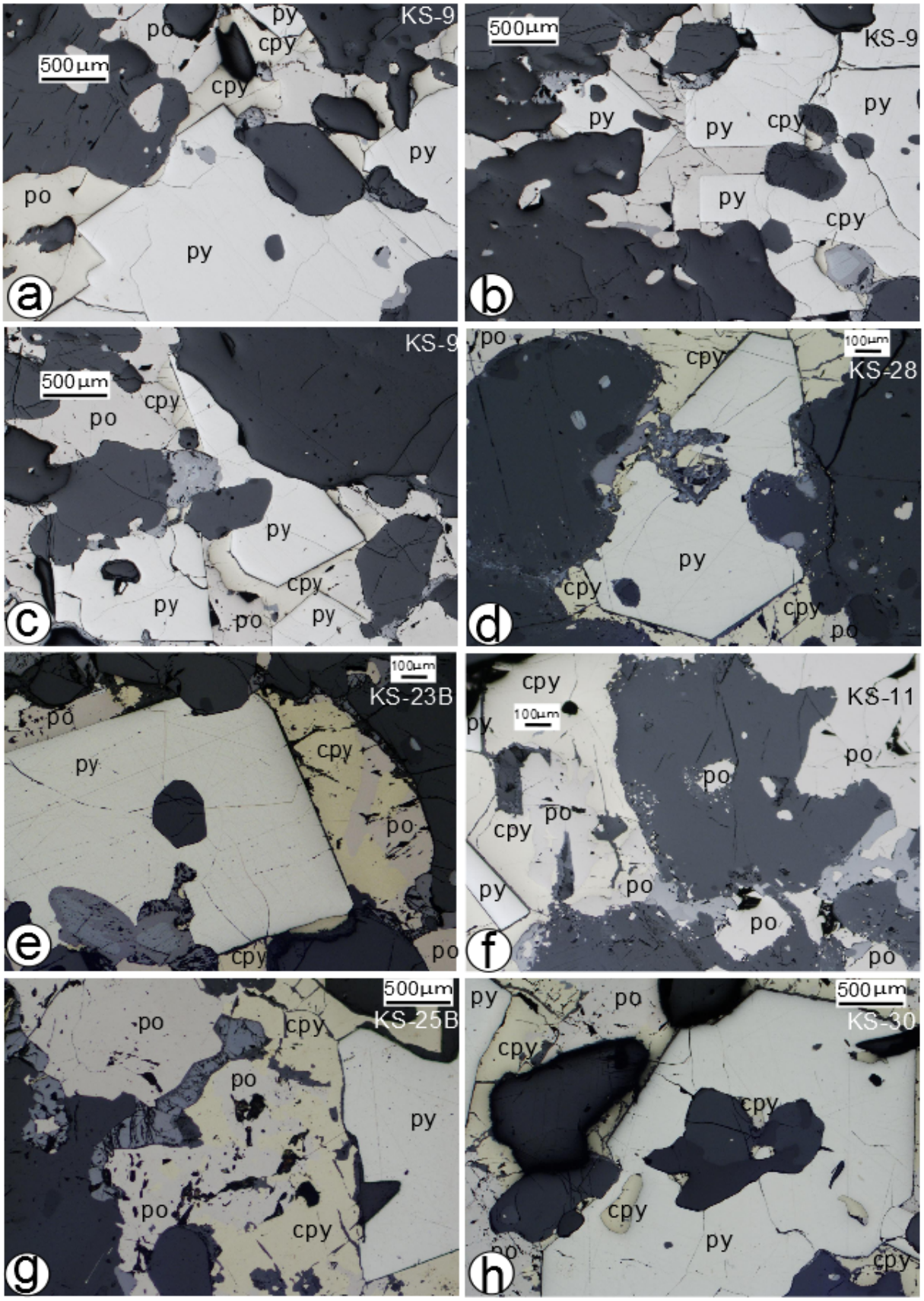

Reflected light photomicrographs illustrating relevant ore textures. (a-e) Typical euhedral pyrite.(f-g) Characteristic intergrowths of chalcopyrite and pyrrhotite in the matrix enclosing the pyrite. Abbreviations: cpy=chalcopyrite, po=pyrrhotite, py=pyrite.

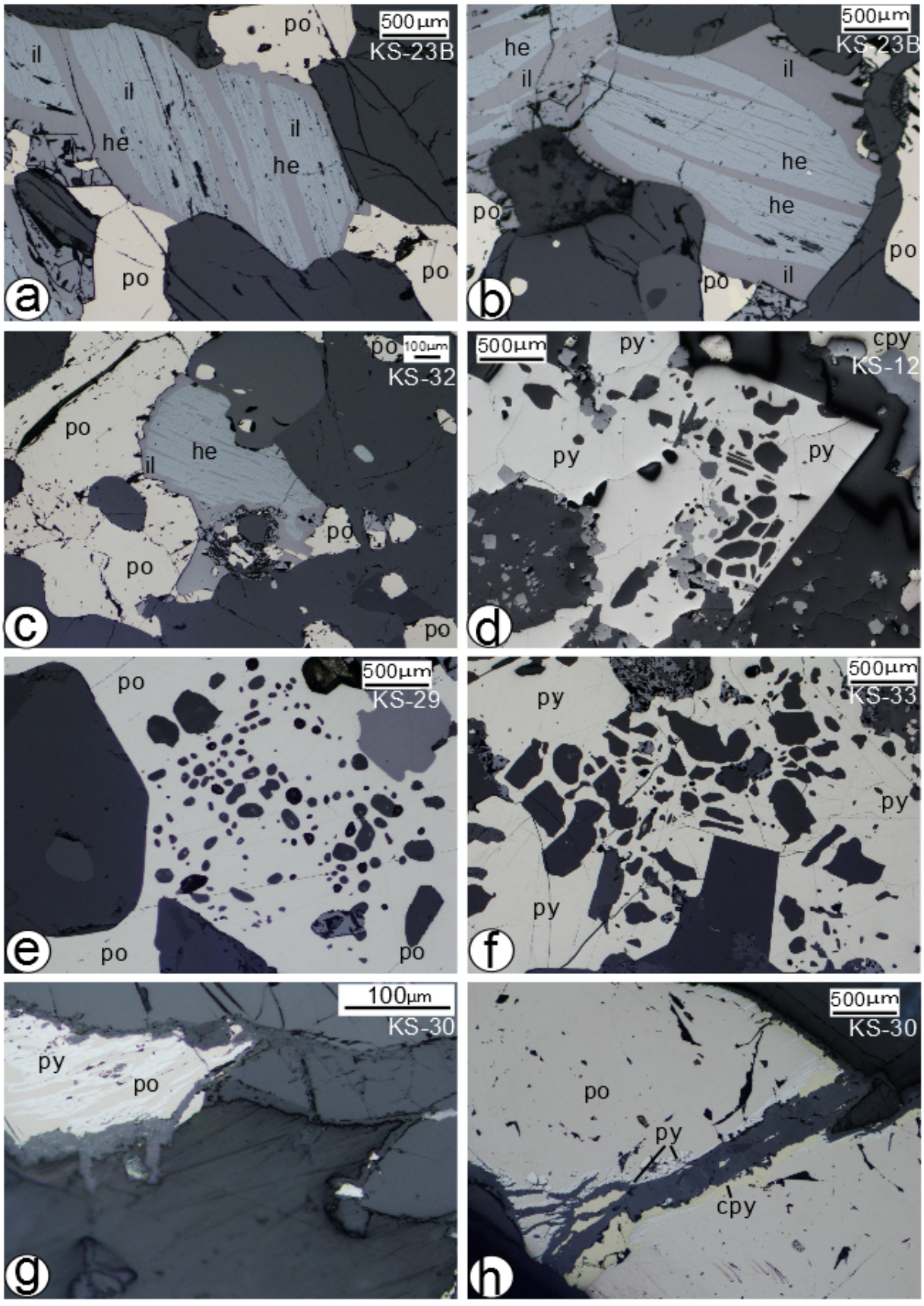

Reflected light photomicrographs illustrating relevant ore textures. (a-c) Exsolution of two iron-titanium oxides (hematite and ilmenite). (d-f) Gangue suspended in pyrite and pyrrhotite matrix.(g-h) secondary pyrite. Abbreviations: cpy=chalcopyrite, he=hematite, il=ilmenite, po=pyrrhotite, py=pyrite.

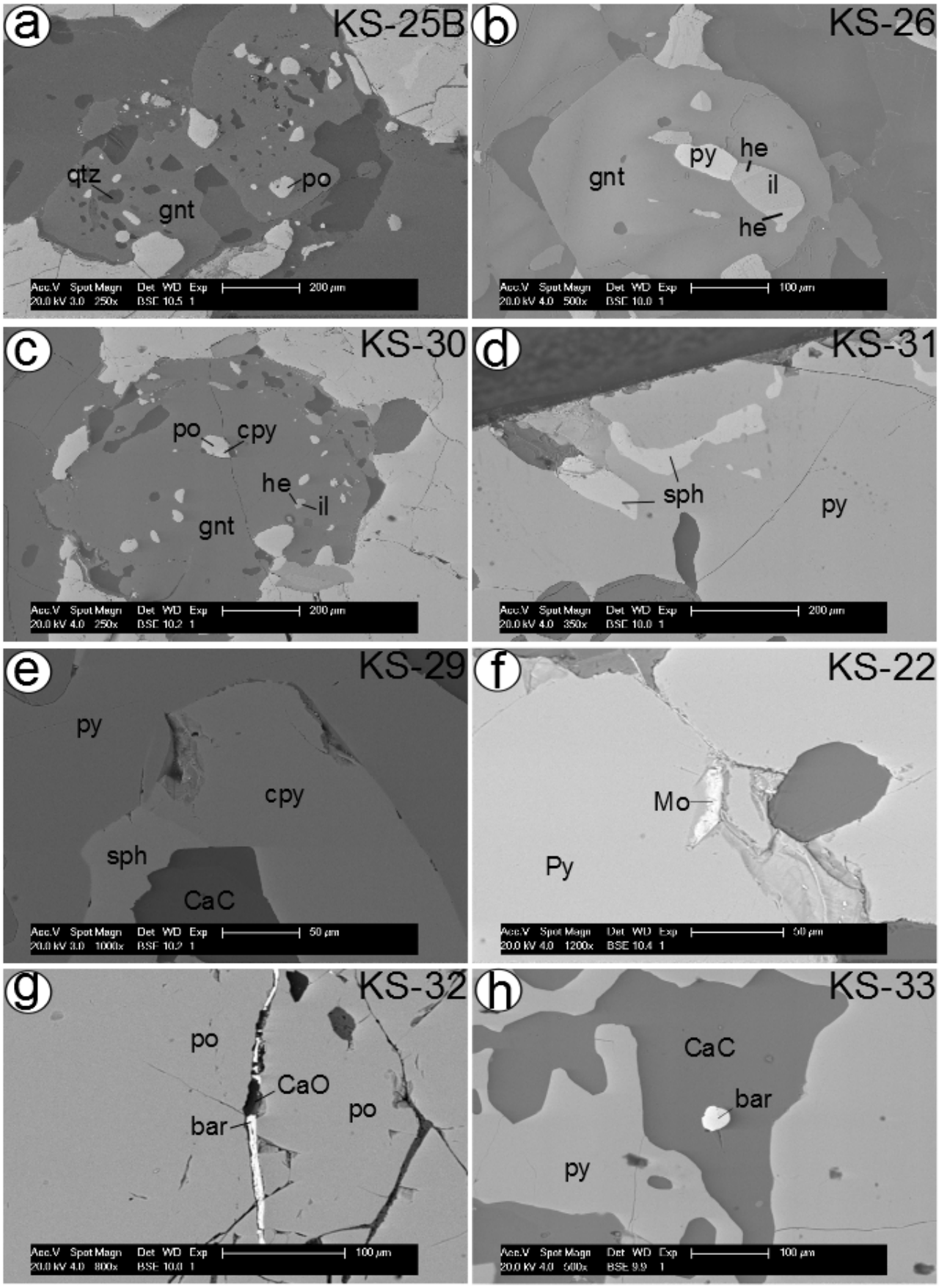

Back scatter electron images illustrating relevant mineral interactions. (a-c) Inclusions of sulphide in garnet. (d-e) Occurrence of sphalerite. (f) Occurrence of molybdenite. (g-h) Occurrence of baryte. Abbreviations: bar=baryte, CaO=calcium carbonate, cpy=chalcopyrite, gnt-garnet, he=hematite, il-ilmenite, mo=molybdenite, po=pyrrhotite, py=pyrite, sph=sphalerite.

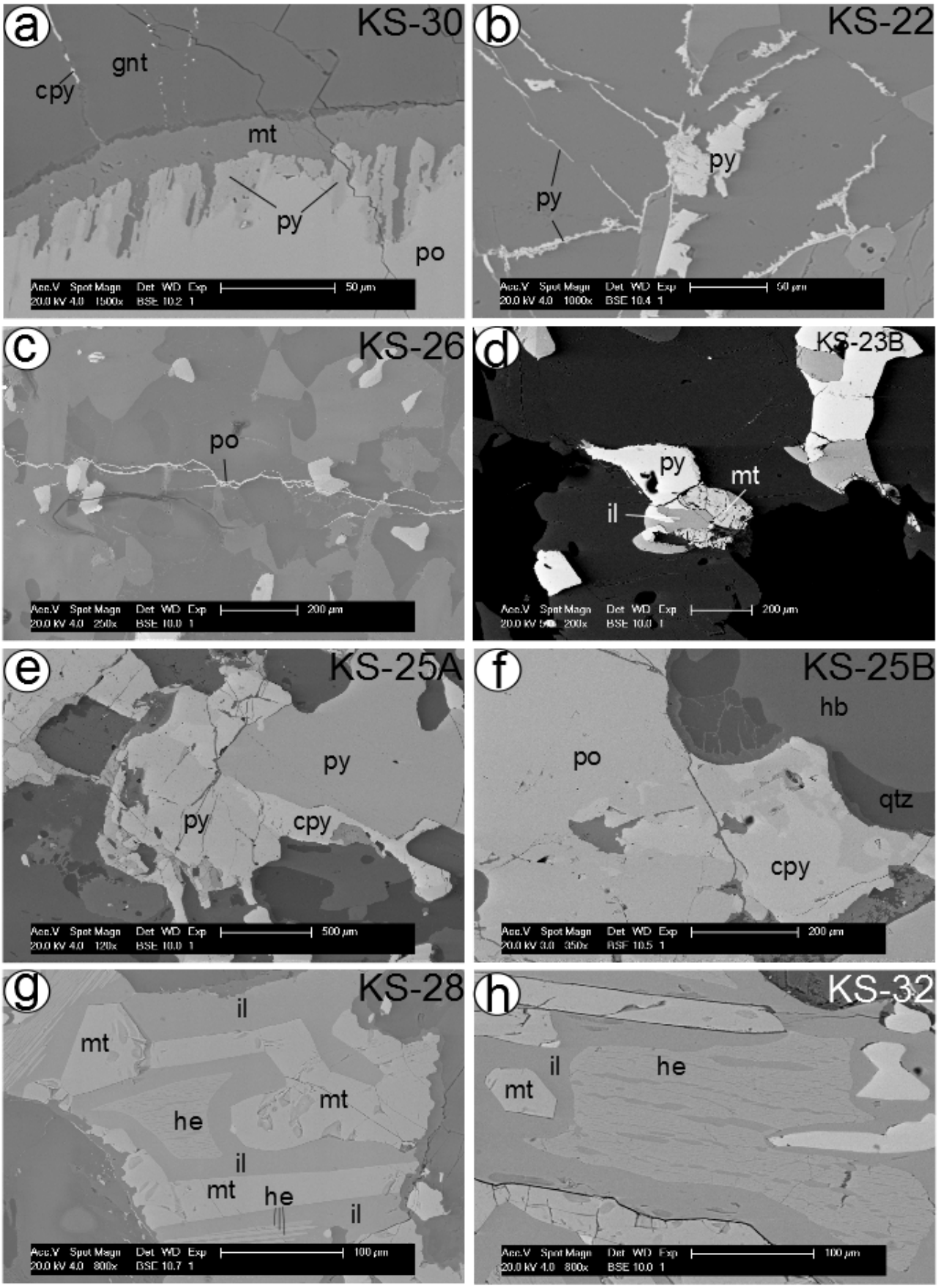

Back scatter electron images illustrating relevant mineral interactions. (a) Secondary pyrite. (b-c) Sulphide veining. (d) Occurrence of magnetite. (e-f) Characteristic intergrowths of chalcopyrite and pyrrhotite in the matrix enclosing the pyrite. (g-h) Exsolution of two iron-titanium oxides (hematite and ilmenite). Abbreviations: cpy=chalcopyrite, gnt=garnet, hb=hornblende, he=hematite, il=ilmenite, mt=magnetite, po=pyrrhotite, py=pyrite, qtz=quartz.

APPENDIX E: FULL DATASET OF LA-ICP-MS ANALYSIS OF PYRITE GRAINS

Element	V	Cr	Mn	Co	Ni	Cu	Zn	Se	Mo	Ag	Sb	Te	Au	Hg	Tl	Pb	Bi
KS-25b																	
KS-25b_01	0.06	0.58	0.56	5094	11	1.7	<1.7	14	<0.11	<0.04	<0.06	<0.59	<0.06	0.24	<0.02	0.04	0.31
KS-25b_02	0.32	<0.59	54	945	373	0.79	<1.5	39	0.25	0.37	<0.09	<0.94	<0.09	<0.29	<0.03	0.13	0.05
KS-25b_03	0.07	0.36	0.35	6754	11	0.78	<0.7	14	<0.09	<0.03	<0.05	<0.48	<0.04	<0.15	<0.01	0.05	0.01
KS-25b_04	0.05	<0.32	0.67	5784	7.4	0.25	0.5	10	<0.09	<0.03	<0.05	<0.47	<0.05	0.19	<0.01	0.03	<0.01
KS-25b_05	<0.12	<2.0	<1.0	5064	7.2	<0.36	<0.4	<7.6	<0.02	<0.02	<0.01	<0.14	<0.00	0.06	<0.00	0.04	<0.00
KS-25b_06	<0.12	<1.4	3.4	3601	5.5	1.0	<0.3	<3.7	<0.02	0.02	<0.01	<0.10	<0.00	0.06	<0.00	0.03	0
KS-25b_07	<0.12	<1.6	4	5087	6.5	<0.50	<0.3	9	<0.02	<0.02	<0.01	<0.01	<0.00	0.07	<0.00	0.02	0
KS-25b_08	<0.21	<2.0	4.2	6434	7.7	<0.53	<0.4	6.3	<0.04	<0.02	0.01	<0.06	<0.00	0.07	<0.00	0.04	<0.00
mean n=8	**0.13**	**1.1**	**8.4**	**4845**	**54**	**0.74**	**0.73**	**13**	**0.08**	**0.67**	**0.03**	**-**	**-**	**0.14**	**-**	**0.05**	**0.05**
KS-11																	
KS-11_01	0.07	<0.56	0.67	1741	5.5	0.63	1.3	<6.4	<0.09	<0.03	<0.04	<0.38	<0.05	<0.15	<0.01	0.03	0.015
KS-11_02	<0.04	<0.47	0.75	2508	11	0.41	<0.75	5.6	<0.09	<0.03	0.05	<0.41	<0.04	<0.15	<0.01	0.06	<0.01
KS-11_03	<0.05	<0.56	0.56	2464	13	1.2	<0.89	<5.5	<0.12	<0.04	<0.05	<0.59	<0.05	0.2	<0.02	0.04	<0.02
KS-11_04	0.05	<0.51	0.81	1762	11	0.83	<0.72	<4.5	<0.11	<0.04	<0.06	<0.62	<0.07	<0.19	<0.02	0.11	<0.02
KS-11_05	0.06	<0.42	0.27	4058	13	0.37	1.6	<3.5	<0.09	<0.03	0.15	<0.48	<0.05	<0.16	<0.02	0.05	<0.01
KS-11_06	9.1	<0.38	2.1	4112	10	1	<0.49	5.5	<0.10	<0.03	0.06	<0.44	<0.05	0.19	<0.01	0.69	1.9
KS-11_07	<0.14	<2.6	3	500	26	2.9	<0.50	<9.9	0.02	0.14	<0.01	0.21	<0.00	0.07	<0.00	0.85	3.6
KS-11_08	<0.18	<1.9	3.3	2244	11	1.5	<0.46	<5.7	0	<0.02	<0.01	<0.13	0	0.04	<0.00	0.12	<0.00
KS-11_09	<0.16	<1.8	5.8	2334	16	0.47	<0.63	<4.6	<0.03	<0.02	<0.01	<0.12	<0.00	0.1	0	0.02	<0.00
KS-11_10	<0.27	<2.1	5	964	8.9	1.3	<0.57	<4.6	<0.05	<0.03	0.01	0.1	<0.00	0.1	<0.00	0.10	0.01
KS-11_11	<0.26	<2.1	3.1	3988	8.9	2.4	<0.74	7.3	<0.05	<0.03	<0.01	<0.06	<0.00	0.12	<0.00	0.13	0
KS-11_12	<0.27	<2.2	5.5	2364	14	0.93	0.93	6.3	<0.03	0.03	0.01	<0.12	<0.00	0.09	0	0.21	0
mean n=12	**0.89**	**-**	**2.6**	**2420**	**12**	**1.17**	**0.73**	**5.8**	**0.64**	**0.04**	**0.04**	**0.30**	**0.03**	**0.13**	**0.01**	**0.20**	**0.47**

Element	V	Cr	Mn	Co	Ni	Cu	Zn	Se	Mo	Ag	Sb	Te	Au	Hg	Tl	Pb	Bi
KS-09																	
KS-09_01	0.05	<1.7	<0.70	3605	3.5	0.95	<0.42	<11	<0.03	<0.02	<0.02	<0.15	0.02	0.24	<0.01	0.07	<0.01
KS-09_02	0.04	<0.73	<0.34	4780	5.0	0.66	0.28	7.9	<0.04	0.06	0.06	<0.20	<0.03	<0.11	<0.01	0.38	0.6
KS-09_03	0.09	<0.65	<0.32	6222	8.4	1.7	<0.35	8.1	<0.07	<0.03	<0.04	<0.29	<0.04	<0.13	<0.01	0.24	<0.01
KS-09_04	0.06	<0.63	0.84	4834	3.9	1.6	0.49	<7.4	<0.10	<0.04	<0.05	<0.41	<0.05	<0.16	<0.02	0.82	<0.02
KS-09_05	0.05	<0.50	0.88	5457	7.3	1.4	0.92	13	<0.09	0.03	<0.04	<0.43	<0.05	<0.16	<0.01	0.21	<0.02
KS-09_06	<0.04	<0.48	0.39	4094	4.5	0.85	0.65	11	<0.11	<0.04	<0.05	<0.42	<0.06	<0.17	<0.02	0.15	<0.02
KS-09_07	<0.21	<1.9	5.1	4028	4.4	0.57	<1.5	13	<0.03	<0.02	<0.01	<0.10	<0.00	0.18	<0.00	0.08	<0.00
KS-09_08	<0.21	<2.0	5.2	2990	3.8	1.0	<1.2	8.4	0.04	<0.03	<0.01	<0.07	<0.00	0.16	0	0.07	0
KS-09_09	<0.25	<2.3	6.2	7384	4.4	0.94	<1.2	16	<0.03	<0.03	<0.01	<0.08	0.01	0.18	<0.00	0.18	0.01
KS-09_10	<0.29	<2.6	5.1	4701	6.9	2.1	<1.2	11	<0.04	<0.04	<0.02	<0.09	0	0.1	<0.00	0.05	<0.00
KS-09_11	0.63	<2.9	6.0	5109	5.5	2.7	<1.2	8.7	<0.05	1.2	0.29	1.1	<0.01	0.21	0.06	5.7	9.2
KS-09_12	<0.53	<3.1	6.6	5466	6.4	3.5	1.1	17	<0.10	<0.04	0.09	0.14	<0.01	0.24	0	0.32	0
mean n=12	**0.21**	**-**	**3.1**	**4889**	**5.3**	**1.5**	**0.87**	**11**	**0.06**	**0.13**	**0.06**	**0.29**	**0.01**	**0.17**	**0.01**	**0.69**	**0.78**
KS-30																	
KS-30_01	<0.03	<0.74	<0.45	763	13	0.91	0.28	<9.2	<0.04	<0.03	<0.03	<0.24	<0.03	<0.12	<0.01	0.02	<0.01
KS-30_02	<0.04	<0.62	<0.38	2322	11	1.9	1.1	15	<0.09	<0.04	<0.05	<0.33	<0.05	<0.16	<0.01	0.18	0.02
KS-30_03	0.06	<0.50	0.53	302	41	0.45	4.1	<7.1	<0.11	<0.04	<0.05	<0.37	<0.06	0.17	<0.02	0.10	<0.02
KS-30_04	<0.24	<7.3	<3.3	1274	21	1.4	<0.42	<18	0.02	<0.03	0.01	0.03	<0.00	0.16	0	0.19	0
KS-30_05	<0.13	<1.9	3.4	5166	3.4	1.9	1.0	<3.9	<0.02	<0.02	<0.01	<0.10	<0.00	0.05	0	0.04	<0.00
KS-30_06	<0.26	<2.7	6.5	5181	15	1.4	0.86	5.4	<0.04	<0.02	0.01	<0.07	<0.00	0.05	<0.00	0.09	<0.00
KS-30_07	<0.18	<2.2	5	134	65	2.1	<0.42	28	0.01	0.03	0.01	<0.10	<0.05	0.14	0	0.08	0
KS-30_08	<0.31	<3.0	6	137	84	1.2	<0.55	42	0.19	<0.03	0.02	0.07	<0.00	0.10	0	0.38	0.20
KS-30_09	<0.27	<3.2	3.9	95	35	4.3	<0.77	32	0.01	<0.04	0.03	0.02	<0.05	0.13	0	0.11	0.03
mean n=9	**0.17**	**-**	**3.3**	**1708**	**32**	**1.7**	**1.06**	**18**	**0.06**	**0.03**	**0.02**	**0.15**	**-**	**0.12**	**0.01**	**0.13**	**0.03**

APPENDIX F: FULL DATA SET OF LA-ICP-MS ANALYSIS OF PYRRHOTITE GRAINS

Element	V	Cr	Mn	Co	Ni	Cu	Zn	Se	Mo	Ag	Sb	Te	Au	Hg	Tl	Pb	Bi
KS-6																	
KS-6_01	<0.07	<2.9	<1.4	198	84	1.5	1.3	23	<0.05	0.05	<0.02	0.08	0.01	<0.16	<0.01	0.24	0.06
KS-6_02	0.74	<0.49	<0.25	184	63	0.6	<0.12	<4.5	0.04	0.34	<0.01	<0.08	<0.01	<0.05	<0.00	2.4	0.36
KS-6_03	<0.02	<0.35	<0.18	181	76	0.08	0.29	7.2	0.04	0.03	0.03	<0.14	<0.02	0.08	<0.01	0.02	0.01
KS-6_04	3.1	<9.8	<4.9	746	247	3.9	5.7	<33	0.37	0.45	0.00	<0.28	0	0.15	0	0.8	0.21
KS-6_05	1.2	<4.6	13	666	202	5.5	<1.7	<10	0.18	0.74	0.01	<0.29	<0.01	0.07	0	10	1.8
KS-6_06	<0.40	<5.0	5.3	707	286	3.2	<1.6	13	0.12	0.11	0.01	0.23	<0.01	0.11	<0.00	0.13	0.02
KS-6_07	<0.73	<6.7	7.3	706	292	9.4	<1.5	29	<0.10	0.15	0.04	<0.24	0.01	0.15	<0.00	0.62	0.13
mean=7	**0.87**	**-**	**4.6**	**484**	**179**	**3.4**	**1.7**	**17**	**0.13**	**0.27**	**0.02**	**0.19**	**0.01**	**0.11**	**0.00**	**2.1**	**0.37**
KS-11																	
KS-11_01	<0.10	<1.3	2.4	10.9	203	5.6	<4.8	9.7	0.08	0.09	0.03	<0.46	<0.01	0.23	<0.00	0.58	0.06
KS-11_03	<0.14	<1.3	1.3	10.8	218	<2.4	<3.1	14	0.08	0.44	0.03	<0.45	<0.01	0.24	<0.00	2.7	0.85
KS-11_04	<0.14	<1.3	2.0	11.4	210	<4.1	<5.4	19	<0.06	0.29	0.04	<0.44	<0.02	0.30	<0.01	0.75	0.46
KS-11_05	<0.10	<1.1	127	10.6	204	2.9	<2.2	12	0.12	0.10	0.03	<0.38	0.01	0.18	<0.00	0.98	0.19
KS-11_06	<0.90	<28	<11.6	15.2	346	4.4	<1.6	<27	<0.05	0.11	0.00	<0.07	<0.00	0.09	0.00	0.20	0.04
KS-11_07	0.39	<8.9	6.1	18.3	338	4.6	<0.58	<28	0.12	0.38	0.01	<0.22	<0.01	0.24	0.00	1.1	0.48
KS-11_08	<0.34	<5.4	111	14.6	260	<1.4	<1.1	<13	2.4	9.9	0.02	<0.41	0.01	0.14	0.01	5.9	9.0
mean=7	**0.30**	**-**	**37**	**13**	**254**	**3.6**	**-**	**18**	**0.41**	**1.6**	**0.02**	**-**	**0.01**	**1.4**	**0.00**	**1.7**	**1.6**
KS-28																	
KS-28_01	<0.17	<3.8	<4.4	569	315	<0.68	1.6	<21	0.08	0.22	<0.02	0.23	0.01	0.62	0.00	0.18	0.10
KS-28_02	<0.10	<1.2	1.2	419	178	2.4	<1.1	7.2	0.09	0.35	0.03	<0.29	<0.01	0.20	<0.00	0.36	0.23
KS-28_03	0.14	1.2	4.3	445	193	1.7	1	11	0.24	0.74	0.04	<0.34	<0.01	0.15	<0.00	0.71	1.4
KS-28_04	<0.09	<1.0	2.7	393	181	0.9	<1.0	7.1	0.11	0.20	0.03	<0.30	<0.06	0.11	<0.00	0.13	0.06
KS-28_05	0.11	<1.1	1.4	418	176	<1.1	<1.2	12	0.09	0.07	<0.01	<0.35	0.01	0.16	<0.00	0.06	0.01
KS-28_06	0.49	5.6	288	396	225	5.1	3.9	8.4	0.12	1.8	0.03	0.41	<0.00	0.24	<0.00	1.2	0.34
KS-28_07	<0.41	<12	<5.1	385	212	0.9	<0.8	<7.7	0.01	0.01	<0.00	<0.02	<0.00	0.02	<0.00	0.00	0.00
KS-28_08	<0.43	<9.7	<5.3	757	233	4.4	<0.8	<30	0.09	0.34	<0.02	<0.18	0.01	0.31	0	0.10	0.05
KS-28_09	<0.37	<5.1	5.5	561	263	1.8	1.7	<13	0.05	0.14	0.01	<0.34	<0.01	0.08	<0.00	0.07	0.08
KS-28_10	<0.40	<5.0	5.5	592	282	<1.4	<1.1	<9.4	0.19	0.21	0.01	0.42	<0.00	0.10	<0.00	0.12	0.10
mean=10	**0.27**	**4.574**	**32**	**493**	**226**	**2.0**	**1.4**	**13**	**0.11**	**0.40**	**0.02**	**0.29**	**0.01**	**0.20**	**0.00**	**0.29**	**0.24**

Element	V	Cr	Mn	Co	Ni	Cu	Zn	Se	Mo	Ag	Sb	Te	Au	Hg	Tl	Pb	Bi
KS-30																	
KS-30_01	<0.08	<1.3	<1.3	1.2	319	0.68	<0.84	<6.3	<0.04	0.04	0.03	<0.18	<0.00	0.12	<0.00	0.04	0.01
KS-30_02	0.14	<1.1	67	2.6	309	2.2	1.9	<4.5	0.06	0.11	0.03	<0.25	<0.01	0.12	<0.00	0.56	0.06
KS-30_03	<0.10	<1.1	1.2	4.4	334	2.1	<1.2	8.5	0.08	0.06	0.03	<0.29	<0.01	1.4	<0.00	0.05	0.01
KS-30_04	<0.11	<1.3	1.8	0.64	295	1.4	<1.6	19	0.09	0.11	0.02	<0.49	<0.01	0.28	<0.00	0.08	0.07
KS-30_05	<0.14	<1.5	1.2	8.7	377	2.2	<1.3	11	0.04	0.20	0.09	<0.59	<0.01	0.32	<0.00	0.12	0.01
KS-30_06	<0.07	<0.73	1.1	809	35	2.1	0.88	6.5	<0.04	0.06	0.02	<0.28	<0.01	0.24	0	0.21	0.02
KS-30_07	0.25	<1.6	<1.3	2.1	407	2.5	<1.7	18	0.19	0.08	0.03	<0.73	<0.02	0.31	0	0.12	0.03
mean=7	**0.13**	**-**	**11**	**118**	**297**	**1.9**	**1.3**	**11**	**0.08**	**0.09**	**0.04**	**-**	**-**	**0.40**	**0.00**	**0.17**	**0.03**
KS-32_01	<0.10	<2.1	<2.5	145	237	1.5	<1.1	<12	0.25	0.10	<0.01	0.36	0.01	0.25	0	0.15	0.03
KS-32_02	<0.10	<1.3	<1.1	132	209	3	1.3	<5.7	0.11	0.04	<0.01	<0.22	<0.01	0.16	<0.00	0.11	0.01
KS-32_03	<0.10	<1.1	6	132	204	<0.79	<1.0	8.6	0.29	0.35	<0.01	<0.27	<0.01	0.13	<0.00	0.71	0.42
KS-32_04	<0.12	<1.1	1.1	135	208	<1.1	<1.1	11	0.13	0.10	0.04	0.58	<0.01	0.16	<0.00	0.05	0.01
KS-32_05	<0.12	1.3	2.2	130	182	2.4	1.5	14	0.16	0.84	0.03	<0.45	<0.01	0.20	<0.00	0.45	0.02
KS-32_06	<0.13	<1.3	2.6	143	208	2.5	1.8	14	0.23	1.3	0.05	<0.54	<0.01	0.23	0.01	1.4	0.09
KS-32_07	<0.14	<1.3	2.4	142	230	<1.5	<1.5	16	0.26	0.17	0.03	<0.62	<0.01	0.26	0	0.16	0.02
mean=7	**-**	**1.4**	**2.6**	**137**	**211**	**1.8**	**1.3**	**13**	**0.20**	**0.41**	**0.03**	**0.43**	**0.01**	**0.20**	**0.00**	**0.44**	**0.08**
KS-25A_01	0.21	9.8	<3.9	968	645	4.5	2.0	17	0.35	0.24	0.02	<0.19	0	0.53	<0.00	0.27	0.13
KS-25A_02	0.46	5.4	5.6	829	311	14	6.5	11	0.24	3.4	0.04	1.7	<0.01	0.13	<0.00	1.1	0.32
KS-25A_03	<0.10	<1.1	1.3	794	339	2.2	1.1	14	0.15	0.11	0.04	0.38	<0.01	0.19	0	0.13	0.05
KS-25A_04	0.18	1.7	2.2	782	353	2.5	1.1	21	0.22	0.24	<0.01	0.4	<0.01	0.08	0	0.5	0.02
KS-25A_05	<0.10	2.5	<0.9	742	435	1	1.5	22	0.29	0.15	0.02	<0.32	<0.01	0.21	0	0.08	0.01
mean=5	**0.21**	**4.0**	**2.8**	**823**	**416**	**4.8**	**2.4**	**17**	**0.25**	**0.82**	**0.03**	**0.61**	**0.01**	**0.23**	**0**	**0.41**	**0.11**

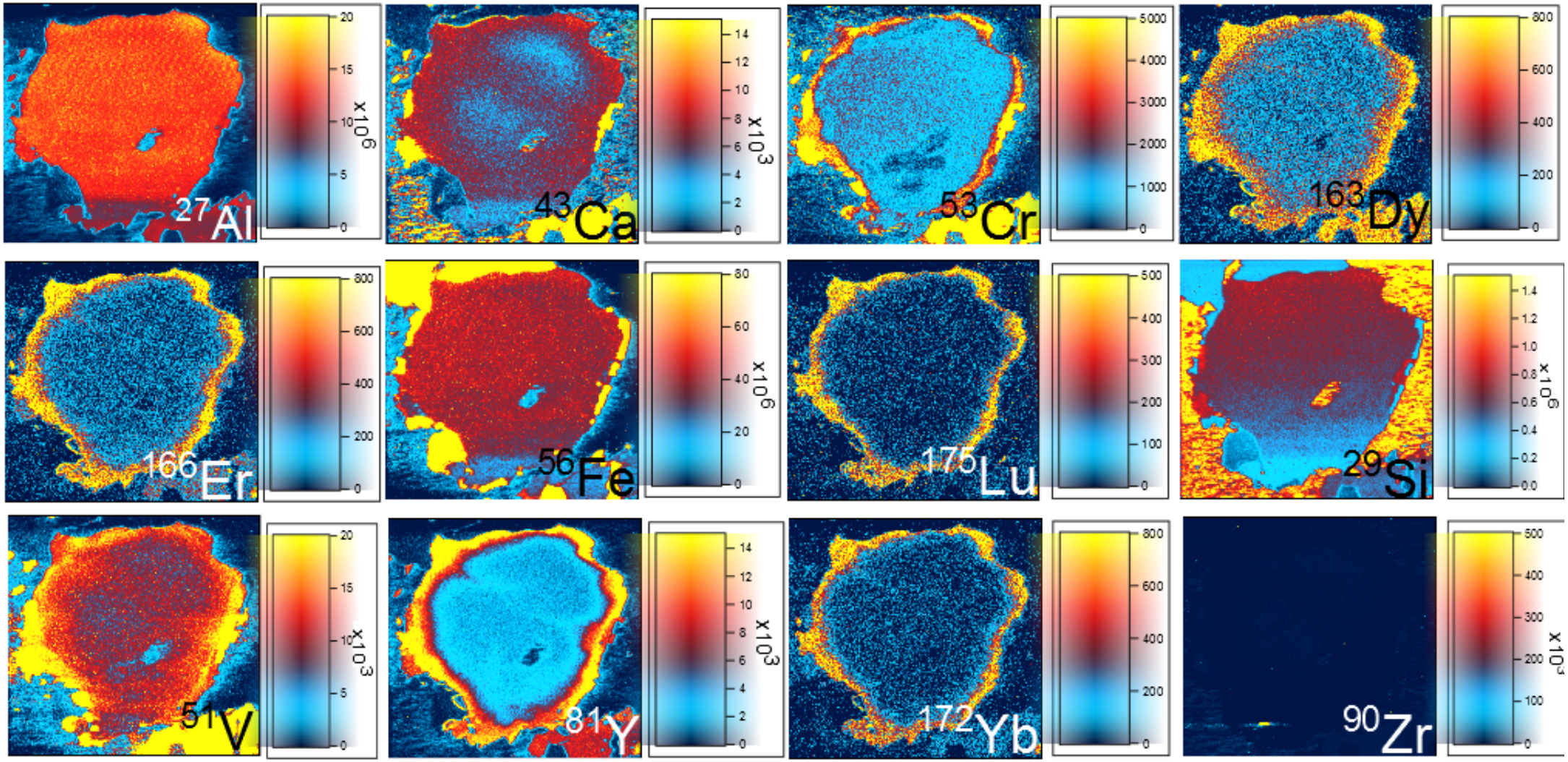

LA-ICP-MS element mapping of a metamorphic garnet grain. Notice that heavy rare earth elements (Dy, Er, Ly, Y, Yb), and Cr and V show compositional zoning, with enrichment in the core. Whereas elements that usually define compositional zoning, such as Al, Ca, Fe and Si show no compositional zoning.

APPENDIX H: ORIGINAL DRILLHOLE LOGS OF DIAMOND DRILLHOLES LB027DD AND LB035DD

HOLE # LB027DD Page 1 of 4					E:	N:	DIP:	AZI:	TD:
Structure	**Geology**	**Rock Type**	**Minerals**	**Sulphides**	**Comments**				
		Sand			0-4m : Sand cover.				
4		Calcrete	cb		4-6m : calcrete.				
6									
10		Weathered Amph.	a-p-q-cy-g		6-16.6 : Weathered amphibolite. minor garnet				
20		"	a-p-q-cy		16.6-21.6 : as above no garnet.				
∝ 57°									
* 30	qtz-cb vein	Amph	a-p-q-tx (px)	tr	21.6-47 : mg, dkgy, wf inplaces Amphibolite. : weak-mod qtz rich "sweats" throughout interval : two matic minerals (amph + px?) : qtz-cb altn vein @ 31-31.2m				
40									
47									
* 50		Amph	a(px)-p-q-tx	tr	47-52 : As above. Very low Cu assay 9ppm WHY?				
52									
					52-65.7m :				
60		Amp	a-(px)-p-q-tx	tr	As 21.6-47 with very minor tr garnet.				
65.7									
66.7		shear	cy-c-g		65.7-66.7 : sheared amphibolite with garnet.				
69.25	qtz vein	Amp	a(px)p-q-tx-g	1% suls py	66.7-74.2 : dkgy, mg, mass amphibolite, qtz sweats, minor garnet. 10cm qtz vein 68.1-68.2m				
70					69.75-70.1 qtz (minor cb) vein ± chlorite				
				tr suls.	72.4-72.45 qtz vein				
74.2m		Amp		tr py	74.2-81 : dkgy, mg, mass amphibolite, qtz sweats, minor garnet, tr suls. v minor qtz veins				

HOLE # LB02700 Page 2 of 4					E:	N:	DIP:	AZI:	TD:
Structure	**Geology**	**Rock Type**	**Minerals**	**Sulphides**	**Comments**				
mf ∝ 36°		Psamite ± minor amphibolite	q-b-a-p±g		81-91.57: gy, mf, mg-fg Metasediment? : 86.5-86.75 qtz vein x-cuts fol. : minor amphibolite as bands in interval.				
90									
91.57		Gneiss	q-p-a-1x		91.57-103.4: gy, mf mg-cg Gneiss (felsic amph) + qtz sweats : 102-102.5 cg-peg q-a-p vein : 102.8-103 qtz vein. : internal gradational with unit below.				
100									
103.4		Amph	a-q-p±g-1x		103.4-111: dgy, mf, mg Amph with comm qtz sweats : trace garnet : gradational to interval below.				
100									
111					111-136.8: dkgy, mf-mass, mg Amph, common qtz sweats, : 2-3% garnet over interval but concentrates in narrow bands				
120		Amph	a-p-q-g-1x	tr sulfs.					
130									
136.8									
140		Amph/ Csg	a-g-q-p-1x	1% sulfs.	136.8-142.3: dkgy±pk, mg-cg, mass Amph with common garnet-amph-qtz intervals (csg) to 80cm thick. Garnet, vcg to 2cm across, minor sulphides.				
142.3									
		Amph	a-p-q-g-1x	1% sulfs	142.3-151.37: dkgy, mg, massive, common qtz sweats, minor sulfs. : garnet common, concentrated in narrow intervals, <10cm ~2-3% garnet overall.				
150									
∝64° 151.37 151.85 152.31		vein	q	2-3% sulfs	151.37-151.85: cm, massive, minor "veins" hbl, dissem sulfs.				
			cg-p-q-a		151.85-152.31: SHEAR ZONE, clay & fe dominant core ∝ 64° (11 to 51).				
		Csg/Amph SMS	a-g-p-q-1x-cb mt	1±% sulfs 8% po 3% py <1% cpy	152.31-160.53: Csg/Amp (50:50), bands sulfs as matrix sulphides, rounded "clasts" of mela amph common in sulphide bands garnet "clasts" also present. qtz sweats common throughout. cg mt in qtz sweat. 1% fg diss sulfs in mela amph "clasts"				

HOLE # LB027 DD pg 3 of 4	E:	N:	DIP:	AZI:	TD:

Structure	Geology	Rock Type	Minerals	Sulphides	Comments
160.53					160.53 - 172.37 : mg, massive, qtz sweats, dkgy. weak sulphides, mainly as veinlets (x cutting) becomes more garnet rich toward base of interval
		Amph	a-p-q-g-1x	tr-1	
190					
172.37		Amp/SM$ Csg	a-p-g-q-1x cb	30% suls overall, po 20% cy 8% cp 2%	172.37 - 175.86 : Sulphide rich interval. Thick "bands" of sulphide to 50% suls. @ 173m 50% sulphide "bands" cross cut amph = late remob of suls? (PHOTO). Amph 70 : Csg 30% qtz sweats common
175.86		SHEAR zone	cg-a-g-q		
177.25		Amph	a-p-q-g-1x	tr	175.86 - 177.25 : bngy, fg-mg shear zone ~ 38°
178.38					
180		SM$	a-g-q-p-mt ·cb	50% Suls. po - 4% py - 8% cp - 2%	177.25-178.38 : dkgy, mg, qtz sweats, massive weak suls. minor garnet.
187.38					178.38-187.38 : semi-massive po-py-cpy dominat sulphides with magnetite. Some qtz sweats. very homogeneous unit & no fabric. very minor <5cm "bands" or "layers" of barren amph. Some "clasts" of mela amphibolite also. cb common throughout.
190		Amph	a-g-q-p±cb	2-3% po-py-cp	
191.72					187.38 - 191.72 : dkgy, massive, qtz sweats, garnet common (to 4cm across) occ band/layer of po-py-cp (30%) to 10cm but 2-3% suls overall
~60°		Amph	a-q-p-g-1x±cb	tr suls	
195.77					195.72 - 195.77 dkgy, wf, qtz sweats common garnet (in layers). minor chlorite altn. thin massive sulphide vein x-cutting @ 191.4° to core axis py-cp-po-mt 80%-10%-5%-5%.
~60°		cb Altered Amph	a-cb-q-p-g	1-2% po-py-cp	
200					
201.28					195.77 - 201.28 : cb altered amph? wf mg gy-gn. garnet minor. toward base (last 2m) of interval some bands/layers of sulphides (to 10-15%) over 10cm.
~66		Amph	a-q-p-1x	tr-1% suls.	
207.46		sm$	q-a-mt-cb	py-po-cpy 60%	201.28 - 207.46 : dkgy, mg, wf, qtz sweats, no garnet
207.87		cb-c-mt altered amph	a-q-cb-c-mt	tr-1%	
210					207.46 - 207.87 : bk+yl, mg-cg 60% suls 30% py 29% po <1% cpy. Mt common, minor cla, some mafic "clasts" and some qtz "clasts". ARE the qtz clasts relic qtz sweats & sulphides invaded + replaced them. Implications for timing. sulphides enplaced post peak meta?
~51°					
213.43		①	40% q-a-p±g-mt	30% py-30% po 1% cp	
215					
220		②	50% a-q-g-p±cb mt	40% po - 8% py - 2% cp	207.87 - 213.43 : bk&wt wf mg-cg unit. common cb, chlorite (as "clots") and cg magnetite altn of Amphibolite?? minor sulphides. Some very mafic layers in this interval similar to mafic "clasts" in SM$.
227.1					① - py-po rich & qtz+ amph "clasts" to 2cm, rare garnet. veg
230		③	50% a-q-g-p±cb mt	25% py - 23% po - 2% cp	② - po rich : common "clasts" and "layers" of mafic (a-mt), with lesser qtz-g layers. garnet and qtz "clasts" common too to 2cm. vfg suls in garnet.
231.7					③ py-po rich: as layer 2 with clasts. 3-4 intervals (up to 30cm thick) of py rich sulphides (40% py)
		④	40% q-g-a-mt	45% po - 12% py - 3% cp	④ po rich : homogeneous massive material. cg qtz ± garnet "clasts", amphibolite mt "clasts" more mg. pyrite subhedral and cpy common "rims" py. Garnet rich "layer" 233.1 - 233.3m disseminated sulphides (5%) common in garnet layer. Upper margins of "layer" has 5mm py rich selvage.
237					
240		⑤	40% q-g-q-p-mt	40% py 19% po 1% cp	⑤ py rich - up to 50% py - 10% po-cpy last 2m of interval. clasts common as above.

HOLE # LB027 DD pg 4 of 4					E:	N:	DIP:	AZI:	TD:
Structure	**Geology**	**Rock Type**	**Minerals**	**Sulphides**	**Comments**				
242.43		⑤							
∝49°		Amph	a-q-p-c-lx	tr	242.43-246.7: dkgy, weakly banded, qtz sweats, occasional gt bands, chlorite alteration. minor sulphides. Towards end of unit possible mela-amphibolitic clasts. m-c grained.				
246.7		Alt. Amph	a-q-p-	5-10% py mt	246.7-247.6: dkgy, m grained, massive, alt. amph. slug (10cm) semi-massive, py, mt in centre of interval. Thin veinlets of py, random orientation. Weak dissemnations.				
247.6									
250		Amph	a-p-q-cb-lx	tr	247.6-255.3: dkgy, m-grained, quartz sweats, massive. Trace gt. Cut by abundant thin cb veinlets at random orientations.				
255.3		fault	a-p-cb		255.3-255.5: fault breccia. cb common				
255.5									
260		Amph	a-q-p-g-lx	tr	255.5-268.84: dkgy, m-grain, mod foliated becoming strongly foliated towards base. Common gt,				
∝70°									
268.84									
∝72° 270		Amph	a-q-p-g-c-lx	1-2% py	268.84-269.9: strongly foliated to sheared amph. dkgy, f-m grained. veinlets of py parallel to foliation and cross cutting. Cb veinlets also				
		Amph	a-p-q-lx	tr	269.9-277.3: dkgy, m-grained, massive, qtz sweats. very rare gt				
277.3					EOH				
280									

HOLE # LB035 DD pg 1 of 5					E:	N:	DIP:	AZI:	TD:
Structure	**Geology**	**Rock Type**	**Minerals**	**Sulphides**	**Comments**				
		sand			0.–3.5m : sand cover				
3.5		calcrete	cb		3.5–5.65 : calcrete				
5.65		weathered Amph	a-p-q-cy-cb		5.65 – 7.3 : weathered amphibolite with cb veinlets.				
7.3		Amph	a-p-q-lx-cb	tr	7.3–39.6 : dkgy, m-grained, mod-foliated. : cb veinlets at top of unit : areas of lighter grey foliated layers : quartz sweats : occasional gt present towards bottom of interval : trace pyrite towards bottom of interval : m-c grained lx in some places.				
10									
20									
α 61°									
30									
39.6		fault	a-p-q-lx	tr	39.6 – 40.1 : shear zone, amphibolite. 3cm qtz vein, trace pyrite.				
40		Amph	a-p-q-gt-lx	tr	40.1 – 59.9 : gy, m-grained, massive : qtz sweats : gt rich zones, usually formed in bands of gt. <1% gt : trace amounts of pyrite : rare veins of cb : gt becoming less abundant towards bottom of interval				
50									
60		fault	a-p-q	tr	59.9 – 60.1 : shear zone, mainly matic minerals. trace pyrite, sheared amph.				
α 53°		Amph	a-p-q-gt-lx	tr	60.1 – 96.2 : dkgy, m-grained, weakly foliated in some places. : qtz sweats : rare gt zones : trace pyrite and pyrrohtite : same as 40.1 – 59.9 minus gt rich zones and massive texture. : last 3m increase in carbonate veining				
70									
80									

HOLE # LB035 DD pg 2 of 5					E:	N:	DIP:	AZI:	TD:
Structure	**Geology**	**Rock Type**	**Minerals**	**Sulphides**	**Comments**				
90									
98.2 100 100.7		Amph	a-p-q-cb-lx		98.2 - 100.7: amph as above. Broken core due to carbonate vein parallel to core axis.				
∝53° 110		Amph	a-p-q-cb-lx	tr	100.7 - 111.2: dkgy, weakly foliated, m-grained. Thin carbonate veinlets minor gt towards top of interval. Qtz sweats. Broken core from 105.8 - 106.4m.				
111.2		Amph cb alt	q-p-q-lx	tr	111.2 - 113.4: dkgy, massive amph. med-grained. cb alt feldspar rich, giving lighter colour, no qtz in cb alt. 40% cb alt, 60% amphibolite.				
∝60° 113.4 114.5	∿∿∿∿∿	shear	cy-cb-a-q-p		113.4 - 114.5: sheared amphibolite				
120		Amph	a-p-q-gt-lx	tr	114.5 - 126: dkgy, moderately foliated, medium grained amphibolite. Qtz sweats. garnet rich layers (1% gt) 1cm thick quartz vein @ 124.5m.				
126									
130 ∝69° 134.9		psammite + minor amph	q-b-a-p-lx	tr	126 - 134.9: - grey, strongly foliated, m-grained : minor amphibolite interbedded between psammite layers : gradational boundary between previous unit and psammite.				
∝59° 140		Gneiss + minor amph	a-p-q-lx -cb	tr	134.9 - 145: grey, moderately foliated, m-c grained : interbedded with small amphibolite bands : coarse grained lx. : carbonate veins running parallel to core axis, some hosting sulphide mineralisation.				
145									
150 ∝60° 160		Amph	a-p-q-lx	tr	145 - 165: m-grained, dkgy, moderately foliated amphibolite. : gradational boundary between previous gneiss and amph. : rare garnet band. : 3cm quartz vein cross cutting foliation @ 155.2m : quartz sweats : minor cb : low Cu values				

HOLE # LB035 DD pg 3 of 5	E:	N:	DIP:	AZI:	TD:

Structure	Geology	Rock Type	Minerals	Sulphides	Comments
165					
170		Amph	a-p-q-g-1x -cb	tr	165-185.2: dkgy, m-grained, moderately foliated amphibolite : gt-rich zones (1% gt) : cb veinlets : qtz vein from 166.1-166.5m and 172.5-172.6m : trace pyrite and pyrrhotite. : qtz sweats
∝65°					
180					
185.2		SHEAR	a-p-q-cy		185.2-185.5: sheared amphibolite with quartz veinlets.
185.5					
190		Amph	a-p-q-g-cb-1x	1%	185.5-199.2: dkgy, med-grained, mod foliated amphibolite : minor gt (<1%) : quartz sweats : cb veinlets, some which host sulphide mineralisation. : pyrrhotite slug, semi-massive sulphides. po, py, cp @ 188.1-188.5 po (85%)
∝67°					
199.2					
200		Csg	g-q-a	2-3% po-py-cp-	199.2-208.3: dkp, vcgrained, massive, gt dominant (60%) 2cm across : pyrrhotite and pyrite in equal abundances and very little chalcopyrite. : sulphide is disseminated equally throughout interval.
208.3					
210		Amph	a-p-g-q	1%	208.3-212.1: dkgrgy, massive, f-m grained. Gt m-c grained, gt equally distributed throughout interval, 5-10% of interval. occasional qtz sweat
212.1		Amph	a-p-q	3%	212.1-216.4: dkgy, massive, f-m grained. Mela amphibolite. Rare garnet. Banded (2cm) sulphide
216.4					
220		Amph/SM$	a-g-q-mt	35% 25% po 8% py 1-2% cp	216.4-227.9: br gy, m-cgrained, massive gt up to 8cm, gt very common 'bands' 'clasts' of mela-amphibolite common. occasional coarse grained quartz. Gt commonly contain sulphide inclusions, timing? Slug of po, py, cp @ 227.50m. cb-alt
227.9		Csg	a-g-q	1%	227.9-230.5: dkgn-p, massive, vcgrained. disseminated and banded sulphides
230					
230.5		Amph/SM$		20% 12% po 6% py 1-2% cp	230.5-236: dkgy-brgy, moderately foliated amphibolite, m-cgrained. Sulphide zones are massive in appearance, contain up to 60% sulphide. Sulphides follow banding but also cross cut in places. Coarse gt common, up to 6cm, mt inclusions pyrrhotite towards bottom of interval
∝62°					
236		Amph	a-p-q-	1%	236-242.95: dkgy, massive, m-grained amphibolite. Qtz sweats, 1% sulphides including pyrite stringers rare garnet. Becoming more sulphide rich towards bottom of unit.
240					

HOLE # LB035DD pg 1 of 5					E:	N:	DIP:	AZI:	TD:
Structure	**Geology**	**Rock Type**	**Minerals**	**Sulphides**	**Comments**				
242.95		SM$	g-a-q	60% 40% po 17% py 2-3% cp	242.95-250 - brown-brassy, c-grained, massive. c-grained gt with inclusions of sulphides and mt, to 3cm Mela-amphibolite clasts, sub-rounded, up to 3cm. cb. Alt.				
250		Amph/ SM$	a-q-g-mt	35% 18% po 1% cp 16% py	250-257: dkgy-bry, c-grained, massive. Alternating bands of amph and sulphides. Sulphides becoming pyrmt rich towards bottom half of interval. Py-sub-hedral Alternating sulphides between po rich and py rich over the meter. cb Alt scale. Po rich zones, m-c grained, with gang min assem. of a-g-q. Py-rich zones, generally a-g-mt-gt (lesser gt) py-c grained. Sharp contacts between sulphide zones				
257									
260		SM$/ Amph	a-q-mt -g	40% 34% py 1% cp 5% po	257-262.5: y-dkgy, massive (amph intervals have mod-foliation of 55°) m-c grained py-dominant, common mt, gt coarse grained where present. siliceous. massive texture, 70% SM$ + 30% AMPH over interval cb-alt.				
262.5		SM$	a-g-q-mt	50% 38% po 2% cp 10% py	262.5-267.2 bry, c-grained, massive, vc-grained pyroxene? crystals, inclusions of sulphides @ 264.9m. cb alteration. 'Clasts' to 3cm in interval, of mela-amph.				
267.2									
270		SM$	a-p-q-gt	50% 40% py 8% po 2% cp	267.2-277: y-dkgy, c-grained, massive. coarse grained pyrite. occasional qtz sweats. occasional gt grains up to 2cm, included with mt. Mela-amph 'clast' up to 6cm, included with gt and sulphides. Pyrrohtite rich zone towards bottom of interval				
277									
280		SM$	a-p-q-gt-mt	35% 20% po 12% py 3% cp	277-297.2: dkgy-brassy, m-grained, massive. m-grained pyrrohtite. layers of dkgy massive amph @ 279.9-280.1 and 280.9-281.2m. Becoming more felsic (qtz rich) towards bottom of interval. vc-grained gt, up to 10cm, included with mt. Mela-amph 'clasts' up to 8cm, with inclusions of sulphide.				
290									
297.2									
300		SM$	a-p-q-gt-mt	40% 25% py 1% cp 14% po	297.2-302.1: y-dkgy, massive, c-grained. c-grained py, gt up to 3cm, inclusions of mt & sulph. Mela-amph 'clasts' up to 5cm, inclusions of mt.				
302.1									
x55°		Amph	a-p-q-gt	1-2%	302.1-307.05: dkgy, moderately foliated, m-grained amphibolite. Qtz sweats. 1% gt, becoming more abundant towards bottom of unit (<2cm crystals). Bands of sulphide that follow the foliation. Py and po with trace amounts of cp.				
307.05		SM$	a-p-q-gt	20% (10 py, 9 po, 1 cp)	307.05-308.7: y dkgy, massive, m-c grained, mela-amph 'clasts' up to 10cm, 2cm gt clasts.				
308.7		Amph	a-p-q-g	1-2%	308.7-310.5: dkgy, m-f grained, strongly foliated. minor bands of sulphide 3% gt				
<70° 310	310.5	Amph	a-p-q-lx	tr	310.5-326.5: dkgy, m-grained, massive amphibolite. Minor gt 323 → onwards				
320									

HOLE #	LB035 DD	Pg 5 of 5			E:	N:	DIP:	AZI:	TD:
Structure	Geology	Rock Type	Minerals	Sulphides	Comments				
326.5		qtz vein	quartz		326.5 - 327.2 : quartz vein, minor amphibole cluts				
327.2									
330		Amph	a-p-q-1x		327.2 - 334.2 : dkgy with lgy bands (psammite??) m-grained, mod-strongly foliated. 1cm light grey bands. qtz sweats				
∝ 31°									
334.2									
∝ 72°	~~~~	shear	a-p-cb-q-cy		334.2 - 336.5 : dkgy, m-grained, strongly foliated, sheared amphibolite. Intensive carbonate veining				
336.5									
∝ 72°		Amph	a-p-q-1x-gt		336.5 - 339.9 . dkgy, m-grained, weakly foliated, amphibolite. 3% gt (0.5 cm)				
340									
341.8		Csg	g-a-q-mt	2-3% po, py	339.9 - 341.9 : dpk, vcgrained, massive. 60% gt. po, py equally distributed. sulphide disseminated equally through interval.				
343	~~~~	shear	a-p-cb-q-cy		341.8 - 343 : same as above shear zone				
350		Amph	a-p-q-1x		343 - 362.5 : dkgy, m-grained, weakly foliated in places : very minor gt : quartz sweats : minor thin qtz to 3cm				
360									
362.5		peg + amph	p-q-a		362.5 - 366.5 : interval of intense pegmatite veining. 50% peg vein, 50% amph as above				
366.5									
370		Amph	p-a-q-1x -cb		366.5 - 376.5 : dkgy, m-grained, massive : quartz sweats : thin cb veinlets.				
380									